Mechanism of Landslides around China's Three Gorges Dam

by

Yang Li

A Thesis Submitted in Partial Fulfillment of the Requirements for the Degree of

Master of Science

in

Geotechnical Engineering

Department of Civil and Environmental Engineering
University of Alberta

ABSTRACT

In this research, a literature review is conducted for landslide reactivation and movement caused by reservoir water level fluctuation around the world and especially in China in the past decades. Based on the movement patterns and characteristics, landslides triggered by reservoir level fluctuations are broadly classified into two types based on their movement mechanism.

Mechanism 1 refers to landslides which move or move faster when reservoir water level is decreasing. The soil in this type of landslide usually has low permeability and the combination of outward seepage force and lower hydrostatic pressure at the toe makes the landslide less stable when reservoir level is decreasing. Mechanism 2 refers to landslides which move or move faster when reservoir water level is rising. The soil in this type of landslide has high permeability and the increase in landslide movement is caused by decreased effective normal stress in the slip zone. These two types of landslides have been studied using a numerical model with a strain softening and strain rate dependent model adopting Drucker-Prager plasticity using the ABAQUS program.

Three landslides around the Three Gorges dam reservoir have been studied. They are the Shuping landslide, Baishuihe landslide and Muyubao landslide. For Shuping and Baishuihe landslides, with low permeability soils, the calculated changes in groundwater table does not follow the fluctuation of reservoir water level closely and there is a time

lag between movement and changes in reservoir water levels. The changes in the calculated factor of safety follows the expected trend on changes in reservoir water level which increases when reservoir level is rising and decreases when reservoir level is decreasing. In addition, the calculated landslide movement from coupled seepage/stress finite element model with Drucker-Prager constitutive model shows that movement accelerates when reservoir level is decreasing and decelerates when reservoir level is rising. These two landslides belong to Mechanism 1: low permeable landslide material, reservoir drawdown causes outward seepage force and less stabilizing hydrostatic pressure at the toe, which leads to movement acceleration; when reservoir level is rising, the increasing hydrostatic pressure at the toe helps stabilize the slope and decreases the rate of movement.

For Muyubao landslide, which has high permeability material, the calculated groundwater table follows closely with the observed reservoir water level, which indicates that the fluctuating reservoir level has significant influence on the pore water pressure along the slip zone. The calculated factor of safety decreases when the reservoir level is rising and increases when reservoir level is decreasing. In addition, calculated landslide movement from the finite element model accelerates and decelerates when reservoir level is rising and decreasing respectively, which agrees with the observed movement from GPS stations. Hence Muyubao landslide belongs to Mechanism 2: with high permeable landslide material, fluctuations of reservoir water

level induce changes in the pore water pressure and effective normal stress in the slip zone; the effective normal stress and shear resistance decrease when reservoir level is rising, which lead to movement acceleration; the effective normal stress and shear resistance increase when reservoir water is decreasing and decelerate the movement.

Field permeability tests have been conducted on Shuping and Baishuihe landslides. Moreover, laboratory tests such as grain size distribution and Atterberg limits tests have been conducted on the landslide materials. It is recommended that further laboratory tests should be conducted to verify the strain softening and strain rate hardening parameters as well as unsaturated permeability parameters used in the numerical models.

Acknowledgements

I would like to give my deep appreciation to my supervisor Dr. Dave Chan for his support, guidance, and help throughout my study and research. His supervision is critical for me to improve not only on my research but also on how to ask questions and solve problems.

I thank Dr. Guogong Zhang for his support and direction during the research program. His suggestions and instructions on landslide investigations and analysis are invaluable to the accomplishment of this research.

I also thank Dr. Shimei Wang and Dr. Yong Chen for their help with field and laboratory testing. I am grateful for Dr. Yunzhi Tan and Miss Ni Guan for their help with laboratory tests. I would like to express my gratitude to Jialong Liu and Fan Zhang for their help during field investigations and tests.

I would like to thank Li Wang for providing me plan views and sections of Shuping, Baishuihe and Muyubao landslide.

I would like to express my deep and sincere appreciation to my family, especially my wife, Yameng. Her continuous love, encouragement, and support helped me overcome all difficulties during the research. I am grateful for her help and sacrifice during my postgraduate study.

Finally, I would like to express my gratitude to my friends both in Canada and China. Their care and help are priceless to me.

TABLE OF CONTENTS

Chapter **Page**

LIST OF TABLES

Page

LIST OF FIGURES

Page

Chapter 1 Introduction

1.1 Background

The Three Gorges dam is one of the largest hydroelectric power projects in the world. With 32 main turbine generators, it produces 22,500 MW of electricity comparing to 1,212 MW of total installed capacity of the Genesee Power Generating Station which provides power for the City of Edmonton. The water level of the Three Gorges reservoir varies between winter and summer months for flood control of the Yangtze River, China largest and longest river system. The annual water level fluctuation can be as much as 30 meters, which has significant effects on the stability of the slopes surrounding the reservoir. This variation of water level introduces cyclic loading on the slopes. Some slope movements occur during rising of the water level while others move when the water level is being lowered. In 2003, a slope failure occurred in the reservoir resulted a 20-meter wave surge killing 13 people. This surge also adversely affected the ecology in the reservoir area and threatened the safety of the Three Gorges dam.

Since June 2003, GPS monitoring stations have been installed on the ground surface in 37 landslides to monitor landslide movement. Among these landslides, several landslides tend to be more active and move at a relatively faster rate. More attention has been given to these faster moving landslides and boreholes have been drilled to identify underground stratifications and slip zones.

Among hundreds of active moving landslides around the Three Gorges Dam reservoir, three landslides have been selected for this research. They are called Shuping landslide, Baishuihe landslide and Muyubao landslide. Topography, subsurface stratification, groundwater level, and ground surface movement data have been collected and provided by Dr. Guodong Zhang of the China Three Gorges University for this research.

Field permeability tests were conducted on Shuping landslide and Baishuihe landslide. A

set of field permeability test equipment was designed and made for this research. Undisturbed soil samples were obtained using thin-wall tubes and laboratory tests were conducted to obtain density, moisture content, Atterberg limits and grain size distribution of the landslide soil.

In this study, landslides are broadly classified into two main types based on their movement pattern and mechanism of movement in response to reservoir water level fluctuations. Seepage and stability analyses were carried out using SEEP/W and SLOPW/W software. A strain softening strain rate hardening Drucker-Prager constitutive model has been implemented in the commercial finite element program ABAQUS to carry out coupled hydro-mechanical analysis under cyclic loading.

Four scenarios are proposed for the landslides in the Three Gorges reservoir and the factors affecting the mechanisms of landslide movement are studied using SEEP/W, SLOPE/W and SIGMA/W software.

1.2 Objective of the Research

The impact of impoundment and drawdown on the landslide stability and movement has been studied during the past decades; however very little work has been done in understanding the cyclic behavior of soils and its effect on slopes, specifically the landslide behavior under cyclic reservoir water level fluctuation. In this research, a rate dependent constitutive model has been implemented in ABAQUS to study landslide movement due to cyclic reservoir water level fluctuations.

Based on ground surface global positioning system (GPS) observations, landslides around China's Three Gorges Dam can be classified into two main types. The first type of landslide moves faster when the reservoir water level is decreasing. The second type of landslide moves faster when the reservoir water level is rising. It is postulated that the

soil in the first type of landslide has low permeability and the second type of landslide has soils with high permeability. Field permeability tests have been conducted and a cyclic constitutive model has been implemented in ABAQUS to study the mechanisms of these two types of landslide.

The purpose of the research is to use a constitutive model to analyze cyclic movement of landslides and to study the deformation mechanisms. This research will provide a better understanding on landslide movement around the Three Gorges area which will be useful to identify potential slope failures.

1.3 Scope of Research and Organization of Thesis

In Chapter 2, a review of existing literature on landslides around reservoir is presented. This includes a review of research on landslides in the Three Gorges reservoir in China and in other countries. The types of movement are presented and the mechanisms for the landslides are included. In addition, progress of research on the effect of strain rate on the shear strength is presented.

Chapter 3 presents the results from laboratory experiment and field test conducted for this research. In this chapter, the theory for conducting field permeability test and test procedures are described. The procedure of taking undisturbed soil sample in colluvium soil with gravels and boulders using thin-wall tubes is also included in this chapter. Field permeability test results for Shuping landslide and Baishuihe landslide are presented. Several laboratory tests, including density test, Atterberg limits test and grain size distribution test are described and test results are also summarized in this chapter.

In Chapter 4, two types of landslide and their corresponding mechanisms are studied. Drucker-Prager plasticity model with strain rate hardening is implemented in ABAQUS to model movement of a general landslide with high and low permeability under cyclic

reservoir water level fluctuation. It is postulated in Mechanism 1 that for landslide with low permeability, rising of the reservoir water level increases the stabilizing force at the toe and lowering of the reservoir water level leads to outward seepage force and less stabilizing force at the toe. It is postulated in Mechanism 2 that for landslide with high permeability, rising of the reservoir water level increases pore water pressure and decreases effective normal stress in the slip zone resulting in more unstable situation.

In Chapter 5, a case study is carried out on Shuping landslide which moves faster when reservoir level is lowered. Background information of Shuping landslide is discussed. In addition, the observed reservoir water level, ground surface movement and ground water level are also provided. Seepage analysis and stability analysis were conducted using SEEP/W and SLOPE/W software. Coupled pore fluid/stress analysis was carried out using strain rate hardening Drucker-Prager constitutive model in ABAQUS. Permeability and strength parameters that best match monitored ground water level and landslide movement were determined.

Chapter 6 presents the case study of Baishuihe landslide with mechanism 1 type of movement. Backgrounds of the landslide such as areal extend of the slide, subsurface stratification and layout of GPS stations are provided. Moreover, the observed reservoir water level and ground surface movement are presented. Transient seepage and stability analysis under the fluctuating reservoir levels were conducted with SEEP/W and SLOPE/W software. Details of coupled pore fluid/stress analysis with strain softening and strain rate hardening Drucker-Prager constitutive model in ABAQUS are presented in this chapter. The permeability and strength parameters are back calculated for Baishuihe landslide and are also presented in this chapter.

In Chapter 7, the case study of Muyubao landslide is presented which moves faster when the reservoir is rising. The background of this landslide is discussed and the

subsurface stratification is presented. In addition, the observed reservoir water level and ground surface movement pattern are presented. The results of a coupled pore fluid/stress analysis with strain softening strain rate hardening Drucker-Prager constitutive model using ABAQUS are presented in this chapter. The permeability and shear strength on the sliding surface are back calculated for this landslide.

Chapter 8 presents a sensitive study on the factors that affect the mechanism of landslide movement. The influence of water pressure at the toe of a landslide, effective stress at the slip surface, seepage force and weight of water at the toe of a landslide are some of the factors considered in the study.

Finally, conclusions of the thesis and recommendations for further research are summarized in Chapter 9.

Chapter 2 Literature Review on Landslides around Reservoirs

A lot of dams were built worldwide during the past decades. During first impoundment or regular operation of those dams, landslides were reactivated or landslide failures were triggered by the impact of reservoir level fluctuation. Some of the landslides moved or failed during reservoir drawdown; some other landslides were caused by the reservoir impoundment. Researchers worldwide have studied the impact of reservoir water level on landslide by installing instrumentations, conducting laboratory tests to study soil strength behaviors, doing large scale model experiments, and conducting numerical analysis by establishing numerical models.

In Chapter 2.1, current researches on reservoir affected landslides around the world are reviewed. Cases of both types of landslides are illustrated which show that the two types of landslides exist not only in the three gorges reservoir, but also widely around the world.

Chapter 2.2 is focused on the cases and studies of landslides in the three gorges reservoir. Factors affecting landslides in the three gorges reservoir such as geological conditions, rainfall and earthquake are reviewed. Then cases of landslides in the three gorges reservoir which are affected by reservoir drawdown and impoundment are presented, respectively.

Chapter 2.3 puts emphasis on considering not only factor of safety but also motion characteristics of huge slopes. It also gives insights into strain softening and strain rate hardening of soil which was implemented in the modeling part in this research.

2.1 Landslides around Dam Reservoirs Worldwide

Landslides Affected by Reservoir Drawdown

There are many cases of landslides worldwide caused by the drawdown of reservoir water level. In the book *Deterioration of dams and reservoirs: Examples and their analysis* (ICOLD 1980), an upstream landslide in San Luis Dam reservoir in California was discussed. The landslide was caused by the drawdown of reservoir after successful operation of the dam for 14 years.

A number of landslides along the river banks of the Rio Montaro in Peru were triggered by rapid drawdown of the reservoir water level (Lee et al., 1975). Several landslides which were triggered by rapid reservoir drawdown were also analyzed by Sherard et al. (1963).

The Groapa Vântului landslide, a deep-seated landslide which is located in the Siriu Reservoir in Romania, was affected by reservoir water level oscillations according to Micu et al. (2013). In his paper, the reservoir level was maintained up to 10 m above and decreased twice below the normal retention level, which induced the slope base weakening.

The Grasegger slope is located in the reservoir of the Gmünd dam in Austria. In the paper by Leobacher et al. (2010), an estimated volume of 10,000 m^3 at the foot of the slope failed due to high rate of trial drawdown in September 2004.

The stability of the Mississippi earth banks under drawdown effect were analyzed by Desai (1971, 1972, 1977) who conducted both experimental and theoretical studies. Different drawdown rates and permeability of the materials in the slope were considered under semi-rapid drawdown condition.

Morgenstern (1963) mentioned that sudden drawdown can induce landslides in the natural slopes in the reservoir area. He noted that numerous landslides were observed in the Grand Coulee Dam reservoir in the U.S. state of Washington after lowering the reservoir level. In his paper, stability charts for different drawdown ratios are presented.

Lane et al. (2000) noted that the stability of a slope can be affected by forces which include pore water pressure, seepage forces, and hydrostatic and hydrodynamic effects which can be induced by reservoir water and drawdown. He mentioned that for many submerged slopes, the rapid drawdown is the most critical case. As an extension of Morgenstern's chart method, Lane used the finite element method and developed a chart based approach for critical conditions of slopes under rapid drawdown from partial submergence.

Alonso et al. (2008, 2011, 2011) studied the pore water pressure of slopes under rapid drawdown and illustrated case studies of Glen Shira Lower Dam in Northern Scotland and Canalles landslide in Spain. He stressed that a fully coupled flow-mechanical analysis is critical for the analysis of slopes affected by reservoir drawdown.

In this research, fully coupled fluid/stress analyses were conducted for mechanism 1 and mechanism 2 and in all three case studies with transit fluid boundary reflecting the cyclic fluctuating reservoir water level. Mechanism 1 is proposed for the landslide whose movement is affected by reservoir drawdown and it is postulated in this research that this type of landslide has low permeability.

Landslides Affected by Reservoir Impoundment

Besides the above landslide cases affected by the drawdown of reservoir, there are also cases of landslides which are caused by the reservoir impoundment around the world. .

Saurer et al. (2013) mentioned that many reservoir slope stability can be affected by first impoundment and reservoir level fluctuation. He stressed that “the boundary conditions of reservoir slopes may change drastically due to impoundment” and developed a decision matrix for the selection of appropriate landslide stabilization methods.

Thorough investigations for slope stability threatened by water level fluctuation in reservoirs were conducted in Japan (Fujita, 1977). In his paper, cases for the landslides induced by first impoundment (Futase Dam, Kanogawa Dam, and Narugo Dam) were presented.

The Mandria landslide, which is located in Polyphyton reservoir in northern Greece, was reactivated by the first filling of the reservoir. Pytharouli et al. (2010) conducted a thorough study of the landslide by analyzing displacement and reservoir level records using signal analysis techniques. Alexis landslide is also a major landslide in the Polyphyton reservoir. According to Riemer et al. (1996), the landslide movement was affected by the initial filling of the reservoir.

According to Singh et al. (2012), a number of fossil slide sites were reactivated after the Baglihar dam reservoir water level, which is located in Kashmir, increased from 850 m to 870 m level. Singh studied a huge landslide washing out at Assar and concluded that the toe cutting induced by the increased reservoir water level is one of the key factors for the Assar landslide failure.

Sadrekarimi et al. (2007) conducted a thorough review of the Vaiont landslide and concluded that one of the mechanisms that reactivated the ancient landslide was lower effective normal stress and shear strength induced by increasing reservoir level.

In this research, mechanism 2 is proposed for the landslide which moves faster during impoundment. For the study of this mechanism, much emphasis is put on the pore

pressure and effective stress change in the slip zone of the landslide. Muyubao landslide, which is located in the Three Gorges reservoir, is selected for the case study.

2.2 Landslides around the Three Gorges Dam Reservoir

The Three Gorges dam, which is located on the Yangtze River in China, is one of the largest gravity dams in the world. Since the first impoundment of the 660 km long reservoir in May 2003, more than 260 landslides have occurred along the reservoir banks (Hug, 2009).

It is known that landslides in the Three Gorges reservoir can be reactivated and landslide movement can be affected by factors such as landslide geological conditions, topography, precipitation, earthquake, human activities and reservoir water level fluctuation.

Huang (2007) reviewed large-scale landslides in China since the 20th century and concluded that topographical and geomorphological conditions, strong earthquakes, and extreme weather conditions and the global climate change are three main factors that led to large landslides in the Three Gorges reservoir area. It is also concluded in the paper by Du et al. (2013) that reservoir landslide movement can be influenced by geological and hydrological conditions, as well as external factors such as rainfall, earthquake, human activities and reservoir level fluctuations.

Landslides Affected by Geology Related Conditions

The material composition, distribution and geological formation of the Baiyian ancient landslide were studied by Li et al. (2008). Li pointed out that the stability of the Baiyian landslide is not only controlled and affected by its current state, but also by its geological evolutionary history.

Lu et al. (2012) pointed out that the topography and lithology are two main factors that

inherently influence landslide deformation. He mentioned that the Woshaxi landslide is steep at the toe and the argillaceous siltstone and mudstone of the landslide are susceptible to wreathing and easy to be softened by water, which makes the landslide easy to slide.

Miao et al. (2014) also noted that lithology can have great impact on landslides. He noted that the interbeded layers of thick silty sandstone and thin sandy mudstone of the Jurassic red strata in the Three Gorges reservoir are important factors for the development of landslides, such as the Chonggang landslide, Jipazi landslide and Qianjiangping landslide.

Qiao et al. (2006) analyzed the impact of the lithological characteristics, slope gradient, slope formation, slope height, and slope orientation on landslide development by studying the data of 205 landslides in the Three Gorges reservoir and he developed a landslide risk level map.

In this research, the geological history and underground stratification are described in each of the three case studies. Geological characteristics of landslide mass and bedrock are considered for permeability and strength in numerical modeling.

Landslides Affected by Rainfall

There are some landslide cases in the Three Gorges reservoir which are affected by the precipitation. Xia et al. (2013) studied the movement records and rainfall data of the Shiliushubao landslide in the Three Gorges reservoir and concluded that rainfall is the main factor affecting the deformation of two shallow blocks of the landslide.

The displacement monitoring data of the Liangshuijing landslide was analyzed with rainfall by Wu et al. (2013) using factor analysis method. It was concluded that the

rainfall two months before and the rainfall of the current month have greater influence on the displacement of Liangshuijing landslide than the reservoir level.

Hou et al. (2013) conducted research about the Houba landslide which is located in the Three Gorges reservoir area. The surface-layer slip zone and the landslide mass above the slip zone are mainly composed of weak-moderate expansive soil. Hou mentioned that the shear strength of the expansive soil could be easily reduced by the saturation-desaturation cycles due to the rainfall. His research shows that localized surface-layer landslide may occur under continuous rainfall conditions.

The saturated/unsaturated seepage of Dashiban landslide in the Three Gorges reservoir under a particular rainfall type was studied by Feng et al. (2011). It was concluded that the resurrection of the landslide in the year 1983 was caused by the saturation of the landslide induced by long period of rain.

Hu et al. (2012) conducted saturated/unsaturated seepage analysis of the Hualianshu landslide on the condition of rainfall and concluded that rainfall causes reduction of matric suction of the unsaturated zone, thus reducing the shear strength of unsaturated soils.

The stability of the Bazimen landslide under the influence of rainfall was studied by Hu et al. (2011). It was concluded that rainfall changes the groundwater infiltration line in the landslide significantly and stability of the landslide decreases with increasing rainfall intensity. Du et al. (2013) studied two landslides in the Three Gorges reservoir, Bazimen and Baishuihe landslide, whose movement is affected by rainfall. Du adopted the BP neural network model in analyzing the accumulated rainfall data.

According to He et al. (2009, 2012), the rainfall records from 1978 to 1985 suggest that the displacement velocity of the Xintan landslide is primarily influenced by rainfall. In his

paper, the relationship between rainfall and landslide movement was studied by using the loading/unloading response ratio method. In the research of Wang et al. (2009), it is also mentioned that precipitation is an important factor for deformation acceleration and reactivation of the Xintan landslide.

Based on Boussinesq's differential equation of unsteady-seepage and boundary condition, Wang et al. (2013) analyzed the stability of the Er-Liban landslide, which is located in the Three Gorges reservoir, with different rainfall intensity. It was found that the factor of safety of the Er-Liban landslide decreases almost linearly with increase in rainfall intensity.

Rainfall was not included in numerical models in this research and it is only qualitatively discussed in Chapter 6. The rainfall impact on landslide stability and movement mechanism can be studied in future research.

Landslides Affected by Earthquake

Seismic load induced by earthquake can have significant adverse effects on landslide stability. An earthquake fault zone was discovered in the Maluxiang - Changduhe area in the Three Gorges reservoir and Li et al. (2013) conducted a thorough study and presented the fault distribution and geographical conditions of the site. According to Li, the active fault zone has the ability to nurture devastating earthquakes which can be triggered by reservoir fluctuations and can lead to reactivation of old landslides.

Tang et al. (2012) investigated the stability and movement pattern of the Zhaoshuling landslide under the influence of seismic load by conducting physical model tests. His research shows that landslide will deform and lose stability partly when earthquake load reaches certain intensity with the normal reservoir level.

The factor of safety of a reservoir landslide under the influence of earthquake was studied by Deng et al. (2011) with Strength Reduction FEM. The research shows that the landslide is not stable under the earthquake load with normal reservoir level. Based on the modeling results and geological conditions, Deng proposed a treatment plan of unloading the back edge of the landslide.

Besides the above factors that can lead to landslides in the Three Gorges reservoir, landslide reactivation and movement in the Three Gorges reservoir can also be induced and significantly affected by reservoir drawdown and impoundment.

Landslides Affected by Reservoir Drawdown

There are many cases of landslides which are affected by the drawdown of Three Gorges reservoir level. In Hug's (2009) research, site investigations and stability calculations were conducted on the Qiao Tou landslide in the Three Gorges reservoir. Hug studied the landslide stability under 95 m, 145 m, 175 m and falling from 175 m to 145 m AMSL water level. She concluded that 95 m and 175 m AMSL water level were stable and the falling from 175 m to 145 m AMSL was the critical situation (FS<1). She noted that "not a single water level contributes to movements within the slope but the falling water level from 175 m AMSL to 145 m AMSL causes an elevated phreatic surface in the slope and groundwater drainage parallel to the surface of rupture."

Shuping landslide is an ancient landslide located on the main stream of the Three Gorges reservoir. Wang et al. (2007) installed extensometers, conducted 1 m-depth ground temperature measurement for groundwater vein and analyzed GPS monitoring results. In the later research of Wang et al. (2013), extensometer monitoring results at the east boundary of the Shuping landslide showed that the landslide moved when the reservoir level was decreasing. In addition, it was concluded in the paper that "the slope deformation rate is proportional to the water level falling-down rate".

Hu et al. (2013) studied the Zhujiadian landslide, which is located in the Zigui County in the Three Gorges reservoir area, by analyzing monitoring data from extensometers, GPS stations, and inclinometers. Hu's research also shows that the landslide moves faster during the reservoir water level drawdown.

The relationships between landslide stability, permeability and reservoir drawdown speed were analyzed by Liao et al. (2005) using Geo-slope software. Liao's research presented that the factor of safety (FS) was always decreasing for 30-meter drawdown. It was also concluded that the FS decreased with higher rate of drawdown.

The Tangjiao #1 cohesive landslide, which is located in the Wanzhou District in the Three Gorges reservoir, is also affected by the reservoir water level fluctuation. The landslide mass of the Tangjiao #1 cohesive landslide is a low permeability quaternary colluvium. Yang et al. (2013) conducted seepage and stability analysis of the landslide whose research shows that the landslide stability increases when the reservoir water level rises; the factor of safety decreases when the reservoir water level drops. In his research, the factor of safety increases/decreases faster when the reservoir fluctuation rate is higher, which indicates that the stability change rate of the Tangjiao #1 cohesive landslide is closely related to the reservoir water level fluctuation rate.

Zhu et al. (2011) conducted coupled seepage and stress analysis of the Hefeng landslide to study the landslide movement due to fluctuation of the Three Gorges reservoir. In Zhu's research, the permeability of the landslide mass is taken to be 8.41×10^{-7} m/s, which is fairly low. On one hand, it has been shown by Zhu that the saturation line lags behind the reservoir level and seepage force acts almost horizontally inward the landslide, which helps to stabilize the landslide, during rising of the reservoir. On the other hand, Zhu's research shows that seepage force acts both inward and outward of the landslide and the pore water pressure along the slip zone gradually increases during

reservoir drawdown. Zhu concluded that the drawdown of reservoir level lowers the stability and causes the movement at the toe of the Hefeng landslide.

Xia et al. (2013) conducted research about the Shiliushubao landslide movement under the influence of reservoir water level. The landslide consists of a deep-seated main block and two shallow blocks. According to Xia, the reservoir water level fluctuation is the major cause of movement of the main block and the movement accelerates during drawdown of the reservoir level. He also mentioned that the rise of reservoir water level causes seepage force pointing to the inside of the low-permeable landslide body which contribute to the landslide stability while the drawdown of reservoir water level causes outward seepage force which has adverse effect on the stability and movement of the landslide.

Ma et al. (2011) studied the stability of the Nongji Technical School landslide, which has a relatively low permeability, under the influence of the Three Gorges reservoir fluctuation. It is shown by Ma that that the landslide is mostly stable under the reservoir water level at 145 m. It becomes less stable under the reservoir level at 175 m and it is least stable during reservoir drawdown from 175 to 145 m. This indicates that the outward seepage force can have significant adverse effects on the stability of the low-permeable Nongji Technical School landslide.

Li et al. (2010) conducted research on the Baishuihe landslide, which is located 56 km west of the Three Gorges dam. Li noted that most part of the landslide is located below the reservoir water level and the rise of the water level increases the normal stress on the slope surface thus stabilizing the landslide.

There are also researchers who studied the impact of drawdown on landslide stability by conducting laboratory experiments. Three 1:400 scale landslide models were built by Hu et al. (2005) based on the Zhaoshuling landslide in Badong County, which belongs to the

Three Gorges reservoir area. His experiment was focused on the landslide stability under 145 m, 175 m and during the drawdown from 175 m to 145 m reservoir water level conditions. Seepage force was calculated and applied to the landslide model for the drawdown case. In Hu's research, it was found that the least stable landslide case was the one under a seepage force due to water level drawdown from 175 m to 145 m. A more stable model is associated with the water level at 145 m and the most stable model corresponds to the water level at 175 m.

In this research, mechanism 1 is proposed for the landslide which moves faster when reservoir level goes down. It is postulated in mechanism 1 that this type of landslide has low permeability. When the reservoir level rises, the larger hydrostatic pressure and inward seepage force stabilizes the slope. When reservoir level goes down, the outward seepage force and smaller hydrostatic pressure leads to smaller factor of safety and larger movement rate.

Landslides Affected by Reservoir Impoundment

There are also cases of landslides which are affected by the rise of water level in the Three Gorges reservoir. The Huangtupo landslide is a very large-scale landslide which is located in the Three Gorges reservoir area. It is concluded by Deng et al. (2000) that the middle and the toe of the Huangtupo landslide are the most vulnerable parts and they are directly affected by human activity and reservoir filling.

In the research of Luo et al. (2010), movement of the Shiliushubao landslide under the combined effect of the reservoir water level and rainfall was studied. Luo mentioned that the model showed movement of the landslide increased significantly during the impoundment when water level increased from 68 m to 175 m and there was little movement of the landslide during gradual reservoir drawdown from 175 m to 145 m.

The Majiagou landslide was reactivated by the Three Gorges reservoir impoundment in 2003. Li et al. (2009) conducted field permeability tests on the landslide and concluded that the main portion of the landslide mass has high permeability. In his research, the simulated groundwater table in the landslide mass rises and decreases synchronously with the reservoir water level. In addition, his research shows that the landslide stability decreases when the reservoir water level rises from 135 to 165 m.

The Qianjiangping landslide is located on the western bank of Qingganhe River in Shazhenxi Town, Hubei province, China. The landslide occurred on July 14th 2003, after completion of the first impoundment of the Three Gorges reservoir on June 15th 2003. Wang et al. (2004) quoted that "with the slope in a critical state, an increase in the river would decrease the effective normal stress in the toe of the slope, and the shear resistance would decrease at the same time." The reservoir impoundment was the trigger for the occurrence of the Qianjiangping landslide.

The Xietan landslide is located in Xietan Town, which belongs to the Three Gorges reservoir area. Zhang et al. (2009) conducted a model test of the landslide and studied the failure mode and the mechanism of the landslide. The piezometric tube in the landslide model showed that the groundwater table in the foreside of the landslide increased with the reservoir water level. Thus the landslide moved because of increased pore water pressure and correspondingly decreased effective normal stress along the slip zone during reservoir water level rising.

In this research, mechanism 2 is proposed for the landslide which moves faster when reservoir level goes up. It is postulated in mechanism 2 that this type of landslide has high permeability. When reservoir level rises, groundwater table follows closely with the reservoir water level and the increased pore water pressure causes lower effective normal stress along the slip surface. Thus the landslide is less stable and moves faster

when reservoir level goes up.Although a lot of research has been done on the impact of reservoir water level on landslide, little research has been done on the impact of cyclic reservoir water level on landslide movement. In this research, a rate dependent constitutive model was implemented in ABAQUS for both two mechanisms and landslide movement under the impact of cyclic reservoir water level was studied in detail.

2.3 Consideration of Ground Motion and Strain Rate Effect

In the above literature, most of research and analysis were conducted based on factor of safety and little has been done regarding to slope movement. According to Wedage (1995), "*the conventional approach to analyzing such large structures and natural slopes considers only limiting stability conditions, and no account is taken of the actual motions of the soil. The motions of natural slopes can be either slow-stable or accelerating. The slow-stable motions may be acceptable in many situations while accelerating motions may not. In both cases, limit analysis gives the same result".* Therefore, it is necessary to conduct not only limit analysis but also ground motion analysis for landslides.

In landslide risk management, government and regulatory bodies in China making decision to relocate inhabitants living on old landslides are often based on ground surface movement monitoring using GPS. Thus, it is not only important, but also necessary to analyze movement pattern of landslides. In this research, both factor of safety and slope motion have been analyzed for the postulated two mechanisms.

During movement of the landslide, the slip zone shears and strain-softening is usually implemented in the numerical model. According to Skempton (1964), part of the drop in strength from the peak to the residual is due to increasing water content during dilation; another important part is the formation of thin bands or domains in which clay particles reorient in the direction of shear.

Direct shear tests were conducted by Skempton (1964) and it was concluded that from peak to the residual, the cohesion intercept c' disappears completely. During the same process the angle of shearing resistance also decreases; in some clay by only 1° or 2°, but in others by as much as 10°.

In order to better model the observed step-like landslide movement, the impact of strain rate on the soil strength was considered in this research. According to Li et al. (2011), the implementation of viscous component in the dynamic analysis of the landslide can explain the velocity fluctuation of the landslide movement under the effect of reservoir water.

The influence of strain rate on undrained shear strength has been studied for 26 clays by former researches. According to Graham et al. (1983), lightly overconsolidated clays exhibit significant time-dependent stress-strain characteristics; regardless of soil type, undrained shear strengths and preconsolidation pressures change by about 10-20% for a tenfold change in strain rate.

Kulhawy and Mayne (1990) provided a summary of several former laboratory results and concluded that for triaxial compression tests, each log cycle increase in strain rate is accompanied by a 10 percent increase in s_u.

Ring shear test and direct shear test have been conducted on Clearwater clay-shale. The clay-shale, which had a Plasticity Index of 107%, a Liquid Limit of 135%, natural water content of 23% and clay content of 49% showed an improved residual shear resistance at higher rates. It was found that the residual strength was increased by 3.4-3.5%, for a tenfold increase in the strain rate. (Wedage, 1995)

Vaid et al. (1979) conducted isotropically consolidated undrained triaxial tests with heavily overconsolidated Saint-Jean-Vianney clay and found that both the

compressibility and the undrained shear strength of naturally cemented heavily overconsolidated clay were profoundly influenced by the time effects. The results demonstrate that there was a 25% increase in undrained strength with a 100 times increase in strain rate.

Triaxial compression tests were conducted by Richardson et al. (1963) with remolded normally consolidated specimens using two strain rates: 1% strain in 1 minute and 1% strain in 500 minutes. Test results showed that at low strain (0.5% strain), the deviator stress increased about 100%; at larger strain, the peak shear resistance increased about 10%.

Two horizontal investigation tunnels were excavated on the collapsed area of the Qianjiangping landslide. According to Wang et al. (2008), “the upper layer is a black silt layer with calcite blocks while the lower layer is yellow clay”. His research revealed that the two types of soil behaved differently under high shear velocity - the undrained shear strength of the black silt became lower at high shear velocity, whereas the s_u of the yellow clay became higher at higher shear velocity. Li et al. (2013) studied the residual strength of the slip zone soil for the Qianjiangping landslide and Xietan landslide in the Three Gorges area by conducting large drained ring shear tests. It is shown in his research that the residual strength of the Xietan and Qianjiangping landslide can be increased by 15 % to 40 % for tenfold increase in shear rate.

Miao et al. (2014) studied the strain rate dependency of slip zone soil of the Xiangshanlu landslide in the Three Gorges reservoir by conducting ring shear tests with different shearing rates. His research shows that the residual shear resistance doubled when the shear rate increased from 0.0011 mm/s to 175.56 mm/s, and the fitted curve of the shear rate and shear resistance presented a growth-oriented power function.

The above literatures on strain rate hardening for both landslides around the world and

in the Three Gorges reservoir serve as basis for the implementation of stain rate effect in the slope motion modeling in this research.

Chapter 3 Laboratory and Field Test Program

In this chapter, details of boreholes, sampling, and field permeability tests on Shuping and Baishuihe landslide are described. Field permeability test theory, procedure, equipment, and test results are described in detail. Laboratory experiments were also conducted for these two landslides. Laboratory test results of bulk density, moisture content, void ratio, Atterberg limits, specific gravity, as well as particle size distribution are summarized in this chapter.

3.1 Field Permeability Test Theory

In order to determine the permeability of the soil in the landslides, field permeability tests were carried out for Shuping and Baishuihe landslides. The tests were conducted based on ASTM standard D6391-11: Standard Test Method for Field Measurement of Hydraulic Conductivity Using Borehole Infiltration. The equipment used in the field test is shown in Figure 3.1.

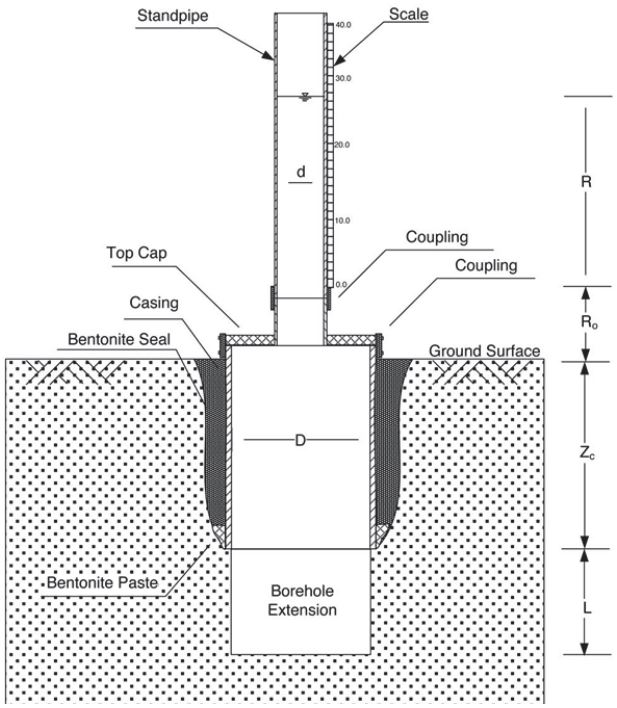

Figure 3.1: Field Permeability Test Equipment (ASTM: D6391-11)

Two methods are described in the ASTM standard. Method A is a falling head test and it is used for soils with anisotropic permeability. Method A has two stages. Stage 1 requires a minimum ground clearance by drilling a borehole, inserting casing and sealing the casing with bentonite before conducting the falling head test. Stage 2 consists of emptying the casing, advancing the borehole, reassembling the system and performing falling head test. Advancing the borehole within the casing requires a well-designed reamer.

For simplicity, Method B is chosen for this research. According to the ASTM standard, Method B is also a falling head test but it is used under the assumption that the soil is isotropic. Method B has only one stage, which is Stage 1 in Method A. The simplified model for Method B is shown in Figure 3.2. The field permeability is given by:

$$K_1 = R_T G_1 \frac{\ln\left(\frac{Z_1}{Z_2}\right)}{(t_2 - t_1)} \tag{3.1}$$

where

$$G_1 = \left(\frac{\pi d^2}{11 D_1}\right)\left[1 + a\left(\frac{D_1}{4 b_1}\right)\right] \tag{3.2}$$

$R_T = 2.2902\left(0.9842^T\right) / T^{0.1702}$ and T is temperature in ℃

$d = ID$ (Inside Diameter) of standpipe (cm)

$D_1 =$ effective diameter of Stage 1 (cm)

$a = 0$ for infinite (>20 D_1) depth of tested material

$b_1 =$ thickness of tested layer between bottom of casing and top of underlying stratum (cm).

$Z_1 = Z_c + R_0 + R$ at time t_1

$Z_2 = Z_c + R_0 + R - c$ at time t_2

$c =$ change in temperature effect gauge (TEG) scale reading between times t_1 and t_2. An increase in the height of water in the TEG standpipe is positive. In this research, $c = 0$.

$t_1 =$ time at beginning of increment(s), and

$t_2 =$ time at end of increment(s)

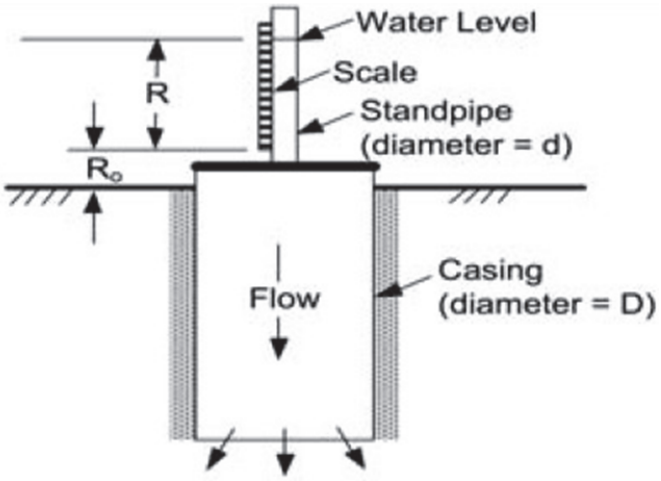

Figure 3.2: Simplified model for method B (ASTM: D6391-11)

3.2 Field Test Procedure

For Shuping landslide, six test holes were drilled and field permeability tests were conducted in the fluctuation zone of the reservoir water level. The water level fluctuates between elevation elevations 145 m and 175 m for flood control and power generation. Test holes were drilled by hand auger (diameter=170 mm) to 1.0 m - 1.5 m below ground surface. The depth of these test holes were controlled by the thickness of top soil and difficulty for workers to drill. Top soil could be identified since it was loose and had little cohesion while the underlying colluvium was blocky and more cohesive. In addition, color contrast and disappearance of grass roots could also serve as evidence of changing from top soil to the underlying colluvium.

After drilling the boreholes, thin-wall tubes (outside diameter=101.6 mm) were connected with a steel rod and were hammered into the soil for 15 cm. Thin-wall tubes were then pulled out of the test hole and the first 15 cm of soil were scooped out and discarded since this segment was strongly disturbed by the head of the hand auger during drilling.

The thin-wall tube was again hammered 30 cm to 50 cm into the soil in the test hole. Heavier hammer with fewer hits are preferred since light hammer and more hammering can lead to more soil disturbance. After hammering, the steel rod connected with the thin-wall tube was gently pushed back and forth to break the soil at the bottom of the thin-wall tube. Then, the steel rod was connected to a wrench and the thin-wall tube was pulled from the ground with the steel rod. Pulling of the thin-wall tube and the sampler are shown in Figure 3.3 and Figure 3.4.

Figure 3.3: Pulling of thin-wall tube

Figure 3.4: Setup of the sampler

The thin-wall tube was then disconnected from the steel rod and rubber plugs were used to seal the tube at both ends. The ends were then wrapped tightly with plastic wrap and with twist-tie bags. The purpose of using rubber plugs, plastic wrap and twist-tie bags was to minimize loss of moisture of the soil samples in the tubes. Thin wall tubes were then placed in steel boxes filled with foam before they were transported to

the laboratory. After obtaining the soil sample with the tube, the borehole segment where the sample was taken was enlarged to a larger diameter (170 mm) for field permeability testing. The larger diameter is for bentonite sealing around casing in later steps.

The casing of the field permeability test equipment was placed in the test hole and temporarily held in place by hand. The annulus was sealed by sodium bentonite placed in two layers. Hydrated bentonite was used for the lower layer and dry bentonite powder was used in the upper layer. The bentonite seal was allowed to hydrate for 12 hours before the standpipe was connected with casing and test was carried out. A schematic of the permeability test equipment is shown in Figure 3.5. The test equipment after completion of installation is shown in Figure 3.6.

The water used in the falling head field permeability test was taken from the Yangtze River. In reality, when reservoir water level rises, water from the Yangtze River flows into the landslide body from the landslide surface. Since chemicals and other particles in the water can influence the permeability test results, the most suitable water for the field permeability test is water taken from the Yangtze River. By using the water from the Yangtze River for the field permeability test, chemicals and other particles in water during the test and in reality are quite similar.

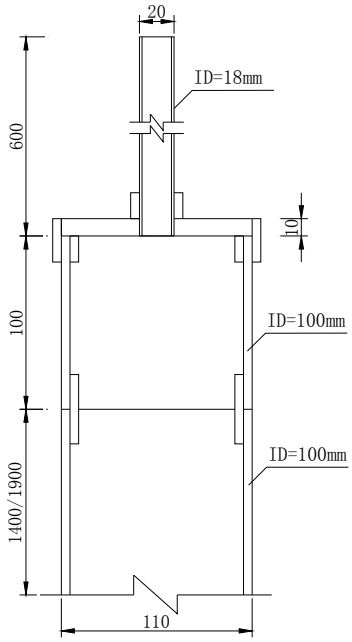

Figure 3.5: Simplified model for method B (Unit: mm)

Figure 3.6: Test equipment after installation

For the falling head test, the beginning time t_1 and the corresponding bottom of the meniscus of the water in the standpipe R_1 were recorded. The time t_2, when the bottom of the meniscus of the water in the standpipe drops to a certain reading R_2 was recorded as well. Temperature of the water for the test was measured during the falling head test. Knowing the dimension of the test equipment, the field permeability was calculated using equation (3.2).

3.3 Shuping Landslide Field Permeability Test Results

Field permeability tests for Shuping landslide were conducted in July 2013 when reservoir water was low (about 145 m). Six test holes were drilled manually with hand auger. The diameter of these test holes ranged from 180 mm to 200 mm and the depth ranged from 1.0 m to 1.5 m. Undisturbed soil samples were taken with tube samplers. The layout of the permeability test holes on the Shuping landslide is shown in Figure 3.7. The research is mainly focused on the impact of seepage through the water level fluctuation zone, thus test holes were all located within the water level fluctuation zone and approximately evenly distributed along the cross section selected for the modeling.

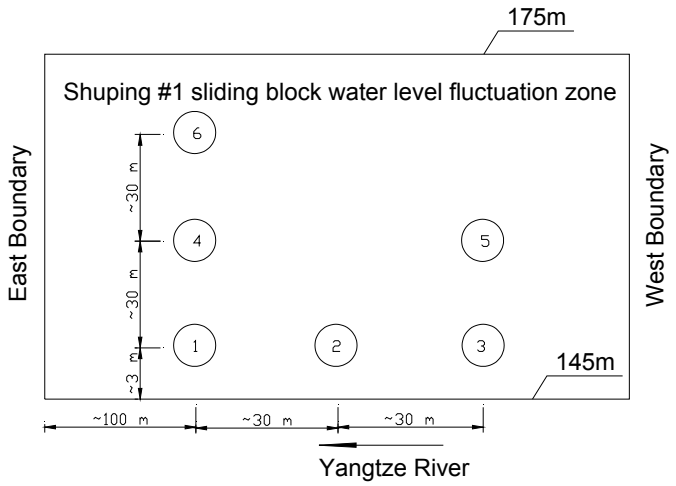

Figure 3.7: Schematic diagram of field permeability test holes on Shuping landslide

Field permeability test results of Shuping landslide are shown in Table 3.2.1. During the drilling of the test holes, more gravel were found in test hole #5 than in other holes. This explained higher permeability at test hole #5. Because test holes #2 and #3 were located very close to the reservoir water level, they were submerged under the fluctuating reservoir water before field permeability test could be conducted. Thus tests were not carried out at these two locations.

Table 3.2.1: Measured soil permeability of Shuping landslide

Test hole #	k (m/day)
1	2.23
4	5.04
5	13.82
6	3.33

Note: The field permeability tests were based on the assumption that the permeability of Shuping landslide is isotropic.

In Table 3.2.1, the field permeability test results show that the saturated permeability of the soil ranges between 2.2 m/day and 13.8 m/day.

3.4 Baishuihe Landslide Field Permeability Test Results

Field permeability tests were carried out at Baishuihe landslide in August 2013 when reservoir water remained low (about 145m). Three test holes were drilled manually with hand auger. The diameter of these test holes ranges from 180 mm to 200 mm and the depth ranges from 1.0 m to 1.5 m. Undisturbed soil samples were taken with tube samplers. The layout of the test holes is shown in Figure 3.8.

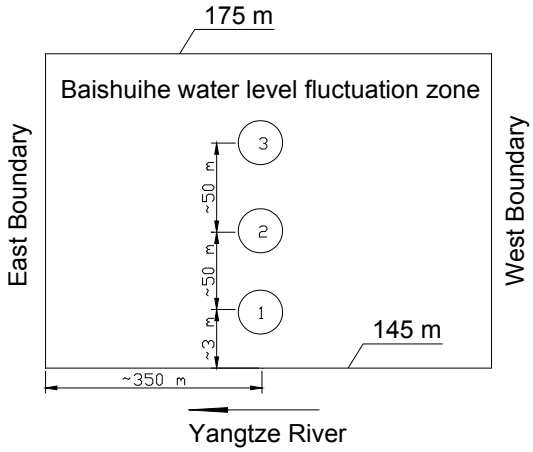

Figure 3.8: Layout of field permeability test holes at Baishuihe landslide

Field permeability test results of Baishuihe landslide are shown in Table 3.3.1. During drilling of the test holes, more gravel was found in Baishuihe landslide than in Shuping landslide. This explains that the soil has higher permeability in Baishuihe landslide than in Shuping landslide.

Table 3.3.1: Field permeability of Baishuihe landslide

Test hole #	k (m/day)
1	7.51
2	12.69
3	4.42

Note: Field permeability tests were based on the assumption that permeability of Baishuihe landslide is isotropic.

In Table 3.3.1, the field permeability test results show that the soil at Baishuihe landslide

has a saturated permeability ranging from 4.4 m/day to 12.7 m/day.

3.5 Laboratory Testing Procedures on Landslides Soils

For Shuping landslide, undisturbed soil samples were obtained from Test Holes #1, #4, #5 and #6. Laboratory experiments were conducted to obtain bulk density, moisture content and void ratio of undisturbed soil samples. Atterberg limits, specific gravity, and particle size distribution were obtained from laboratory experiments as well.

The undisturbed bulk density was taken by pushing the cutting ring into the undisturbed soil in the thin-wall tube. The weight and dimension of the soil sample in the cutting ring were measured and the undisturbed bulk density was calculated.

The specific gravity was obtained by conducting pycnometer test according to Specification of Soil Test SL-237-005-1999. The gradation of soil was taken by conducting sieve test and pipette test according to Specification of Soil Test SL-237-006-1999. Soil samples for the gradation test were taken based on the test specification. Pebbles were removed from soil before conducting the test. The tested soil amount is small compared to the non-uniform nature and the huge volume of the landslide mass. Thus, it should be kept in mind that the particle size distribution curve does not include the pebble content and there is some difference between the curve and true soil gradation. Atterberg limits were obtained by using liquid-plastic limits combined method according to Specification of Soil Test SL-237-007-1999.

For Baishuihe landslide, laboratory experiments were conducted to obtain bulk density, moisture content and void ratio of undisturbed soil samples. In addition, Atterberg limits and particle size distribution were obtained from laboratory experiments as well. Laboratory test methods for Baishuihe landslide were the same as those for Shuping landslide.

3.6 Test Results of Soils from Shuping Landslide

Bulk density, moisture content, void ratio and specific gravity are summarized in Table 3.5.1.

Table 3.5.1: Bulk density, moisture content, void ratio and specific gravity for Shuping

Test Hole #	Bulk Density (g/cm^3)	Moisture Content (%)	Void Ratio	Specific Gravity
1	2.1	20.86	0.52	2.642
3	2.01	21.88	0.62	2.656
4	2.04	20.62	0.56	2.685
6	1.99	18.18	0.57	2.648
Average	2.04	20.39	0.57	2.658

Atterberg limits are shown in Table 3.5.2. Atterberg limits for Shuping landslide are determined from Figure 3.9. The liquid limit is 39 % and the plastic limit is 17 %. The plasticity index for Shuping landslide soil is 22 %. The mass of Shuping landslide has low plasticity.

Table 3.5.2: Atterberg limits experiment results for Shuping landslide

Test #	Penetration (mm)	Ave. Penetration (mm)	Moisture Content (%)
1	8.95	8.80	29.29
	8.80		
	8.64		
2	4.53	4.74	23.64
	4.96		
	4.73		
3	16.68	16.83	38.15
	16.64		
	17.18		

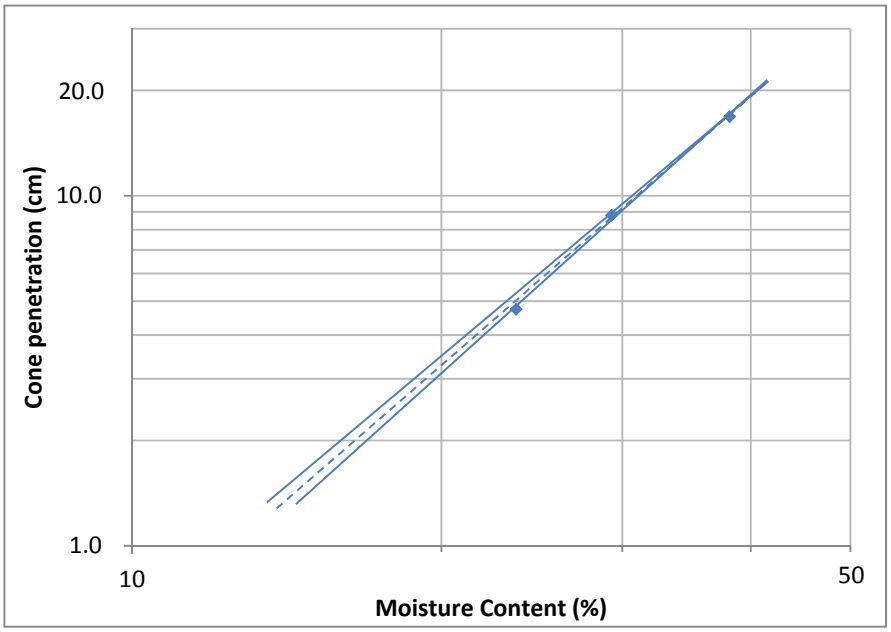

Figure 3.9: Atterberg limits of soils from Shuping landslide

Particle size distribution experiment result of Shuping landslide soil is shown in Figure 3.10. This figure shows that the soil sample is mainly composed of silt and clay, which can give rise to low permeability.

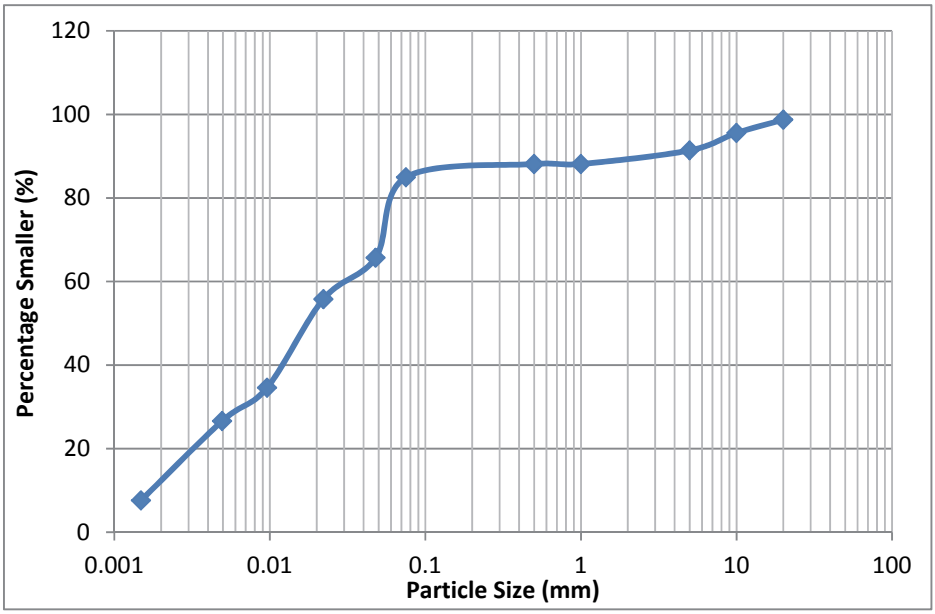

Figure 3.10: Particle size distribution for Shuping landslide mass

3.7 Test Results of Soils from Baishuihe Landslide

Bulk density, moisture content and void ratio are summarized in Table 3.6.1

Table 3.6.1: Bulk density, moisture content and void ratio for Baishuihe landslide

Bulk Density (g/cm^3)	Moisture Content (%)	Void Ratio
1.95	17.94	0.60

Atterberg limits are summarized in Table 3.6.2. Atterberg limits for Baishuihe landslide are determined from Figure 3.11. From this figure, the liquid limit is 29% and the plastic limit is 16%. Thus, the plasticity index is 13%. The mass of Baishuihe landslide has low plasticity.

Particle size distribution experiment result for Baishuihe landslide soil is presented in Figure 3.12. This figure shows that the Baishuihe landslide mass is mainly composed of silt and gravel. Thus its permeability is expected to be low but it can be higher than Shuping landslide.

Table 3.6.2: Atterberg limits experiment results for Baishuihe landslide

Test #	Penetration (mm)	Ave. Penetration (mm)	Moisture Content (%)
1	7.55	7.46	23.31
	7.42		
	7.41		
2	2.38	2.55	17.39
	2.62		
	2.65		
3	14.55	14.74	28.52
	14.58		
	15.08		

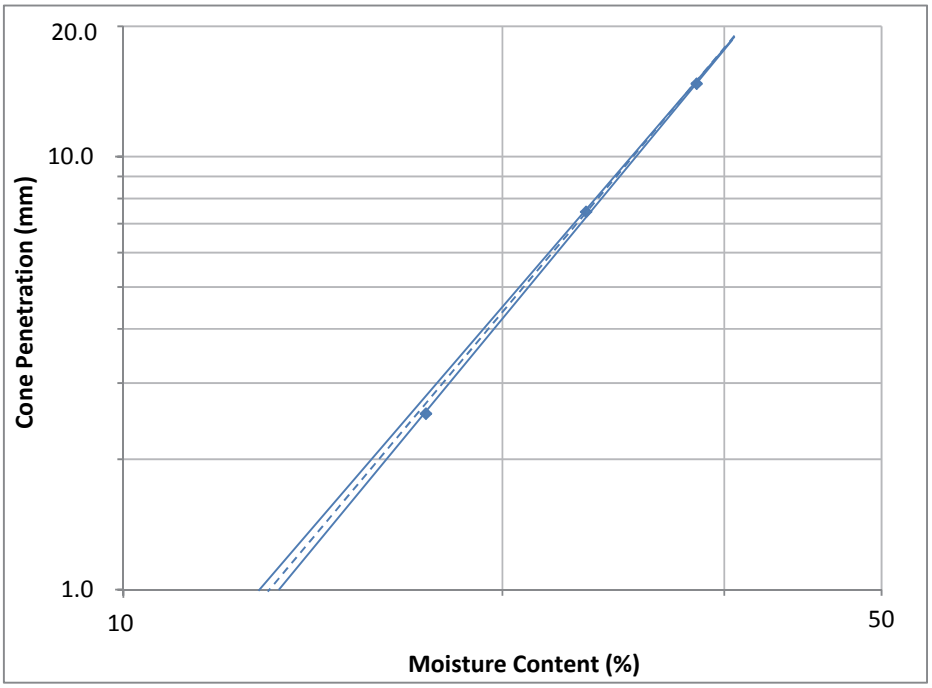

Figure 3.11: Atterberg limits of soils from Baishuihe landslide

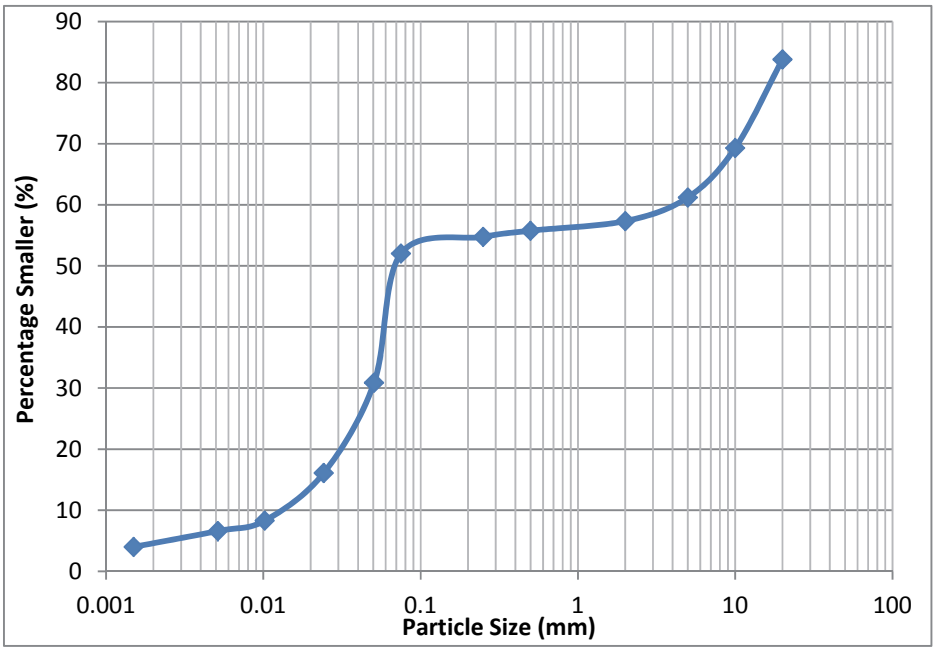

Figure 3.12: Particle size distribution of soils from Baishuihe landslide

Chapter 4 Mechanism of Landslide Movement

Landslides in the three gorges reservoir are generally classified into two types based on the movement pattern. One type of landslide moves faster during the reservoir drawdown; the other type of landslide moves faster when reservoir water level rises. Mechanisms and postulations for the two corresponding types of landslides are explained in this chapter.

The cross section of Shuping landslide was also selected and a finite element model was established based on the selected cross section. Drucker-Prager constitutive model and cyclic reservoir water level were implemented in the model. Modeling results verified permeability postulations for both mechanisms.

4.1 Introduction to Movement Mechanisms of Landslides around the Three Gorges Dam

Selected landslides around the Three Gorges dam reservoir have been monitored using global position system (GPS). GPS provide surface movement of landslides with time. Based on GPS observations, landslide movement due to reservoir level fluctuation can be classified into two main types. The first type is that the landslide moves at a faster rate when the reservoir water level is decreasing. Typical examples for this type of landslide are Shuping landslide and Baishuihe landslide. The second type is that the landslide moves at a faster rate when the reservoir water level is rising. A typical example for this type of landslide is Muyubao landslide.

To explain the response of landslide due to changes in water level of the reservoir, two mechanisms are proposed. For the first type of landslide which moves faster when the reservoir water level is decreasing, referred as Mechanism 1, the landslide soil has a low permeability. When the reservoir water level rises, the groundwater table in the landslide lags behind and the hydrostatic pressure at the toe of the landslide. The

increase in water pressure on the ground surface at the toe increases the stability of the landslide. When the reservoir water level goes down, changes in groundwater table also lags behind and causes an outward seepage force at the toe. In addition, the stabilizing hydrostatic pressure at the toe of the landslide decreases. Thus a combination of outward seepage force and decrease in resistant force at the toe lead to the accelerated movement of the landslide.

For the second type of landslide, which moves faster when the reservoir water level rises, referred as Mechanism 2 here, the landslide soil has a high permeability. When the reservoir water level rises, water can seep into the landslide quickly resulting in a rapid change in the groundwater table in response to the changes in the reservoir water level. The rising ground water level means higher pore water pressure along the submerged slip zone. Since effective stress is defined in ABAQUS as:

$$\boldsymbol{\sigma}' = \boldsymbol{\sigma} + \left(\chi u_w + \left(1 - \chi\right) u_a \right) \mathbf{I} \qquad (4.1)$$

Where

$\boldsymbol{\sigma}'$ is effective stress (negative for compression and positive for tension)

$\boldsymbol{\sigma}$ is total stress (negative for compression and positive for tension)

χ is equal to saturation of the medium

u_w is an average pressure stress in the wetting liquid, called the “wetting liquid pressure”

u_a is an average pressure stress in the other fluid

The increase in pore water pressure causes a decrease of effective normal stress in the shear zone which leads to a reduction in the shear resistance resulting in accelerated movement of the landslide. When the reservoir water level goes down, the groundwater table in the landslide is lowered with the reservoir water level. Pore water pressure in the shear zone decreases which leads to an increase in the effective normal stress and

shear strength. Thus, the landslide becomes more stable and the movement decelerates.

In order to study these two mechanisms of landslide movements, a computer model is developed using the commercial software ABAQUS. The Shuping landslide is chosen for studying the movement mechanisms. The analysis was carried out using ABAQUS/Standard software and the results are presented in the following sections.

4.2 Finite Element Modeling of Mechanism 1

Shuping landslide is located about 47 km upstream of the Three Gorges Dam. Using ABQAUS, a finite element model of the landslide is shown in Figure 4.1. The horizontal length of the model is 890 m with a vertical height of 430 m. The base of the model has an elevation of zero. More detail about the Shuping landslide is provided in Chapter 5. Here the finite element model of the Shuping landslide is used to explore the two mechanisms in explaining landslide movements due to fluctuation of reservoir water levels.

The landslide model is divided into different layers based on the geologic report from the China Three Gorges University (CTGU) (The Ministry of Education Key Laboratory of the Three Gorges Reservoir Geological Disasters, 2012). Layer 0 represents top soil. The landslide mass consists of Layers 1, 2, and 3. Layer 4 represents the slip zone. Layers 5, 6 and 7 represent different types of bedrock. The bedrock is inclined. Boundaries between Layer 5, 6, 7 in Figure 4.1 show general inclination directions of bedrock layers. Bedrocks are mainly bedded silty sandstone, mudstone and marlstone with intermediate layer thickness. The hard rock layer and soft rock layer are interbeded. Bedrock is generally intermediately weathered and susceptible to water softening. Dip angle for bed rock ranges between 10 to 35 degrees. (The Ministry of Education Key Laboratory of the Three Gorges Reservoir Geological Disasters, 2012)

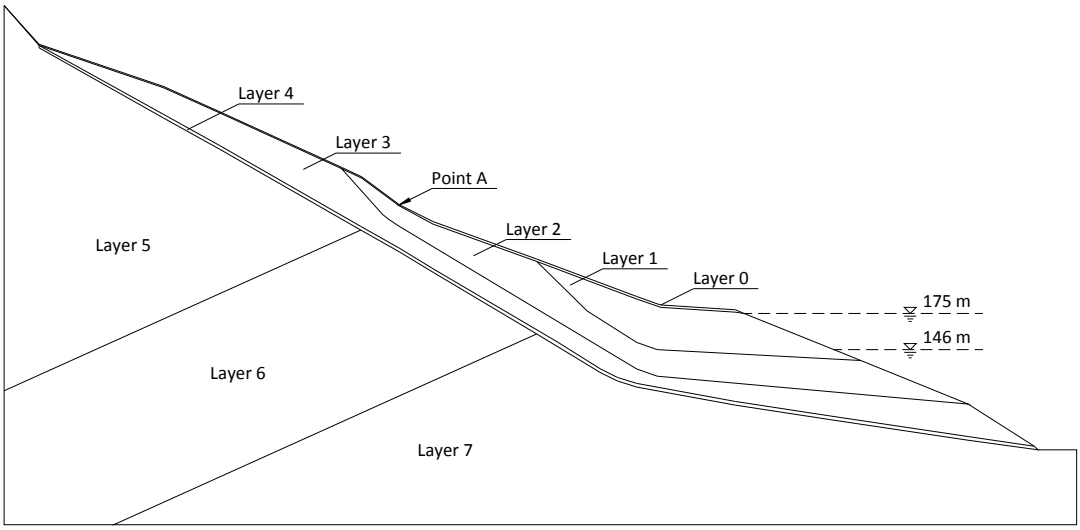

Figure 4.1: The configuration of ABAQUS model for Mechanism 1 and Mechanism 2

Mechanism 1 assumes that the landslide has relatively low permeability. The permeability of each region in the model is summarized in Table 4.2.1.

Table 4.2.1: Assumed permeability of each layer for Mechanism 1

Layer No.	K_H (m/day)	K_V (m/day)
0	2	2
1	0.1	0.01
2	2	0.2
3	0.1	0.01
4	0.1	0.1
5	0.5	0.5
6	1	1
7	0.5	0.5

GPS data show step-like movements of Shuping, Baishuihe and Muyubao landslide. Such cyclic movement patterns indicate changes of movement rate which lead to the change of mobilized strength parameters. If there is no viscous effect of the material, the landslide will be stable enough and will not move after the first cycle of reservoir water level fluctuation. It is because movement results in a more stable landslide configuration

than before. Therefore, a strain rate dependent viscous constitutive model is needed to study cyclic landslide movement. Since ABAQUS/CAE (version 6.12) does not provide options of strain-rate hardening/softening for Mohr-Coulomb constitutive model, a strain rate dependent Drucker-Prager plasticity constitutive model is implemented into ABAQUS to model the deformation of the landslide mass and slip zone. Linear elasticity is assumed for the bedrock.

The Linear Drucker-Prager failure criterion is chosen in the ABAQUS software and it is written as:

$$F = t - p\tan\beta - d = 0 \tag{4.2}$$

where

$$t = \frac{1}{2}q\left[1 + \frac{1}{K} - \left(1 - \frac{1}{K}\right)\left(\frac{r}{q}\right)^3\right]$$

$$p = -\frac{1}{3}trace(\boldsymbol{\sigma})$$

$$q = \sqrt{\frac{3}{2}(\boldsymbol{S} : \boldsymbol{S})}$$

$$r = \left(\frac{9}{2}\boldsymbol{S}\cdot\boldsymbol{S} : \boldsymbol{S}\right)^{\frac{1}{3}}$$

$\beta(\theta, f_i)$ is the slope of the linear yield surface in the p-t stress plane;

d is the cohesion of the material. In this study, the cohesion d is defined by the uniaxial compression yield stress σ_c, thus $d = \left(1 - \frac{1}{3}\tan\beta\right)\sigma_c$;

$K(\theta, f_i)$ is the ratio of the yield stress in the triaxial tension to the yield stress in the

triaxial compression;

$\boldsymbol{S}$ is the stress deviator, defined as $\boldsymbol{S} = \boldsymbol{\sigma} + \boldsymbol{pI}$.

The plastic potential G for this model is defined as:

$$G = t - p\tan\psi \tag{4.3}$$

where

ψ is the dilation angle.

The evolution of the yield surface with plastic deformation is described in terms of the equivalent stress $\overline{\sigma}$. The strain rate hardening, which is independent of plastic strain in this study, is written as

$$\overline{\sigma} = \sigma_0 R$$

(4.4)

where

σ_0 is the static stress-strain behavior;

R is the ratio of the yield stress at nonzero strain rate to the static yield stress.

Based on the landslide report from CTGU (The Ministry of Education Key Laboratory of the Three Gorges Reservoir Geological Disasters, 2012) and laboratory test results, the elastic modulus, Poisson's ratio, density, and strength parameters are summarized in Table 4.2.2. The selected strain rate hardening parameter R is based on the research of Graham et al. (1983) and presented in Table 4.2.3.

Table 4.2.2: Elastic and plastic parameters

	Dry Density (kg/m^3)	E (MPa)	Poisson's Ratio	Friction Angle β(∘)	Flow Stress Ratio	Dilation Angle ψ(∘)	Uniaxial Compression Stress(kPa)
Landslide Mass	1630	20.8	0.21	34.4	1	10	54.0
Slip Zone	1630	20.8	0.21	30.0	1	10	47.0
Bedrock	2000	61000	0.28	-	-	-	-

Table 4.2.3: Strain rate hardening parameter R

Yield Stress Ratio	1.0	1.1	1.21	1.331	1.4641	1.61051
Equivalent Plastic Strain Rate (s^{-1})	0	1.16E-09	1.16E-08	1.16E-07	1.16E-06	1.16E-05

November 1, 2009 is chosen as the beginning time (0 day) for the finite element model. In this model, the first step is to perform a steady-state geostatic analysis. The boundary condition for the reservoir water level at the toe of the landslide is set at 171.0 m. The left and right boundaries of the landslide are fixed horizontally. The bottom of the landslide is fixed in both horizontal and vertical directions.

Transient analyses are carried out in subsequent steps. Reservoir water level at the toe of the landslide decreases, stays at the lowest level and then increases. The reservoir water level stays at the highest level for several steps and then enters into a new cycle of reservoir water level fluctuation. The elevations for the reservoir water level are based on the observed water level at the Three Gorges reservoir. Slight modifications such as smoothing short-term sharp changes or back-and-forth changes of reservoir water level have been made to the original recorded reservoir water level for better convergence of the numerical model. Detail of the reservoir water level implemented in the finite element model is shown in Figure 4.2.

In the finite element model as shown in Figure 4.1, point A is located on the ground

surface in the top soil layer. The relationship between horizontal movement and time at point A from the finite element modeling is plotted in Figure 4.2. It can be seen from this figure that the calculated horizontal landslide movement at Point A accelerates when the reservoir water level decreases. When the reservoir water level remains low, the horizontal movement decelerates; and when reservoir water level rises and stays high, there is small horizontal movement towards the river channel.

Typical groundwater table in the model at the toe of the landslide when the reservoir water level reaches the peak level and the lowest level are shown in Figures 4.3 and 4.4 respectively. The groundwater table is indicated by the boundary between the dark and the light colored areas. The dark area represents submerged soils.

In Figure 4.3, when the reservoir water level rises, the groundwater table in the landslide lags behind the reservoir water level. In this figure, the groundwater table is much lower than the reservoir water level which means the pore water pressure along the slip zone does not increase much during the rise of the reservoir level. The rising hydrostatic water pressure at the ground surface acts as an increasing stabilizing force at the toe of the landslide.

In Figure 4.4, when the reservoir water level is decreasing, the changes in groundwater table in the landslide lags behind the reservoir water level. Some water near the ground surface seeps out of the landslide quickly; however, most groundwater lags behind and creates a relatively large hydraulic gradient between the slip zone and the ground surface. This hydraulic gradient causes seepage force which acts on the landslide body towards the river channel. In addition, the drawdown of the reservoir water level leads to lower hydrostatic pressure on the ground surface, which means smaller stabilizing force at the toe.

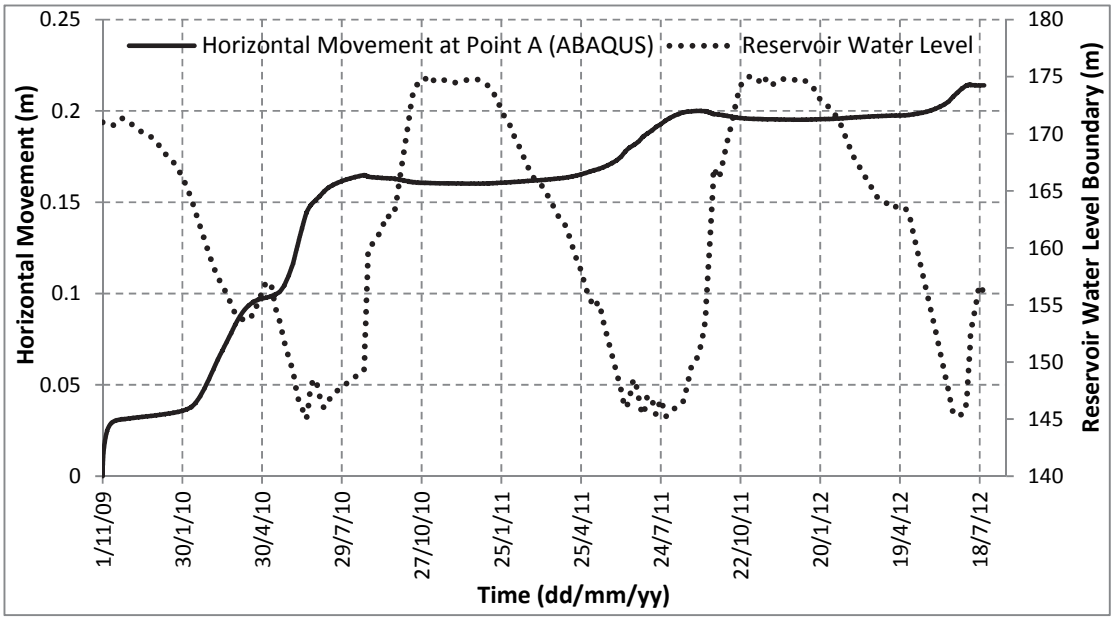

Figure 4.2: Horizontal movement at point A and reservoir water level (Mechanism 1)

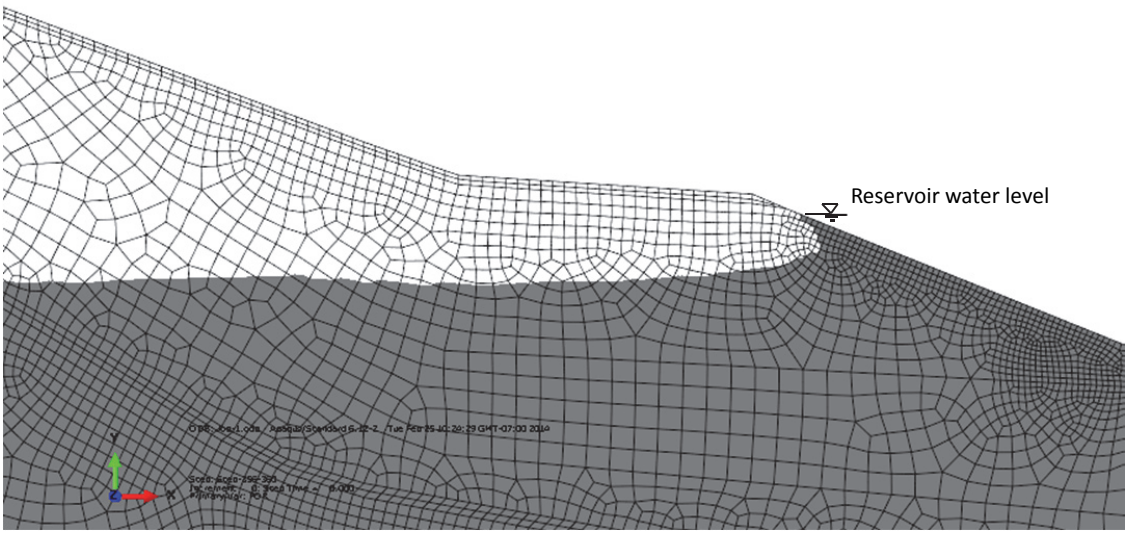

Figure 4.3: Groundwater table when reservoir reaches the peak level (Mechanism 1)

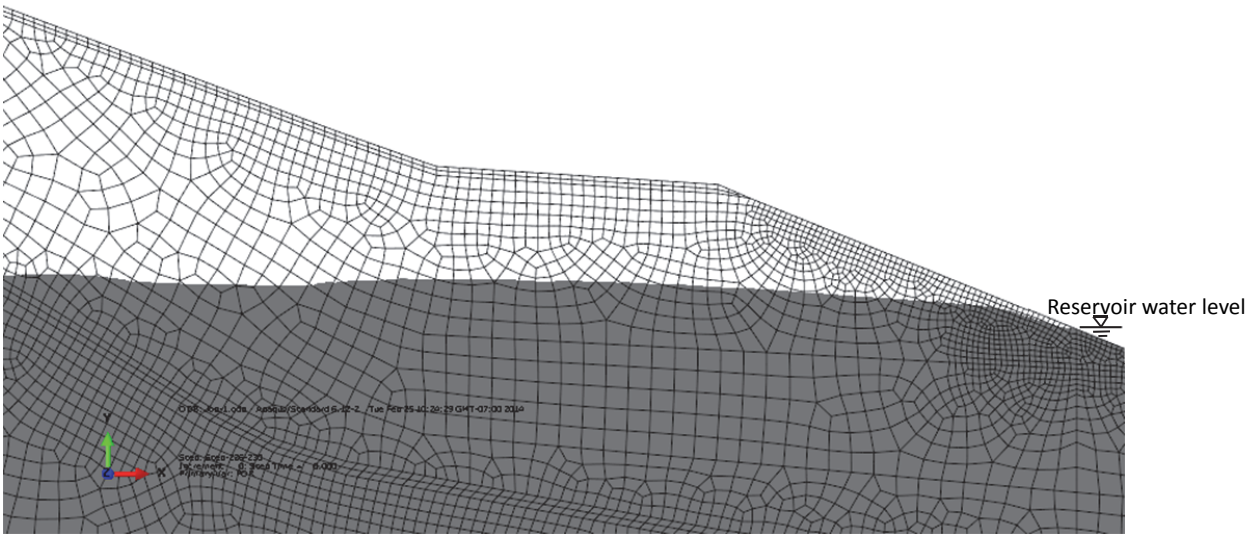

Figure 4.4: Groundwater table when reservoir reaches the lowest level (Mechanism 1)

The calculated landslide movement and groundwater table in Figure 4.2 to Figure 4.4 verify the assumption of Mechanism 1. For a landslide with low permeability, the groundwater table lags behind during both reservoir rising and decreasing. Rising reservoir water level creates larger stabilizing force at the toe, making the landslide more stable and leads to slower landslide movement. Decreasing reservoir water level leads to smaller stabilizing force and higher outward seepage force at the toe, making the landslide less stable with faster landslide movement.

4.3 Finite Element Modeling of Mechanism 2

Mechanism 2 assumes that the landslide which moves faster when the reservoir water level rises has relatively higher permeability.

ABAQUS software is used to analyze landslide movement with high permeability. The schematic of the finite element model used to study Mechanism 2 is the same as that for Mechanism 1 and it is shown in Figure 4.1.

The permeability for all soil layers in the finite element model for Mechanism 2 is

assumed to be isotropic and it is equal to 0.01 m/s, which is 864.0 m/day.

Strain-rate dependent Drucker-Prager plasticity is implemented for the landslide mass and slip zone regions of the finite element model. Linear elastic model is used for the bedrock. To compare the results with Mechanism 1, same material properties such as elastic modulus, Poisson's ratio, density, strength parameters and strain rate hardening parameter R are used in studying Mechanism 2. These parameters are summarized in Tables 4.2.2 and 4.2.3.

September 7, 2009 is chosen as the beginning time (0 day) in the finite element model for Mechanism 2. In this model, the first step is to perform a steady-state geostatic analysis. The reservoir water level at the toe of the landslide is set at 146.0 m. Left and right boundaries of the landslide are horizontally fixed. The bottom of the landslide is fixed both in the horizontal and vertical directions.

Transient analyses are carried out in subsequent steps. Reservoir water level at the toe of the landslide increases, stays at the highest level and then decreases. The reservoir water stays at the lowest level for several steps and then enters into a new cycle of reservoir water level fluctuation. Elevations for the reservoir water level are based on the observed water level at the Three Gorges Dam. Detail of reservoir water level implemented in the finite element model is shown in Figure 4.5.

The relationship between horizontal movement and time at point A from the finite element calculation is shown in Figure 4.5. Typical locations of the groundwater table at the toe of the landslide when the reservoir water reaches the peak level and the lowest level are shown in Figures 4.6 and 4.7 respectively.

It can be seen from Figure 4.5 that the calculated horizontal landslide movement at Point A accelerates when the reservoir water level rises. During the time when the

reservoir water level is decreasing and stays at the lowest level, movement of the landslide towards the river channel decelerates.

In Figure 4.6, when the reservoir water level rises, the groundwater table in the landslide follows the reservoir water level closely and there is almost no time lags between the reservoir level and the ground water table. Rising groundwater table in the landslide causes higher pore water pressure and lower effective normal stress along the submerged slip surface. This leads to lower shearing resistance along the slip surface.

In Figure 4.7, when the reservoir water level is decreasing, the groundwater table in the landslide follows the reservoir water level closely and there is also no time lag. Decreasing groundwater table in the landslide means lower pore water pressure and higher effective normal stress along the slip surface. This increase in effective normal stress causes higher shear strength along the slip surface.

The landslide movement pattern and groundwater table in Figures 4.5 to 4.7 verify the assumption of Mechanism 2. For a landslide which has high permeability, there is almost no time lag of the groundwater table during both reservoir rising and decreasing. The groundwater table follows rising reservoir water level which causes higher pore water pressure, lower shear strength and faster horizontal movement. When the reservoir water level is decreasing, the pore water pressure along the slip zone decreases correspondingly, the shear strength increases and the horizontal landslide movement decelerates.

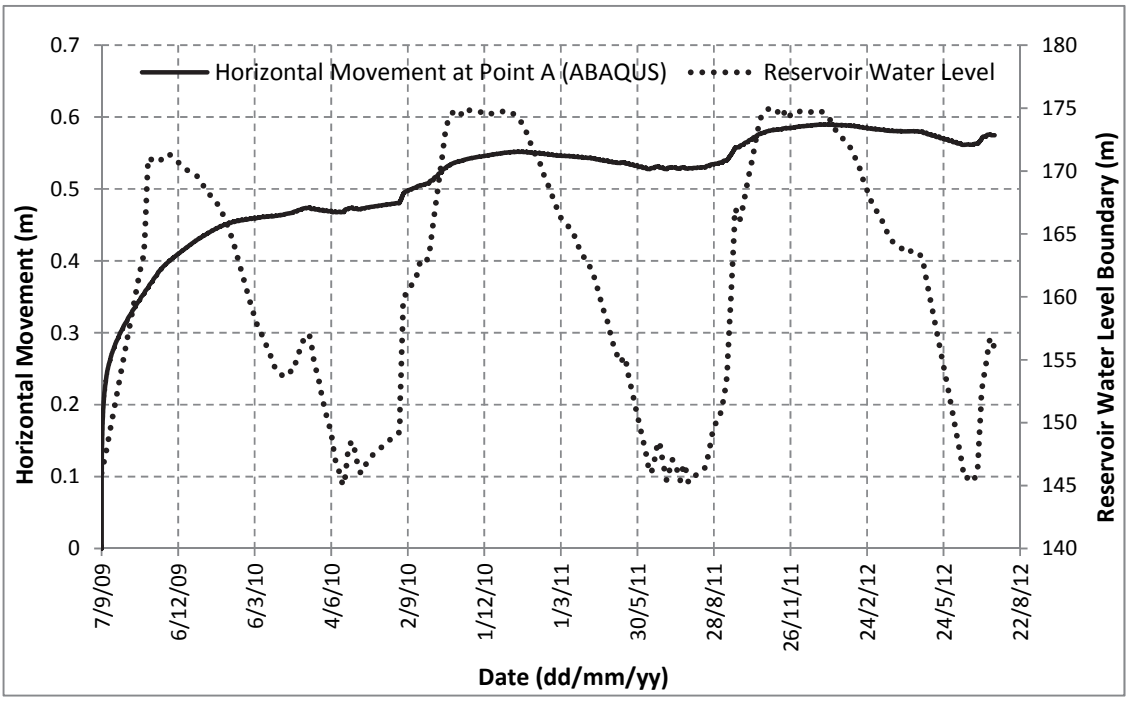

Figure 4.5: Horizontal movement at point A and reservoir water level (Mechanism 2)

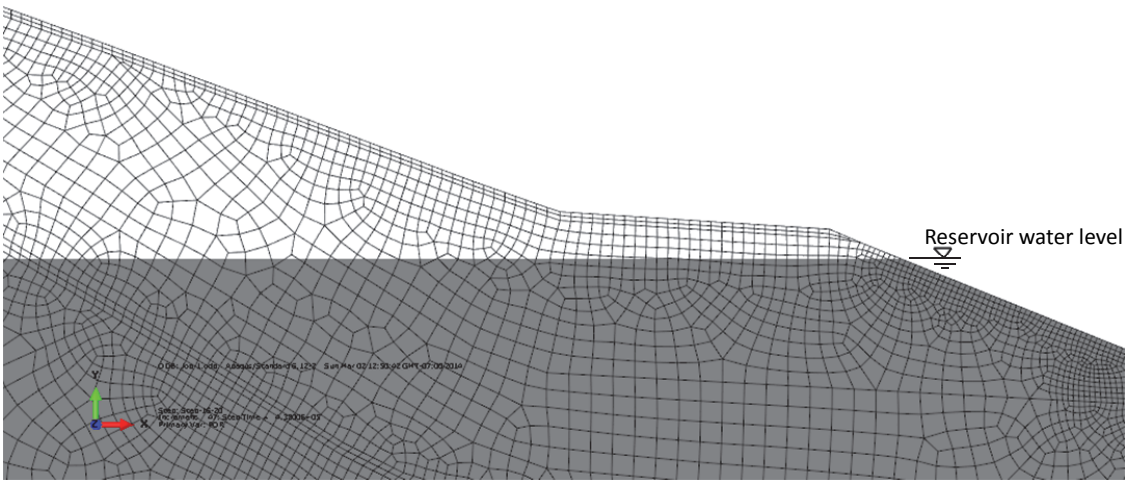

Figure 4.6: Groundwater table when reservoir reaches the peak level (Mechanism 2)

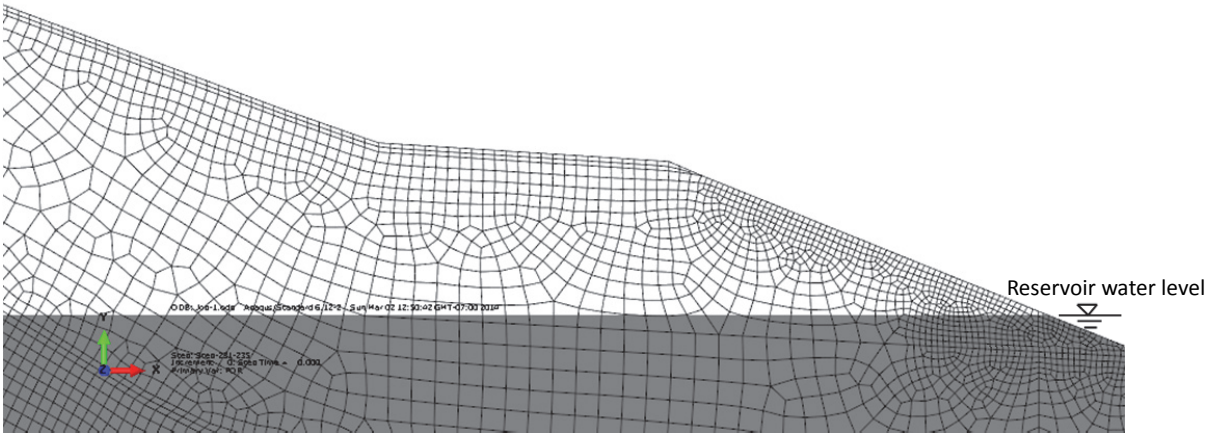

Figure 4.7: Groundwater table when reservoir reaches the lowest level (Mechanism 2)

Chapter 5 Case Study 1-Shuping Landslide-Based on Mechanism 1

An introduction (including plan view, cross section, geology, and observation instrumentations) to the Shuping landslide is given in the first part of this chapter. Then the observed landslide movement, groundwater table and reservoir water level are illustrated and discussed. Based on the observation results, a seepage model was established with SEEP/W and permeability of the landslide was back calculated. Stability analysis was conducted to study factor of safety change with fluctuating reservoir water level and to obtain back calculated strength parameters for the slip zone material. Then coupled fluid/stress analysis is described and modeling results show Shuping landslide belongs to Mechanism 1.

5.1 Introduction to Shuping Landslide

Shuping landslide is an old landslide which once slipped before. This landslide is located in the Three Gorges reservoir area in Zigui county, Hubei province, China. The landslide is located on the southern bank of the Yangtze River and it is about 47 km upstream from the Three Gorges Dam.

The landslide mass is quaternary colluvium (Q^{del}), which consists of silty clay, fine to coarse gravels and cobbles. The gravels and cobbles are mainly weathered angular sandstone, mudstone and marlstone, with diameters ranging from 1 cm to 110 cm. Within a relatively shallow depth from the ground surface, the mass ratio of silty clay to gravels is about 9:1. At deeper depths, the mass ratio of silty clay to gravels and cobbles varies significantly from place to place ranging from 8:2 to 3:7. Therefore there is significant more gravels and cobbles in the deeper landslide body. (The Ministry of Education Key Laboratory of the Three Gorges Reservoir Geological Disasters, 2012)

The slip zone lies at the boundary between colluvium and bedrock. The soil in the slip zone is mainly composed of silty clay and subangular to subrounded gravel whose

diameter ranges from 0.2 to 2.0 cm. The mass ratio of silty clay to gravels lies between 8:2 and 7:3 for the soil in the slip zone.

The bedrock of Shuping landslide belongs to the Middle Triassic Period T_2b. The bedrock is composed of tilted interbeded silty sandstone, mudstone and marlstone. The bedrock is moderately weathered and susceptible to water softening. The dip direction of the interbeded bedrock is opposite the slip direction of the landslide. (The Ministry Of Education Key Laboratory of the Three Gorges Reservoir Geological Disasters, 2012)

The north-south length of the landslide is about 800 m and the east-west width is around 700 m. The landslide is moving north towards the Yangtze River. The slip zone is exposed at the toe of the landslide at an elevation of 60 m and the elevation of the back scarp lies between 380 and 400 m. The depth of the slip zone lies between 30 and 70 m. Thus, the average depth for the slip zone is about 50 m and the estimated total volume of the landslide is 27.5 million m^3.

GPS monitoring of the landslide movement started from June 2003 and landslide movement data are available from July 10, 2003 to July 25, 2012. Thirteen GPS monitoring stations have been installed on the ground surface of Shuping landslide. Among these GPS monitoring stations, eight of them work well and consistently collect landslide movement data. These eight GPS monitoring stations are: ZG 85, ZG 86, ZG 87, ZG 88, ZG 89, ZG 90, SP 2 and SP 6.

Plan view of Shuping landslide and locations of GPS monitoring stations are presented in Figure 5.1.

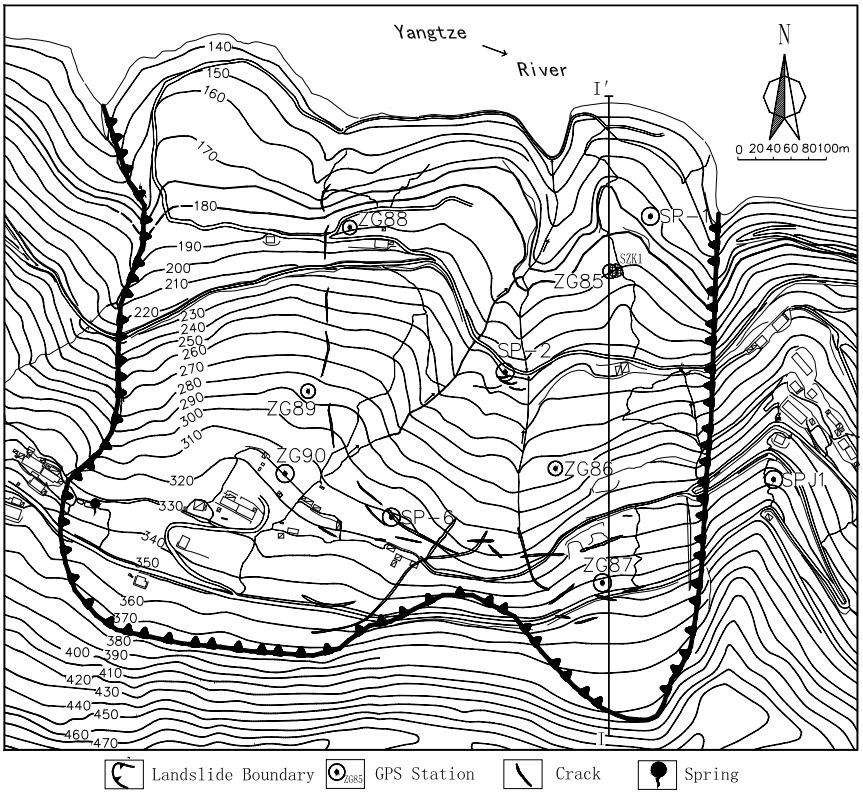

Figure 5.1: Plan view of Shuping landslide and locations of GPS monitoring stations

A groundwater monitoring station SZK-1 is located near ZG 85 at an elevation of 183 m. Three GPS monitoring stations (ZG 85, ZG 86, and ZG 87) are relatively close to line I-I' in Figure 5.1. In addition, according to GPS monitoring data, landslide movement along line I-I' is larger than that in other regions. Thus, Section I-I' has been chosen for 2D landslide modeling. A cross sectional profile of Section I-I' is shown in Figure 5.2. The reason not conducting 3D analysis for Shuping landslide is that landslide is wide and not arc shaped. In addition, based on the current limited data, more assumptions are needed for conducting 3D modeling of Shuping landslide. Thus, 2D seepage, stability and movement analysis are conducted in this research.

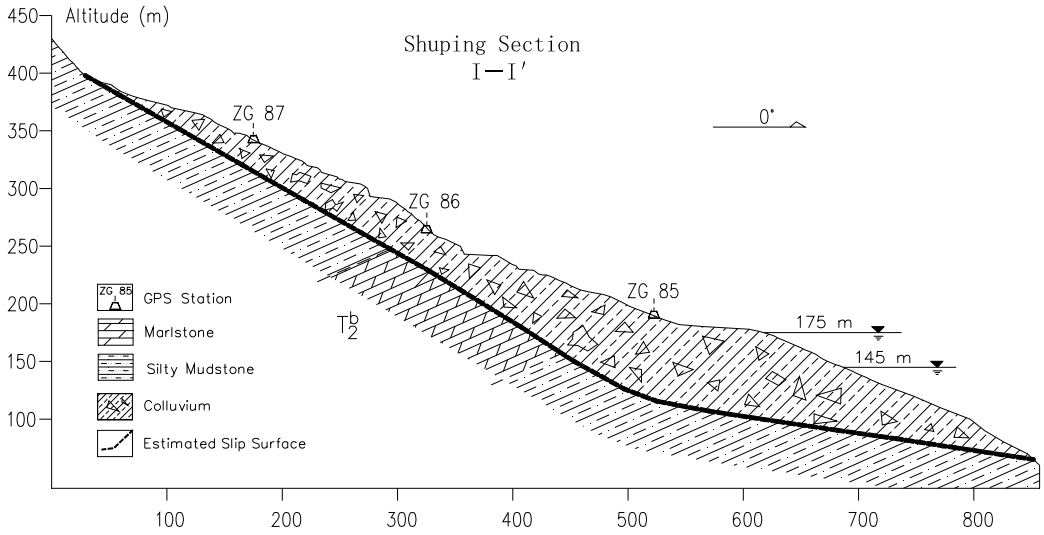

Figure 5.2: Section I-I' of Shuping landslide

In Figure 5.2, the thick line is the observed slip zone drawn based on borehole information. According to Shuping landslide report (The Ministry of Education Key Laboratory of the Three Gorges Reservoir Geological Disasters, 2012) from CTGU, the thickness of the slip zone ranges between 1.0 m and 1.2 m.

5.2 Reservoir Water Level and Shuping Landslide Movement

Before the construction of the Three Gorges dam, the water level of the Yangtze River at the Shuping landslide was about 74 m. Since the year 1996, observations of the landslide showed that the landslide was undergoing localized movement. Movement of the landslide had caused excessive deformation of 15 houses and 60 local residents had to move away from the landslide.

The Three Gorges dam started its first impoundment in May 2003. The reservoir water level at the dam was raised to 135 m in early June 2003. Several GPS monitoring stations were installed on the landslide on June 10, 2013. Reservoir water level and horizontal GPS movement along the Section I-I' are plotted in Figure 5.3. Between June 2003 and August 2006, the reservoir water level fluctuated yearly between elevation 135 m and

140 m. During this period of time, GPS at ZG 85, ZG 86 and ZG 87 was moving at an almost constant rate. Figure 5.3 shows that the landslide moved faster in the middle and slower at the toe. The top of landslide moved the slowest. The average movement rate at ZG 86 was about 0.60 mm/day. The accumulated deformation at ZG 86 during this period of time was about 0.69 m.

During October 2006, the reservoir water level at the Three Gorges dam was raised to 155 m. During October 2006 to September 2008, the reservoir water level fluctuated yearly between elevation 145 m and 155 m. Accelerating horizontal movement of the landslide was observed when the reservoir water level decreased from 155 m to 145 m. The horizontal movement of the landslide slowed down when the reservoir water level stayed low at 145 m and when the reservoir water level rose from 145 m to 155 m. From October 2006 to September 2008, the largest horizontal movement rate, which was 3.7 mm/day at GPS ZG 86, was observed between April 19, 2007 and July 24, 2007. The accumulated horizontal movement at ZG 86 between April and July in 2007 was about 0.35 m. Because of the accelerating movement process, the accumulated horizontal movement at ZG 86 during October 2006 to September 2008 was about 1.03 m.

The reservoir water level at the Three Gorges dam was raised to around 175 m at the end of September 2008. Since then, the reservoir water level fluctuated yearly between elevation 175 m and 145 m. Accelerating horizontal movement of the landslide was observed when the reservoir water level dropped from 175 m to 145 m. Movement slowed down when the reservoir water level stayed low at 145 m and when reservoir rose from 145 m to 175 m. The highest horizontal movement rate 17.4 mm/day was observed at ZG 86 between May 12, 2009 and June 13, 2009. The accumulated horizontal movement at ZG 86 during September 25, 2008 to September 20, 2009 was about 0.80 m. Because of the yearly cyclic accelerating process, the average horizontal movement at ZG 86 between September 2008 and July 2012 was about 0.64 m/year.

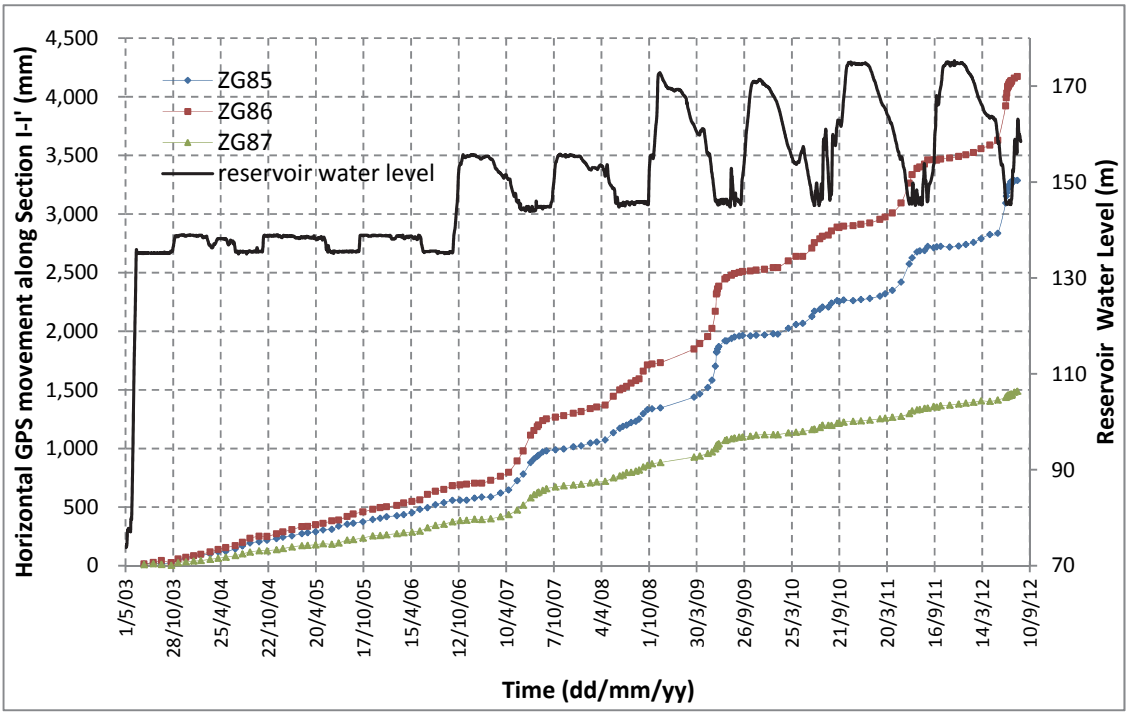

Figure 5.3: Horizontal GPS movement along the Section I-I' of Shuping

5.3 Monitored Ground Water Level of Shuping Landslide

In this research, groundwater information collected in borehole SZK-1 is used. This borehole and its groundwater recording station are located near GPS ZG 85 at a ground surface elevation of 183 m. Groundwater data from other boreholes are not used in this research since the data are not consistent and they have not been collected for long enough time span. The observed groundwater level at SZK-1 and the reservoir water level are plotted in Figure 5.4.

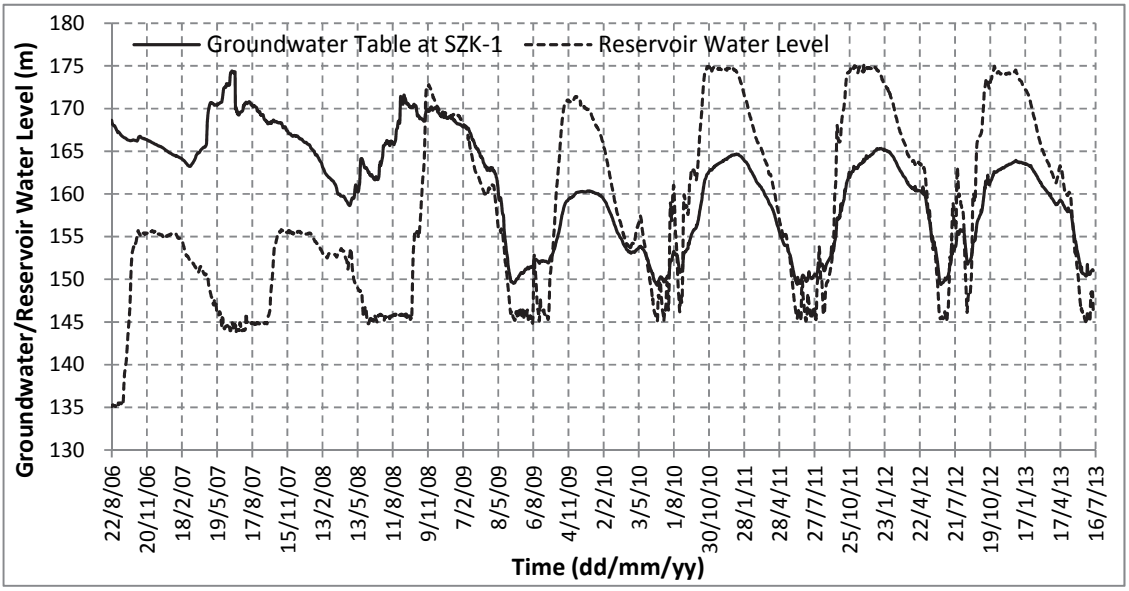

Figure 5.4: Shuping groundwater level at SZK-1 and reservoir water level

In Figure 5.4, the groundwater table during August 2006 to June 2009 is higher than that measured in subsequent years. A likely reason for this is that the slip zone has relatively low permeability and the groundwater in the bedrock is under pressure. From August 2006 to June 2009, the piezometer measured the pressure head in the bedrock, and because of large shear movement along the slip zone, the piezometer broke at the slip surface and the measured groundwater table turned to the groundwater table in the landslide mass.

In Figure 5.4, regular groundwater level fluctuation was recorded from June 2009 to June 2013. In Figure 5.3, the GPS data is only available until July 25, 2012. Thus, June 9th, 2009 and July 23th, 2012 are chosen as the starting day and the last day for the subsequent seepage and stability analysis respectively. The total length of time in the seepage and stability analysis is 1,140 days.

5.4 Seepage Analysis of Shuping Landslide

Seepage analysis was carried out using SEEP/W (GEO-SLOPE International, Ltd., 2008).

Section I-I’ in Figure 5.2 is adopted for the seepage analysis model. Slight modifications have been made to the original Section I-I’ for smoother ground surface and better mesh quality. The seepage model for Shuping landslide is shown in Figure 5.5 and Figure 5.6 with different boundary conditions.

In Figure 5.5 and Figure 5.6, there is one layer of top soil above elevation 175 m. Below 175 m, no top soil is assumed to exist because of annual flooding and washing by the Yangtze River. Based on the geological report from CTGU (Yi et al., 2012), the top soil was found to be 2 m thick between 175 m and GPS ZG 86, and 1 m thick between GPS ZG 86 and the top of the landslide. The landslide body and the bedrock are subdivided into smaller regions according to the geological report from CTGU so that each region represents soil with similar properties. It should be noted that borehole logs are only available at GPS ZG 85 and GPS ZG 86. Thus the boundaries between regions are estimated.

In Figure 5.4.1, the landslide mass is composed of Regions R.1, R.2 and R.3. Region R.1 represents colluvium which is composed of silty clay and fine to coarse gravels. The mass ratio of silty clay to gravels is about 9:1. Region R.2 represents colluvium which composes of silty clay, coarse gravels and cobbles. The mass ratio of silty clay to gravels and cobbles ranges from 7:3 to 3:7. Region R.3 represents colluvium which composes of clay, coarse gravels and cobbles. The mass ratio of clay to gravels and cobbles ranges from 8:2 to 4:6. There is only one region R.4 for the slip zone. Bedrock is composed of three regions, R.5, R.6 and R.7. Among them, R.5 and R.7 represent silty mudstone. R.6 represents marlstone.

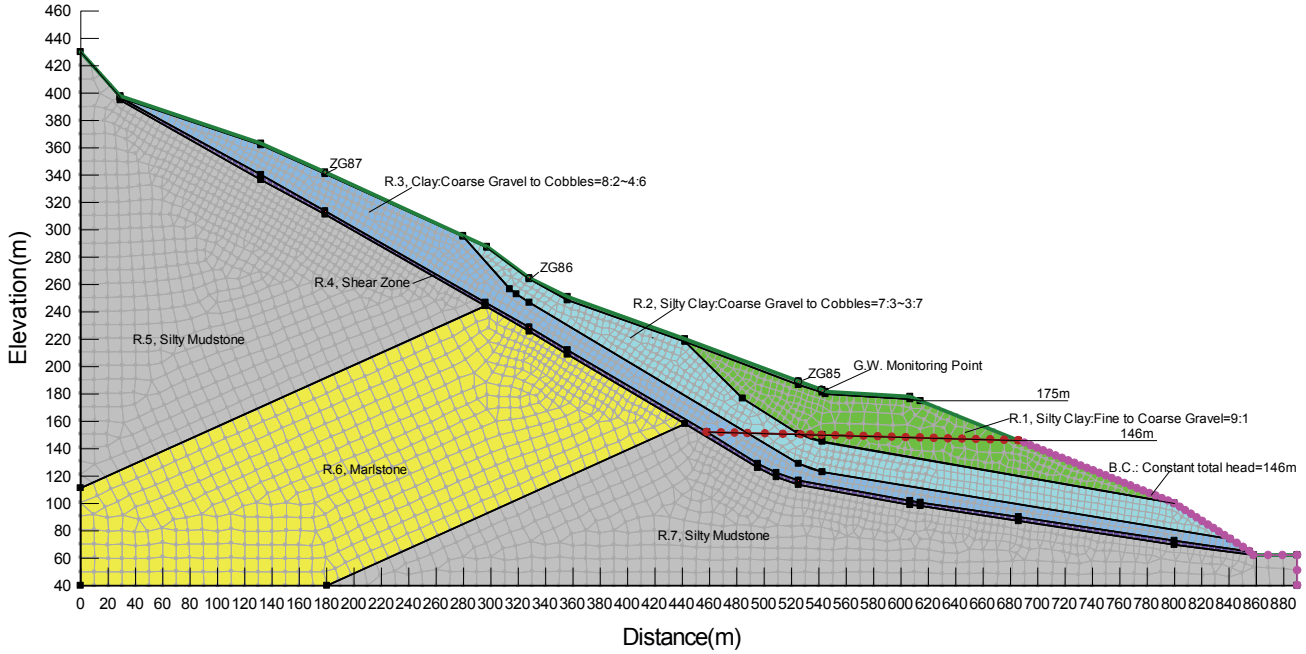

Figure 5.5: Boundary conditions for steady-state seepage analysis of Shuping

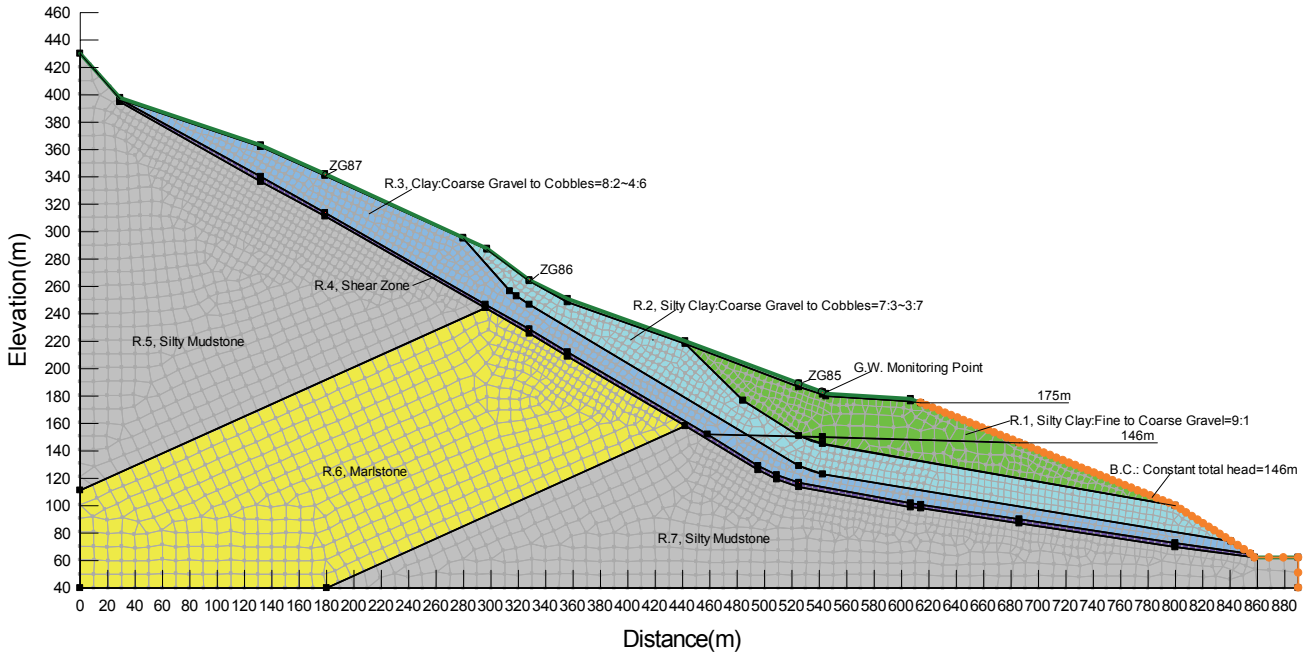

Figure 5.6: Boundary conditions for transient seepage analysis of Shuping

Seepage model as shown in Figure 5.5 and Figure 5.6 for steady-state and transient seepage analysis have the same regions, meshes and material properties; only the boundary conditions are different. Seepage analysis is conducted with the following

boundary conditions and steps:

1. Steady-state seepage analysis. Steady-state seepage analysis is conducted to generate initial groundwater table and initial pore water pressure. The steady-state seepage analysis has only 1 step which lasts for 0 day. A constant total head of 146 m is applied to the ground surface at the toe of the landslide between elevations 40 m and 146 m. The line joined by round dots inside the landslide mass in Figure 5.5 is the boundary that defines the initially inclined groundwater table.

2. Transient seepage analysis. The transient seepage analysis consists of 1,140 steps to simulate real reservoir water level fluctuation for 1,140 days. The initial pore water pressure for this analysis is based on previous steady-state seepage calculation. For the ground surface between elevations 40 m and 175 m, the flow boundary condition is variable total head vs. time, which is based on the observed daily reservoir water level at the Three Gorges dam. The variable total head boundary condition at toe of the landslide for the transient seepage analysis is shown in Figure 5.7.

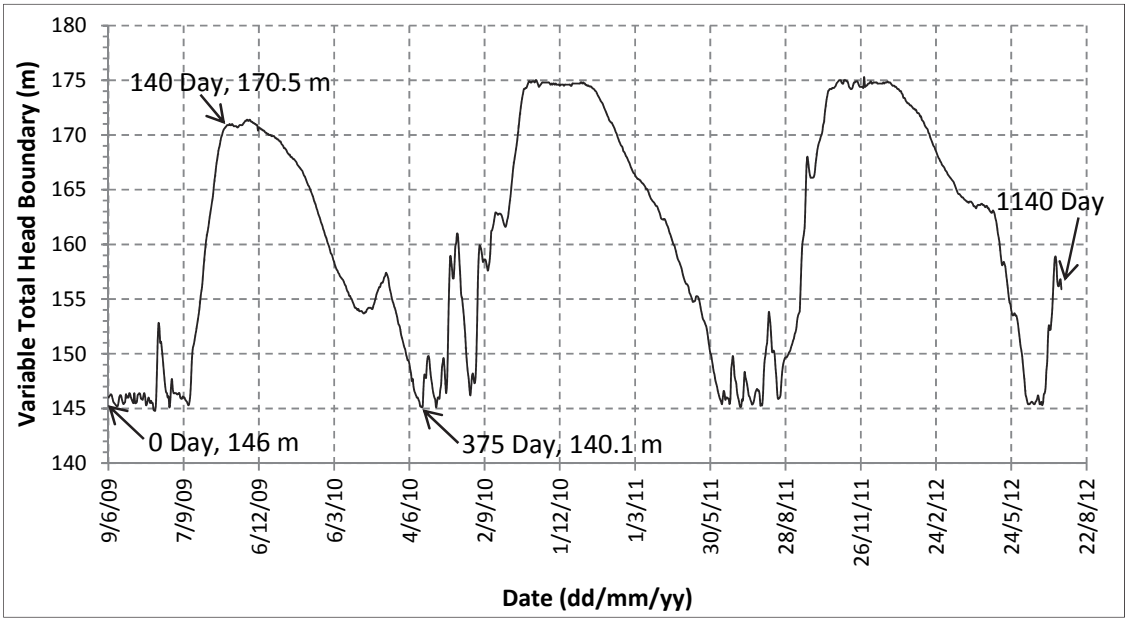

Figure 5.7: Variable total head boundary condition for Shuping transient seepage analysis

Since there is currently no unsaturated laboratory permeability test conducted for the Shuping landslide, the saturated/unsaturated permeability data of Sunjiazhuang landslide, in Xingshan County, which is not too far from Shuping landslide, is used for this analysis.

According to landslide monitoring reports from CTGU, geological history and composition of the Shuping landslide and Sunjiazhuang landslide are quite similar. Shuping and Sunjiazhuang are both colluvium landslides. The material in both landslides are quaternary colluvium (Q^{del}). Bedrocks for both landslides also belong to Middle Triassic Period. The bedrock of Shuping landslide consists of tilted interbeded silty mudstone and marlstone; the bedrock of Sunjiazhuang landslide also consists of tilted interbeded silty mudstone and silty sandstone.

Based on field permeability test results of Shuping landslide and saturated/unsaturated permeability data of Sunjiazhuang landslide, a parameter study with different combinations of permeability is developed to determine the saturated/unsaturated permeability that best represents Shuping landslide. Combinations of the parameter study is shown in Table 5.4.1.

Table 5.4.1: Combinations of permeabilityfor parameter study

Case #	Permeability (m/day)							Anisotropy
	G.S.	R. 1	R. 2	R. 3	R. 4	R. 5&7	R. 6	
1	2	2	4	0.2	0.1	0.1	0.1	Aniso=1 for all regions.
2	2	2	8	0.2	0.1	0.1	0.1	
3	1.5	1.5	3	0.15	0.1	0.1	0.1	
4	0.5	0.5	1	0.05	0.1	0.1	0.1	
5	1	1	2	0.1	0.1	0.1	0.1	
6	0.5	0.5	1	0.5	0.1	0.1	0.1	
7	0.5	0.5	1	0.5	0.1	1	1	
8	0.5	0.5	2	0.5	0.1	1	1	
9	0.5	0.5	0.5	0.5	0.1	0.1	0.1	
10	0.5	0.5	0.1	0.1	0.1	0.1	0.1	

11	0.5	0.5	0.5	0.5	0.1	0.1	0.1	Aniso=0.2 for R. 1,2,3, Aniso=1 for R. 4,5,6,7 and G.S.
12	0.5	0.5	0.5	0.5	0.1	0.1	0.1	Aniso=0.1 for R. 1,2,3, Aniso=1 for R. 4,5,6,7 and G.S.
13	0.5	0.5	5.0	0.5	0.1	0.1	0.1	
14	0.5	0.5	2.5	0.5	0.1	0.1	0.1	
15	0.5	0.5	0.5	5.0	0.1	0.1	0.1	
16	0.5	0.5	0.5	2.5	0.1	0.1	0.1	
17	0.5	5.0	0.5	0.5	0.1	0.1	0.1	
18	0.5	2.5	0.5	0.5	0.1	0.1	0.1	
19	0.5	1.0	0.5	0.5	0.1	0.1	0.1	
20	0.5	1.0	0.5	0.5	0.1	0.1	0.1	Aniso=0.05 for R. 1,2,3, Aniso=1 for R. 4,5,6,7 and G.S.
21	0.5	0.5	5.0	0.1	0.1	0.1	0.1	Aniso=0.1 for R. 1,2,3, Aniso=1 for R. 4,5,6,7 and G.S.
22	0.5	0.4	5.0	0.1	0.1	0.1	0.1	
23	0.5	0.3	5.0	0.1	0.1	0.1	0.1	
24	0.5	0.2	5.0	0.1	0.1	0.1	0.1	
25	0.5	0.1	5.0	0.1	0.1	0.1	0.1	
26	0.5	0.5	0.5	0.1	0.1	0.1	0.1	
27	0.5	0.5	0.5	0.1	0.1	0.1	0.1	Aniso=0.1 for R. 2,3, Aniso=1 for R. 1,4,5,6,7 and G.S.
28	0.5	0.5	0.5	0.1	0.1	0.1	0.1	Aniso=0.1 for R. 1,3, Aniso=1 for R. 2,4,5,6,7 and G.S.
29	0.5	0.5	0.5	0.1	0.1	0.1	0.1	Aniso=0.1 for R. 1,2, Aniso=1 for R. 3,4,5,6,7 and G.S.
30	0.5	0.2	4.0	0.1	0.1	0.1	0.1	Aniso=0.1 for R. 1,2,3, Aniso=1 for R. 4,5,6,7 and G.S.
31	0.5	0.2	2.0	0.1	0.1	0.1	0.1	
32	0.5	0.2	1.0	0.1	0.1	0.1	0.1	
33	0.5	0.2	0.5	0.1	0.1	0.1	0.1	
34	0.5	0.2	3.0	0.1	0.1	0.1	0.1	
35	0.5	0.2	3.0	0.1	1.0	0.1	0.1	
36	0.5	0.2	3.0	0.1	0.01	0.1	0.1	
37	0.5	0.2	3.0	0.1	0.1	1.0	0.1	
38	0.5	0.2	3.0	0.1	0.1	0.01	0.1	
39	0.5	0.2	3.0	0.1	0.1	0.1	1.0	
40	0.5	0.2	3.0	0.1	0.1	0.1	0.01	

41	0.5	0.2	3.0	0.1	0.01	1.0	0.1	
42	0.5	0.2	3.0	0.1	0.01	1.0	0.1	Aniso=0.1 for R. 1,2,3,4 Aniso=1 for R. 5,6,7 and G.S.
43	0.5	0.2	3.0	0.1	0.1	1.0	0.5	Aniso=0.1 for R. 1,2,3, Aniso=1 for R. 4,5,6,7 and G.S.
44	1.0	0.2	3.0	0.1	0.1	1.0	0.5	
45	2.0	0.2	3.0	0.1	0.1	1.0	0.5	
46	4.0	0.2	3.0	0.1	0.1	1.0	0.5	
56	2.0	0.1	3.0	0.1	0.1	1.0	0.5	

Note: G.S. means top soil region at the ground surface. R. 1, R. 2, R. 3, R. 4, R. 5 & 7 and R. 6 represent Region 1, Region 2, Region 3, Region 4, Region 5 & 7 and Region 6 respectively. Aniso means k_y/k_x.

It should be noted that the configuration of each region in Figure 5.5 and Figure 5.6 is based on limited number of geological boreholes.

Table 5.4.2: Parameter study cases for the new SEEP/W model

Case #	Hydraulic Conductivity (m/day)							Anisotropy
	G.S.	R. 1	R. 2	R. 3	R. 4	R. 5&7	R. 6	
47	2.0	0.2	3.0	0.1	0.1	1.0	0.5	Aniso=0.1 for R. 1,2,3, Aniso=1 for R. 4,5,6,7 and G.S.
48	2.0	0.2	2.5	0.1	0.1	1.0	0.5	
49	2.0	0.1	2.5	0.1	0.1	1.0	0.5	
50	2.0	0.3	2.5	0.1	0.1	1.0	0.5	
51	2.0	0.4	2.5	0.1	0.1	1.0	0.5	
52	2.0	0.2	2.0	0.1	0.1	1.0	0.5	
53	2.0	0.1	2.0	0.1	0.1	1.0	0.5	
54	2.0	0.2	1.5	0.1	0.1	1.0	0.5	
55	2.0	0.1	1.5	0.1	0.1	1.0	0.5	
57	2.0	0.1	2.0	0.1	0.1	1.0	1.0	
58	2.0	0.1	2.0	0.1	0.1	1.0	2.0	
59	2.0	0.1	2.0	0.1	0.1	0.5	1.0	
60	2.0	0.1	1.5	0.1	0.1	1.0	1.0	
61	2.0	0.1	1.5	0.1	0.1	1.0	2.0	
62	2.0	0.1	1.5	0.1	0.1	0.5	1.0	

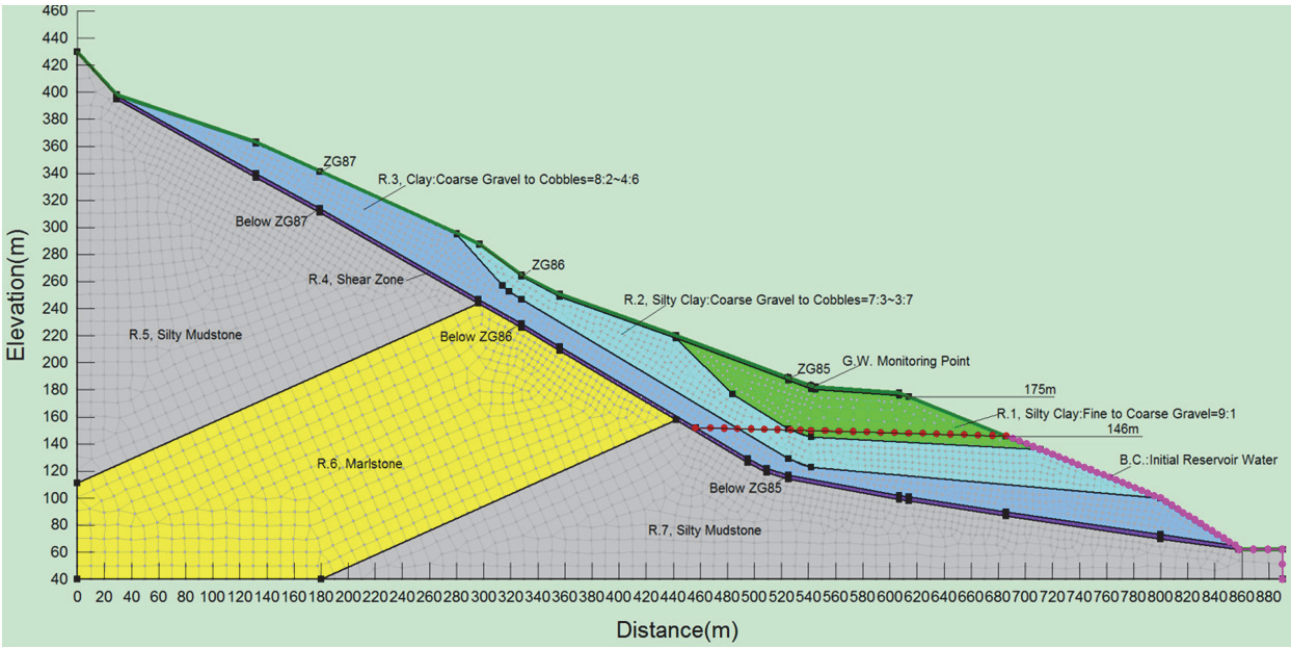

Figure 5.8: Boundary conditions for steady-state seepage analysis of the new model

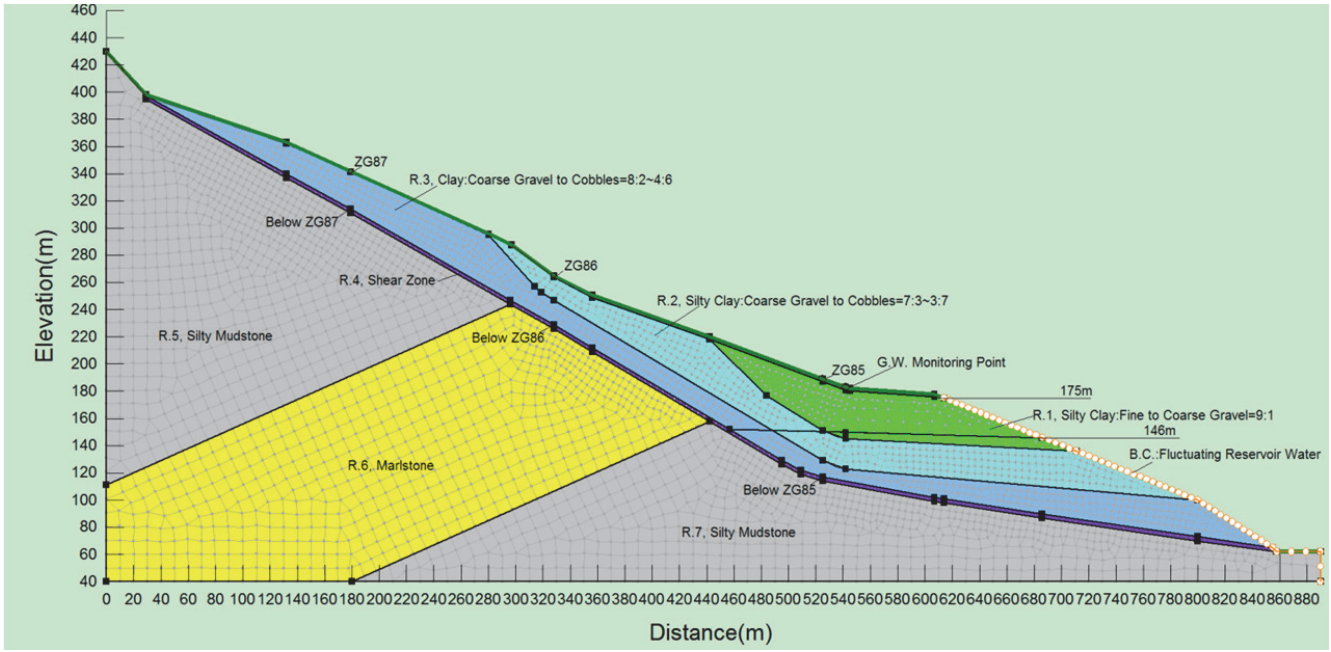

Figure 5.9: Boundary conditions for transient seepage analysis of the new model

Therefore the extents of Regions 1, 2 and 3 are modified and further parameter study have been carried out. The new SEEP/W model after modifying the extents of Regions 1, 2 and 3 is shown in Figure 5.8 and Figure 5.9 The bottoms for Regions 1 and 2 in Figure

5.8 and Figure 5.9 are flatter compared with those in Figure 5.5 and Figure 5.6 The cases considered in the parameter study for the new SEEP/W model are listed in Table 5.4.2.

The calculated groundwater table below SZK-1 from SEEP/W models is compared with the observed groundwater table. The least square method is used to determine the groundwater table that best fits the observed groundwater table. If the groundwater table from the SEEP/W model is denoted as H_i for date i, and the correspondingly observed groundwater table as h_i, the sum of squares to be minimized is $S = \sum_1^N (H_i - h_i)^2$. The sum of squares for each case is calculated and summarized in Table 5.4.3.

Table 5.4.3: Sum of squares for each case

Case #	1	2	3	4	5	6	7	8	9	10
Sum of Squares	6615	6846	6523	5572	6100	5119	3522	3441	5250	6223
Case #	11	12	13	14	15	16	17	18	19	20
Sum of Squares	3532	2663	2613	2365	2957	2797	6597	5419	3662	2765
Case #	21	22	23	24	25	26	27	28	29	30
Sum of Squares	2877	2556	2192	1812	1512	2626	5904	2659	2574	1590
Case #	31	32	33	34	35	36	37	38	39	40
Sum of Squares	1472	1888	2496	1479	1544	1504	1544	1997	1297	1730
Case #	41	42	43	44	45	46	47	48	49	50
Sum of Squares	1565	1679	1445	1445	1443	1539	1429	1294	1055	1557
Case #	51	52	53	54	55	56	57	58	59	60
Sum of Squares	1851	1207	946	1262	971	1217	903	872	779	960
Case #	61	62	-							
Sum of Squares	949	822								

It can be seen from Table 5.4.3 that for the model in Figures 5.5 and 5.6, which have

steeper bottoms for Regions 1 and 2, Case 39 has the minimum sum of the squares. For the new model in Figures 5.8 and 5.9, which have relatively flatter bottoms for Regions 1 and 2, Case 59 has the minimum sum of squares. Compared with Case 39, Case 59 has a smaller minimum sum of squares, which means that Case 59 best fits the monitored groundwater table among all cases. Groundwater table vs. time for Case 39 and Case 59 are plotted in Figure 5.10. The back calculated permeability is about one order of magnitude lower than the field permeability test result. The possible reason for larger field permeability test result is that the field test was conducted 1.0~1.5m below the ground surface and this depth is relatively shallow compared to the thickness of landslide mass. The soil close to the ground surface is susceptible to disturbance such as drying/wetting, weathering, erosion, etc. These disturbances can cause more fissures and larger voids than the undisturbed soil, and lead to higher permeability test results.

Detailed seepage input data of matric suction-k_x relation, and matric suction-volumetric water content relation for Case 59 are summarized in Appendix I. Data in Appendix were obtained by comparison with unsaturated permeability of Sunjiazhuang landslide. Firstly, a ratio was calculated by dividing “saturated permeability of Shuping landslide mass” by “the saturated permeability of Sunjiazhuang landslide mass”. Then the unsaturated permeability corresponding to each matrix suction of Sunjiazhuang landslide was multiplied by this ratio to get the unsaturated permeability for Shuping seepage model. Same method was taken to obtain unsaturated permeability for Baishuihe and Muyubao landslides.

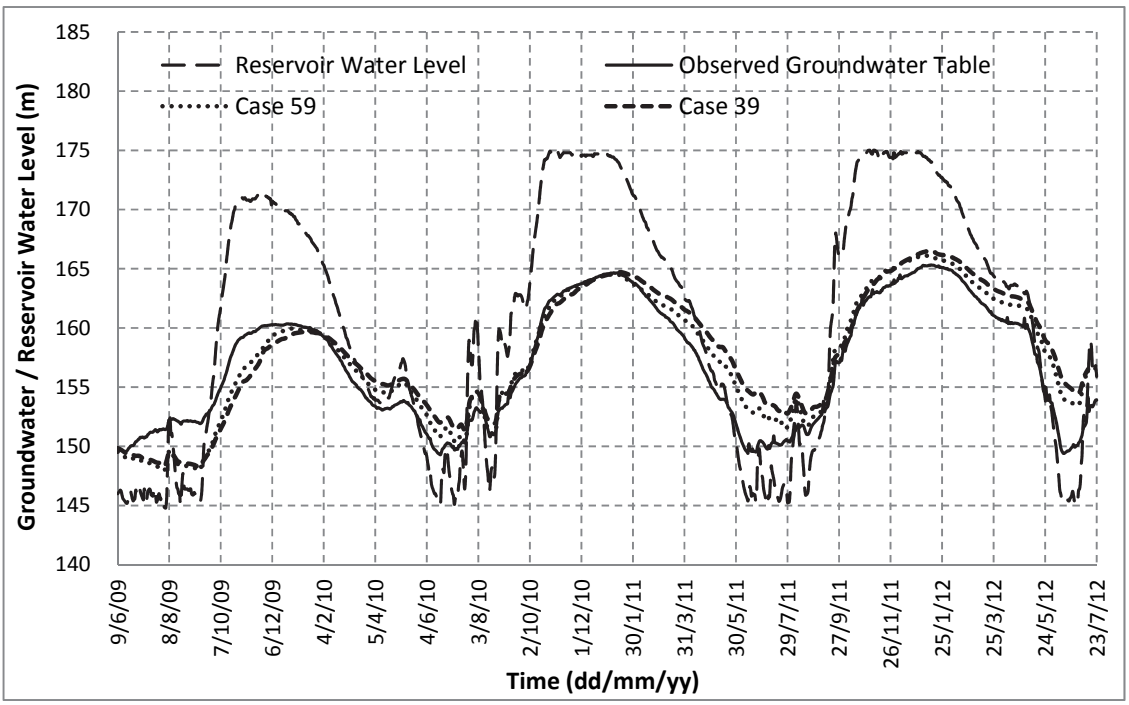

Figure 5.10: Modeled groundwater table for Case 39 and Case 59

The calculated pore pressure contours of Shuping transient seepage analysis (Case 59) for October 27, 2009 (140th Day) and June 19, 2010 (375th Day) are plotted in Figure 5.11 and Figure 5.12, respectively.

Figure 5.11 presents the pore pressure contour when the reservoir just reached the high level. The seepage velocity vectors are mainly inward and upward. The seepage velocity in Region 2 is larger than that in other regions because of the relatively higher permeability of Region 2 material. Because of the low permeability of the landslide mass in Region 1, there is a very distinct time lag between the groundwater table and reservoir water level in Figure 5.11. The groundwater table follows closely with the change of the reservoir water level at the ground surface. However in the area closer to the slip zone, the groundwater table remains almost unchanged and is much lower than the reservoir water level. This indicates that there is no significant increase of pore water pressure along the slip zone when the reservoir water level rises.

Figure 5.12 shows the pore pressure contour when the reservoir just reached the low level. The seepage velocity vectors show that the water is mainly flowing outward and downward of the landslide mass. The seepage velocity is larger in Region 2 because of its relatively higher permeability. Because Region 1 material has low permeability, there is some time lag behind the groundwater table in the landslide mass during reservoir drawdown. The groundwater table is consistent with the reservoir water level at the ground surface. However, it is higher than the reservoir water level in the deeper landslide mass.

The seepage analysis results of Shuping landslide are consistent with Mechanism 1. For Shuping landslide, which has low permeability, the inward and upward seepage force as well as the increasing hydrostatic pressure at the toe makes the landslide more stable when the reservoir water level rises. During the reservoir drawdown, the time lag in the change of the groundwater in the landslide mass leads to outward and downward seepage force. In addition, the hydrostatic pressure at the ground surface decreases during the reservoir drawdown. These adverse effects result in worse condition on the stability of the landslide leading to accelerated viscous movement of the landslide during reservoir drawdown.

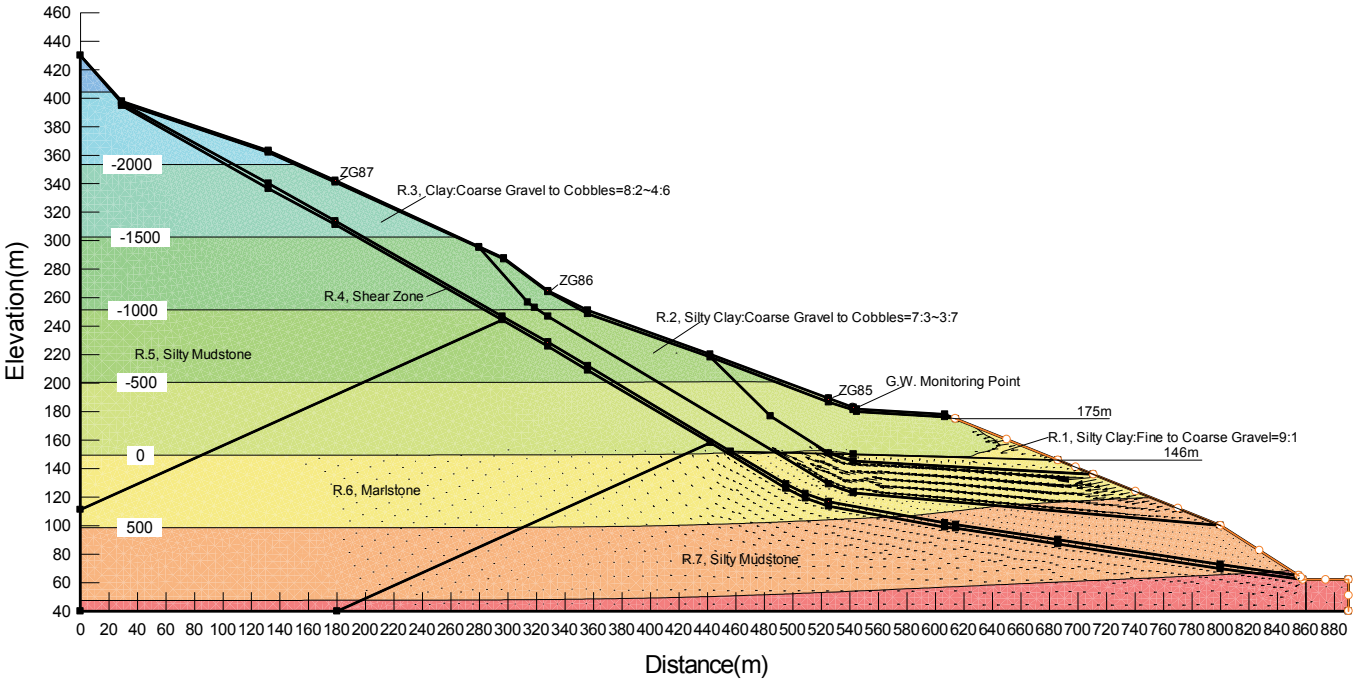

Figure 5.11: Pore pressure contour for Shuping on October 27, 2009 (140th Day)

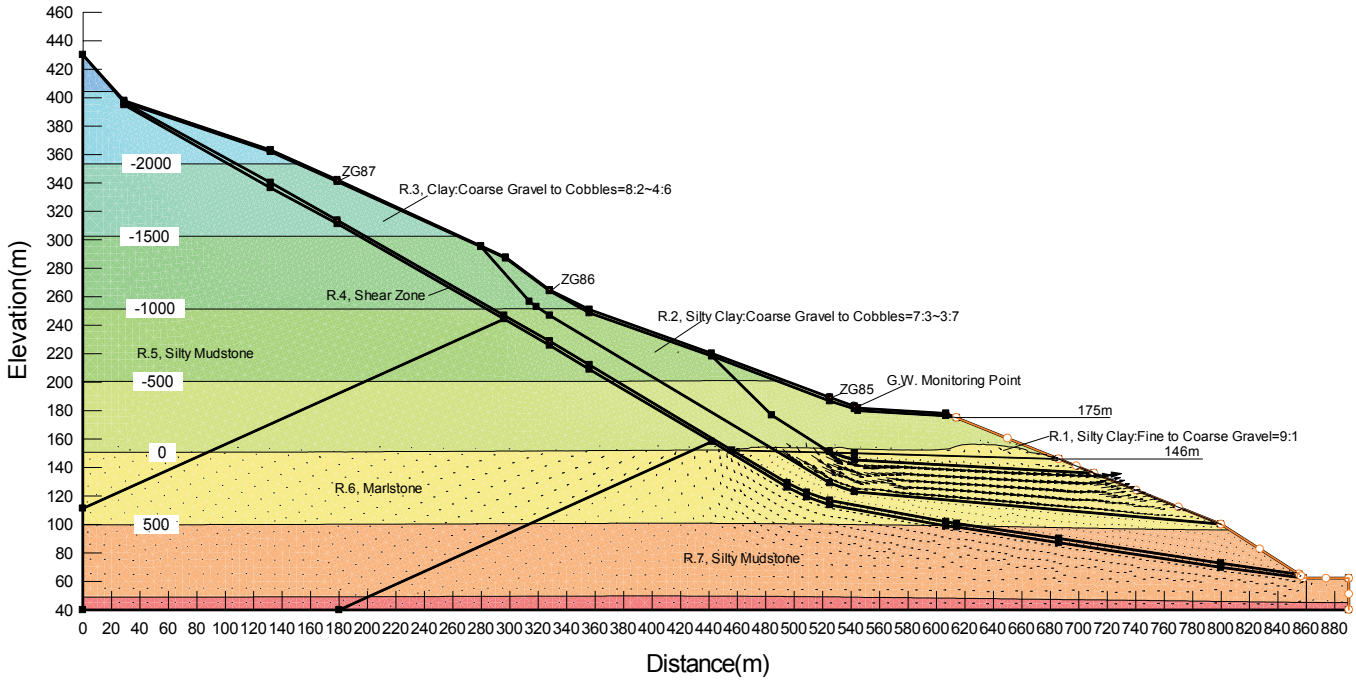

Figure 5.12: Pore pressure contour for Shuping on June 19, 2010 (375th Day)

5.5 Stability Analysis of Shuping Landslide

The gradual step-like movement of Shuping landslide indicates that this landslide has an overall factor of safety slightly above 1.0. Factor of safety of the landslide changes with the fluctuation of reservoir level. The landslide moves faster when factor of safety decreases to closer to 1.0, while it moves slower when factor of safety increases. If the overall factor of safety drops below 1.0, there will be abrupt movement and landslide failure happens.

SLOPE/W (GEO-SLOPE International, Ltd., 2008) is used to analyze the stability of Shuping landslide. In the model, the Morgenstern-Price analysis method is adopted. Pore water pressure calculated from the previous SEEP/W transient seepage analysis (Case 59) is imported to the SLOPE/W model. The slip surface is fully specified which goes through the slip zone region. The configuration of the SLOPE/W model is shown in Figure 5.13.

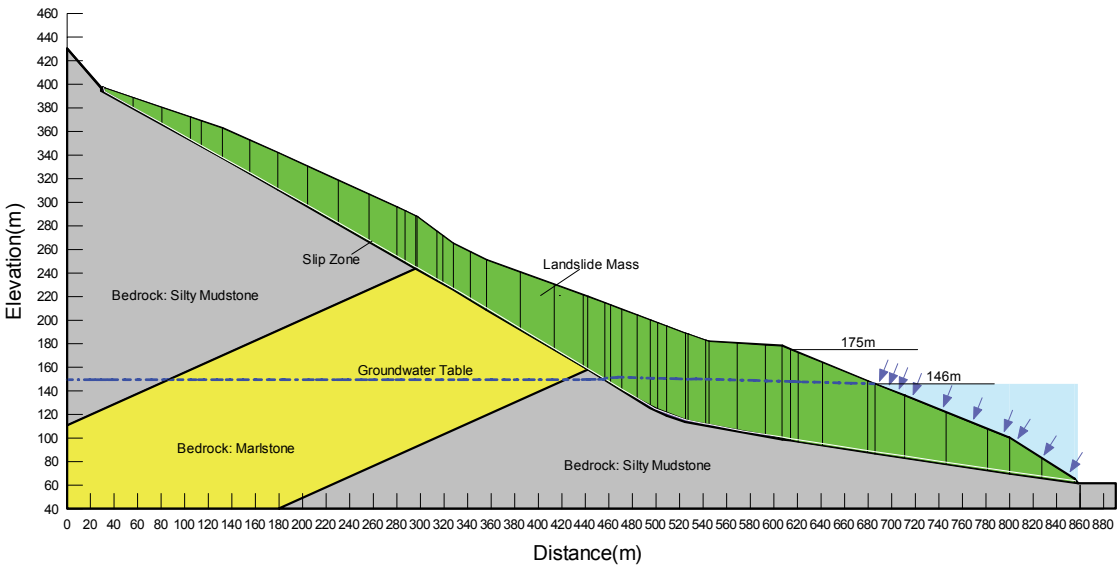

Figure 5.13: Stability model for Shuping landslide

For Shuping landslide, saturated drained direct shear tests were conducted by researchers from CTGU. Maximum, minimum and average values of cohesion and

friction angle for the landslide mass, slip zone and bed rock were obtained and summarized in Table 5.5.1.

Based on the direct shear test result, the following strength parameters in Table 5.5.2 have been selected for Shuping SLOPE/W model for sensitivity study and back calculation of strength parameters. The corresponding factor of safety vs. time is plotted in Figures 5.14 and 5.15.

Table 5.5.1: Strength parameters from saturated drained direct shear test (CTGU)

Landslide Region	Value Type	$c'(\mathrm{kPa})$	$\phi'(\circ)$
Landslide Mass	Maximum Value	23.4	23.4
	Minimum Value	7.7	15.7
	Average Value	15.6	20.0
Slip Zone	Maximum Value	22.4	19.8
	Minimum Value	9.9	14.8
	Average Value	16.6	16.9
Bedrock (Silty Sandstone)	Maximum Value	950.0	41.0
	Minimum Value	520.0	35.0
	Average Value	770.0	37.0
Bedrock (Marlstone)	Maximum Value	3710.0	46.0
	Minimum Value	3050.0	45.0
	Average Value	3380.0	46.0

Stability analyses were carried out and the results are shown in Figure 5.14. In Figure 5.14, a friction angle of 21° is used for the shear zone while the cohesion is decreased gradually. It can be seen that the trend of the change of factor of safety is consistent with the trend of the reservoir water level fluctuation. The factor of safety increases when the reservoir water level rises. It decreases when reservoir water level remains at the peak and during reservoir drawdown. This pattern of factor of safety can also be seen in Figure 5.15, where the cohesion of the slip zone material is fixed at 18 kPa and the friction angle is decreased gradually.

Table 5.5.2: Strength parameters for Shuping SLOPE/W model

Stability Model Region	Unit Weight (kN/m^3)	$c'(kPa)$	$\phi'(\circ)$
Landslide Mass	19.0	23.4	23.4
Slip Zone	19.0	22.0	21.0
		20.0	
		18.0	20.0
			19.0
			18.0
Bedrock	-	-	-

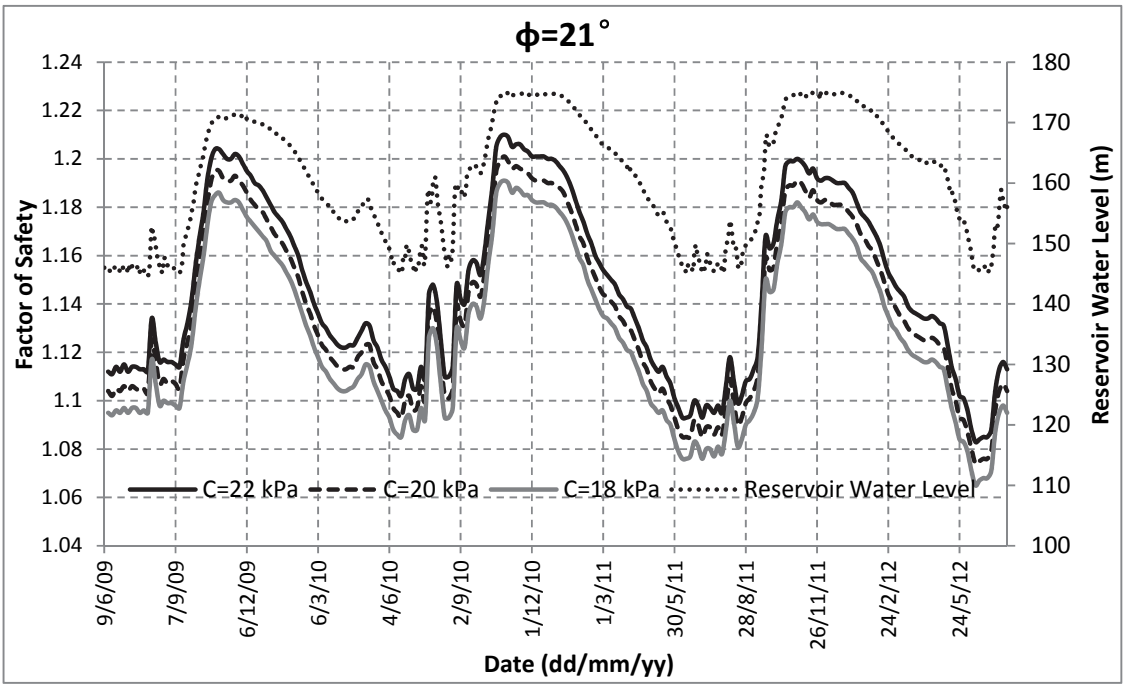

Figure 5.14: Factor of safety vs. time for Shuping landslide (ϕ=21°)

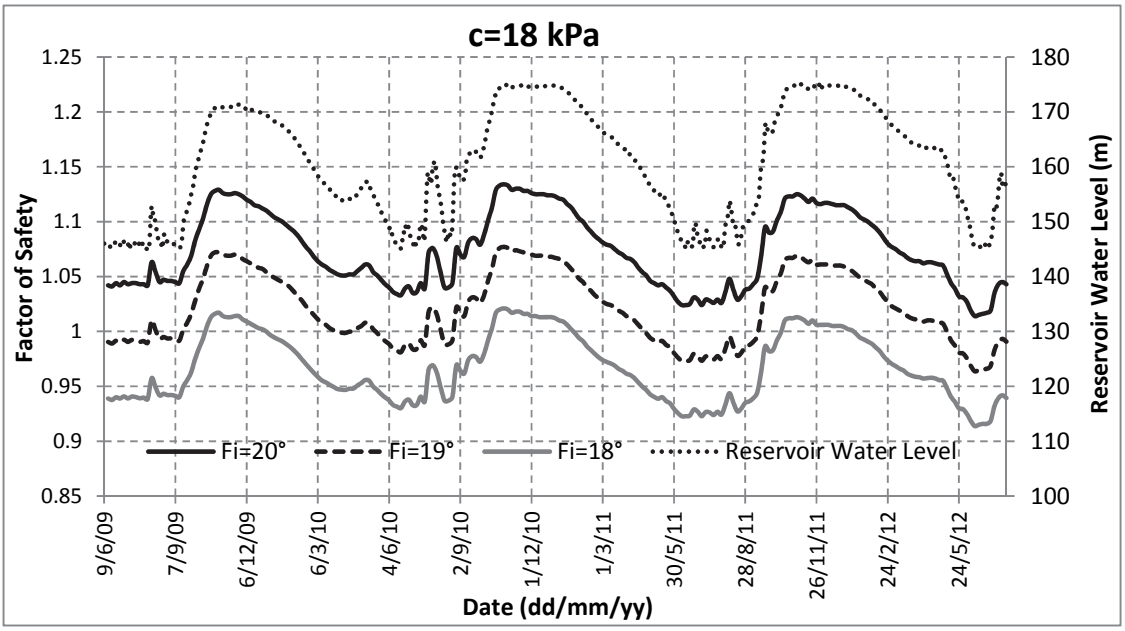

Figure 5.15: Factor of safety vs. time for Shuping landslide (c=18 kPa)

Figure 5.14 and Figure 5.15 also show that the results of the stability analysis of Shuping landslide are consistent with Mechanism 1. On one hand, the landslide material has a low permeability, rising of the reservoir water level increases the hydrostatic pressure on the ground surface and leads to higher factor of safety. As the landslide becomes more stable, its viscous movement rate becomes smaller. On the other hand, the drawdown of reservoir water level means less hydrostatic pressure on the ground surface, which leads to smaller factor of safety. As the landslide becomes less stable, the viscous effect of the material becomes larger leading to accelerated movement.

Comparing Figure 5.14 and Figure 5.15, the factor of safety of the Shuping landslide is more sensitive to changes in friction angle than cohesion of the soil in the slip zone. By decreasing the cohesion from 18 kPa to 14 kPa, the factor of safety on June 9, 2009 only drops from 1.112 to 1.095, which is only a 1.5% decrease. However, by changing the friction angle from 20° to 19°, the factor of safety on June 9, 2009 drops from 1.042 to 0.990, which is a 5.0% decrease.

Figure 5.14 and Figure 5.15 show the change of the factor of safety of Shuping landslide over three years (i.e. three cycles of water level variations). The maximum and minimum factor of safety for each cycle is summarized in Table 5.5.3 and Table 5.5.4. The initial factor of safety on June 09, 2009 (0^{th} Day) is also included in these two tables for comparison. The maximum, minimum and initial factors of safety are plotted in Figure 5.16 and Figure 5.17.

Table 5.5.3: Maximum and minimum factor of safety for each cycle (ϕ=21°)

c(kPa)	Initial FS	Max. FS			Min. FS		
		Cycle 1	Cycle 2	Cycle 3	Cycle 1	Cycle 2	Cycle 3
22	1.112	1.204	1.210	1.200	1.102	1.093	1.083
20	1.104	1.195	1.201	1.191	1.093	1.085	1.074
18	1.095	1.186	1.191	1.182	1.085	1.076	1.065
c(kPa)	Initial FS	Max. FS Increase (%)			Max. FS Decrease (%)		
		Cycle 1	Cycle 2	Cycle 3	Cycle 1	Cycle 2	Cycle 3
22	1.112	8.27	8.81	7.91	-0.90	-1.71	-2.61
20	1.104	8.24	8.79	7.88	-1.00	-1.72	-2.72
18	1.095	8.31	8.77	7.95	-0.91	-1.74	-2.74

Table 5.5.4: Maximum and minimum factor of safety for each cycle (c=18 kPa)

ϕ(°)	Initial FS	Max. FS			Min. FS		
		Cycle 1	Cycle 2	Cycle 3	Cycle 1	Cycle 2	Cycle 3
20	1.042	1.129	1.134	1.125	1.033	1.024	1.014
19	0.990	1.072	1.077	1.069	0.981	0.973	0.964
18	0.939	1.017	1.021	1.013	0.930	0.923	0.914
ϕ(°)	Initial FS	Max. FS Increase (%)			Max. FS Decrease (%)		
		Cycle 1	Cycle 2	Cycle 3	Cycle 1	Cycle 2	Cycle 3
20	1.042	8.35	8.83	7.97	-0.86	-1.73	-2.69
19	0.990	8.28	8.79	7.98	-0.90	-1.69	-2.66
18	0.939	8.31	8.73	7.88	-0.94	-1.73	-2.68

In Figure 5.16 and Figure 5.17, the maximum factor of safety in Cycle 2 is larger than that in Cycle 1 because the peak reservoir water level in Cycle 2 is higher than that in Cycle 1. In addition, the minimum factor of safety in Cycle 2 lies below that in Cycle 1. It is

because the groundwater in the landslide lags behind the reservoir level which helps to build higher pore pressure in the slip zone. This can also explain that the maximum and minimum factor of safety in Cycle 3 are below those in Cycle 2. The groundwater table for the stability analysis is shown in Figure 5.10 (Case 59).

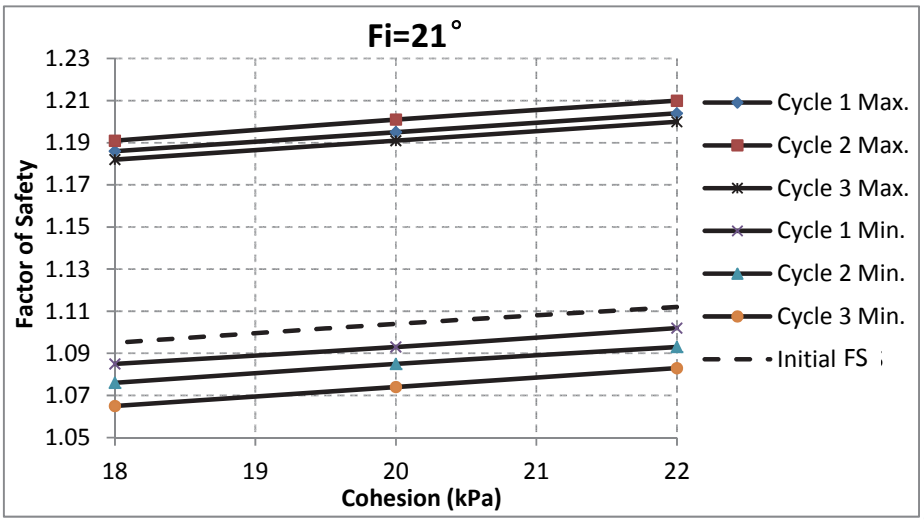

Figure 5.16: Maximum, minimum and initial factor of safety (ϕ=21°)

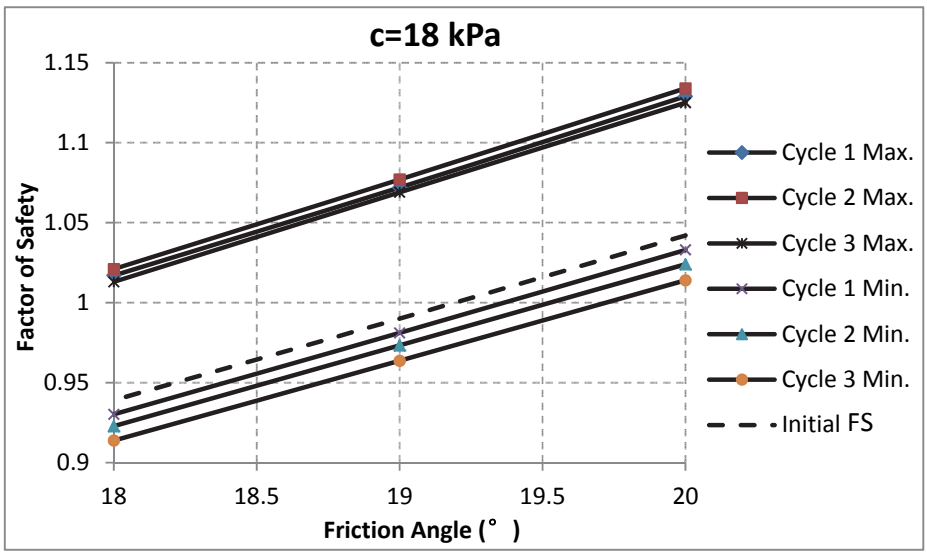

Figure 5.17: Maximum, minimum and initial factor of safety (c=18 kPa)

Figures 5.16 and 5.17 also show that the initial factor of safety, which corresponds to a reservoir water level of 146 m, lie below the maximum factor of safety and above the

minimum factor of safety. Thus, Shuping landslide is most stable when reservoir water level rises and just reaches the peak. The landslide is least stable when the reservoir remains at the lowest level. The worst stability condition for Shuping landslide is during rapid reservoir drawdown.

The maximum percentage increase and decrease from the initial factor of safety are calculated and summarized in Tables 5.5.3 and 5.5.4. It can be seen that the factor of safety of Shuping landslide can be increased by up to 9 % (FOS increased from 1.04 to 1.13)due to rising of the reservoir water. In addition, the factor of safety can be decreased by up to 3 % (FOS deceased from 1.10 to 1.07) because of reservoir drawdown. It should be noted that the adverse effects of seepage force is not included in the SLOPE/W model, thus the factor of safety of the landslide can be smaller than that presented here during reservoir drawdown. In order to avoid failure of Shuping landslide, the drawdown of reservoir level should be under careful control.

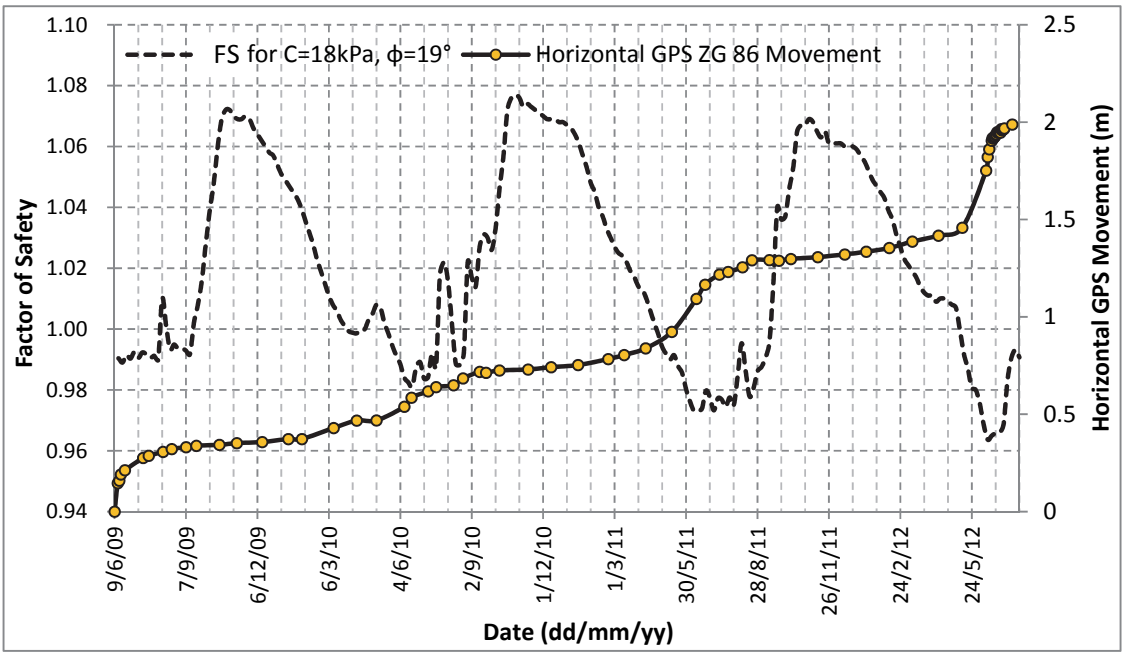

Figure 5.18: Movement and factor of safety of Shuping landslide

The strain rate effect is not considered in the stability analysis because of the limitation of SLOPW/W. The real factor of safety should be higher than 1.0 with current cohesion and friction angle. In fact, the movement rate during acceleration stage is orders of magnitude larger than the “static” state, which means that the soil can be strengthened to a great extent and the real factor of safety can increase to higher than 1.0. A factor of safety of 1.0 chosen here as the starting point for the acceleration stage should be verified in future research. For each real landslide or a specific type of soil, this factor of safety criterion could be 1.00, 1.05 or other values which should be verified based on GPS monitoring data and corresponding movement-based modeling.

Shuping landslide is now in viscous movement stage, and its movement speed is much dependent on the stability condition of the landslide. The movement is slow when the factor of safety is high. During reservoir drawdown, factor of safety is decreased gradually and movement rate of the material in the slip zone increases. To back calculate the cohesion and friction angle for the soil in the slip zone, a criterion is set such that the landslide movement starts to accelerate when the factor of safety is close to one.

The horizontal movement of GPS ZG 86 and the factor of safety for c=18 kPa and ϕ=19° of the soil in the slip zone are plotted in Figure 5.18. In this figure, it can be seen that the landslide movement starts to accelerate every time when the factor of safety is close to 1.0. Thus, c=18 kPa and ϕ=19° are chosen as the back calculated strength parameters for the slip zone soil. Compared with strength parameters from saturated drained direct shear test in Table 5.5.1, the back calculated strength parameters lie within the range of laboratory test results.

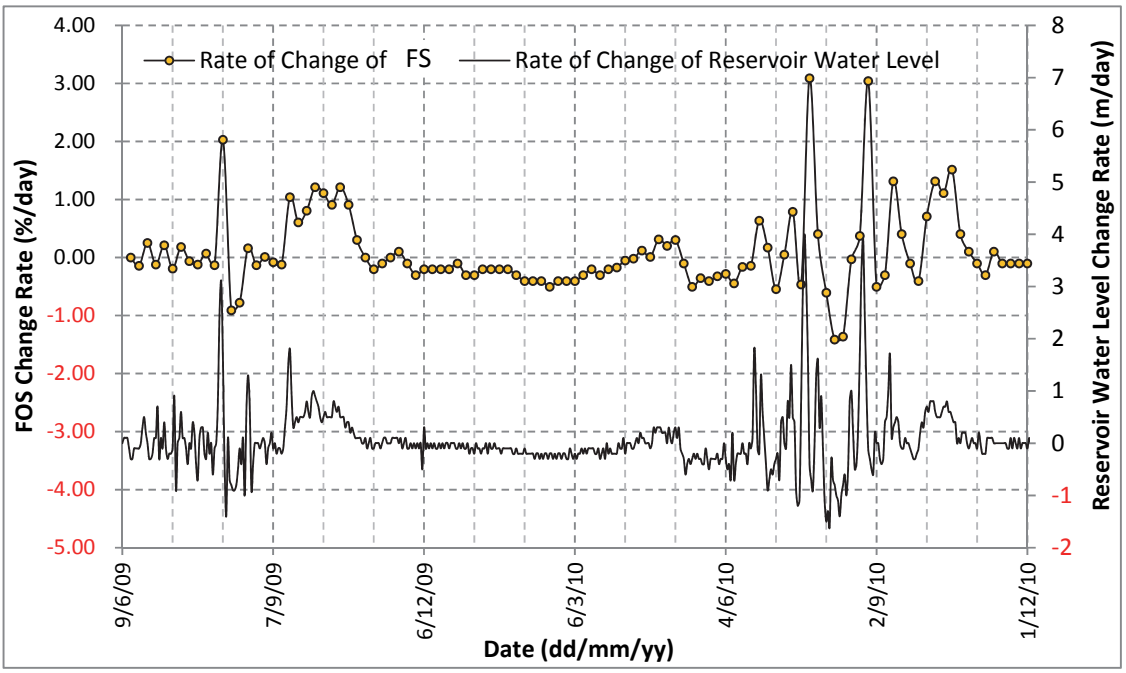

Figure 5.19: Rate of change of factor of safety and reservoir water level for Shuping

Figure 5.19 shows the rate of change of the factor of safety and the rate of change of reservoir water level. It can be seen in this figure that the rate of change of factor of safety is roughly proportional to the rate of change of reservoir water level. The highest rate of rising of the reservoir water level is +3.9 m/day on August 25, 2010 and the corresponding rate of change of the factor of safety is +3.04 %/day. The highest rate of reservoir water level drawdown is -1.5 m/day on August 03, 2010 and the corresponding rate of change of factor of safety is -1.41 %/day. This means that the change of factor of safety is very sensitive to the reservoir water level fluctuation rate. Thus the rate of reservoir drawdown should be well planned and monitored in order to prevent sharp decrease of landslide stability and landslide failure.

5.6 Movement Analysis of Shuping Landslide

For the Shuping landslide, it is observed that the landslide mass and slip zone soil exhibit strain-softening characteristics. If the soil in the landslide mass and slip zone are not strain-softening (for example, perfect plastic), the landslide will become stable enough

after the first cycle of reservoir water level fluctuation and will not move in subsequent cycles. Therefore linear elastic model or elastic-perfect plastic model will not be able to capture the characteristics of these materials. In this model, strain rate-dependent Drucker-Prager plasticity, which is developed in Chapter 4, is implemented to model the landslide mass and slip zone.

According to Graham et al. (1983), for lightly overconsolidated clays, undrained shear strengths and preconsolidation pressures change by about 10-20% for a tenfold change in strain rate. Vaid et al. (1979) conducted isotropically consolidated undrained triaxial tests with heavily overconsolidated Saint-Jean-Vianney clay and found that there was a 25% increase in undrained strength with a 100 times increase in strain rate. Based on several former laboratory results, Kulhawy and Mayne (1990) concluded that there was 10% increase in undrained strength for every tenfold increase in strain rate. In this research, the selection of percentage increase in strength for the strain rate hardening has gone through trial and error in the ABAQUS and it is decided that a 10% increase in cohesion for every tenfold increase in strain rate is used for the movement modeling. Linear elasticity is implemented for bedrock.

The configuration and mesh of the landslide model using ABAQUS are shown in Figures 5.20 and 5.21. The large strain mode is selected. The horizontal length of the model is 890 m, and the vertical height is 430 m. The elevation of the bottom line in the model is zero meter. Region 0 represents top soil. The landslide mass consists of Regions 1, 2, and 3. Region 4 represents the slip zone. Regions 5, 6 and 7 represent different types of bedrock.

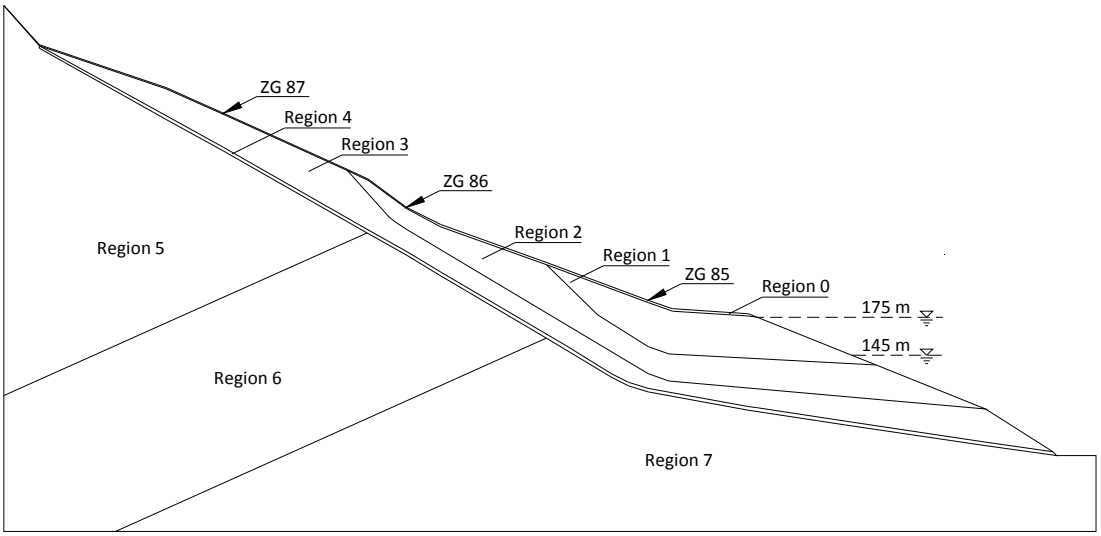

Figure 5.20: Configuration of the Shuping landslide model in ABAQUS

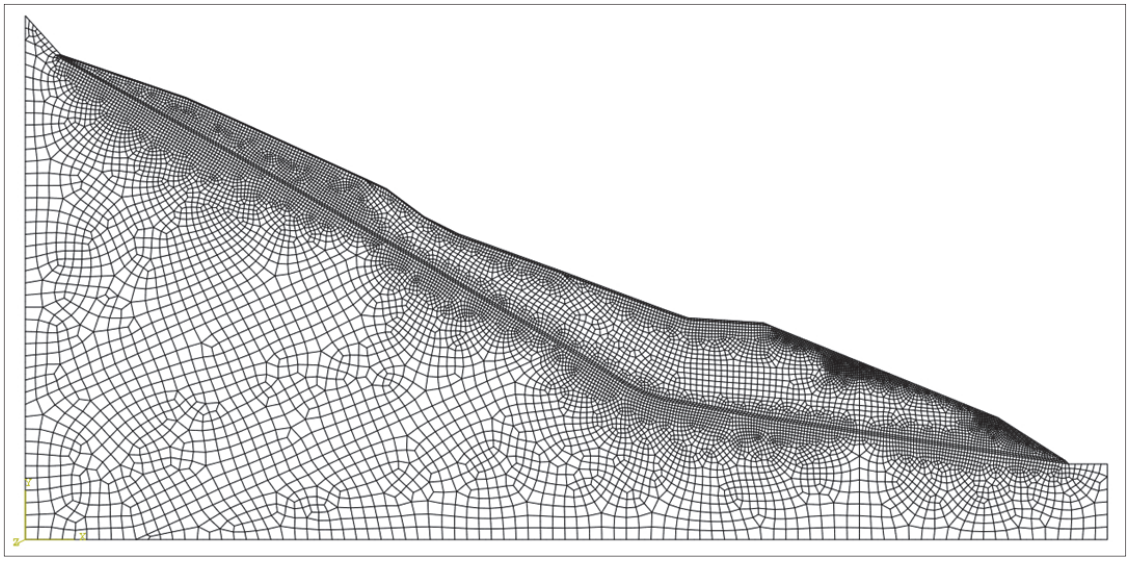

Figure 5.21: Finite element mesh of Shuping landslide using ABAQUS

November 1, 2009, when reservoir level stays at the peak level, is chosen as the beginning of time (0 day) in the model. In this model, the first step is to perform a steady-state geostatic analysis. The initial reservoir water level at the toe of the landslide is set at an elevation of 171.0 m. The left and right boundaries are fixed horizontally but free to move vertically. The bottom is fixed in both horizontal and vertical directions.

Transient analyses were carried out in subsequent steps. The elevations of the reservoir water level are based on the recorded daily reservoir water level at the Three Gorges dam. Slight modifications such as smoothing short-term sharp changes or back-and-forth changes have been made to the original recorded data to make better convergence of the finite element model. The reservoir water level between Nov 2009 and August 2012 is shown in Figure 5.22.

Base on previous seepage analysis using SEEP/W, the saturated permeability for each region in the model have been selected and they are summarized in Table 4.2.1.

In ABAQUS, the unsaturated permeability k_{usat} is defined as:

$$k_{usat} = k_s \times k \tag{5.1}$$

where

k is the saturated hydraulic conductivity.

k_s is a factor which is related to the degree of saturation. The k_s-Saturation relationship can be defined by user in ABAQUS/CAE.

The k_s-Saturation and Saturation-Pore Pressure relationships in the ABAQUS model of the Shuping landslide are based on the unsaturated permeability used in the SEEP/W seepage analysis. Since such relationship exists between volumetric water content and saturation:

$$\theta_w = \frac{e}{1+e} S_r \tag{5.2}$$

The Matric Suction-Permeability and Matric Suction-Volumetric Water Content relationships from the seepage model can be transformed into k_s-Saturation and

Saturation-Pore Pressure relationships in the ABAQUS model. Details of the transformed unsaturated permeability for ABAQUS model are summarized in Appendix I.

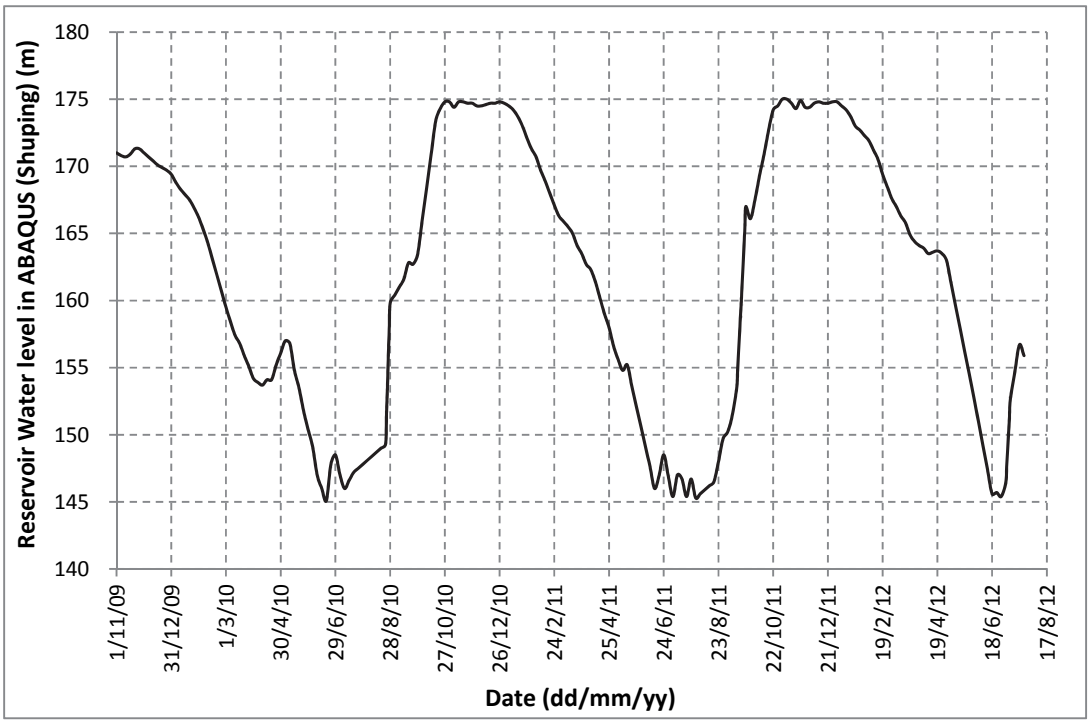

Figure 5.22: Reservoir water level boundary condition for the ABAQUS model (Shuping)

Based on the recorded reservoir level as shown in Figure 5.22, three cycles of reservoir water level fluctuation have been modeled using ABAQUS. The process of drying and wetting cycles can lead to softening of the landslide soil. Li et al. (2007) mentioned that material softening can be caused by long-term soaking. Therefore, besides strain weakening of cohesion for the landslide mass and slip zone materials, some additional weakening of the friction angle and cohesion for the slip zone are assumed and applied on May 11th, 2011 and May 20th, 2012 which represent the beginning of the second and third cycles, respectively. These additional weakening of friction angle and cohesion are assumed and applied in the ABAQUS to model the displacement of the landslide that best fit the observed data at GPS ZG 85. Without additional weakening of the strength properties, the modeled landslide displacement is either smaller than the observed data

or the model cannot converge. A field variable is defined in ABAQUS to account for the additional cohesion and friction angle weakening. The elastic and plastic soil parameters used in the first step of the finite element deformation model are listed in Table 5.6.1. Additional weakening of friction angle and cohesion is applied to the slip zone material and summarized in Table 5.6.2. The strain rate hardening is implemented to Region 0 to 4 based on the assumption that there is a 10% increase in cohesion for every tenfold increase in strain rate.

The strain rate hardening is independent of plastic strain in this study and is written as (Dassault Systèmes Simulia Corp., 2012):

$$\bar{\sigma} = \sigma_0 R \tag{5.3}$$

where

σ_0 is the static stress-strain behavior;

R is the ratio of the yield stress at nonzero strain rate to the static yield stress.

The relationship between yield stress ratio and equivalent plastic strain rate is presented in Table 5.6.3.

Table 5.6.1: Elastic and plastic parameters used in the first step of deformation analysis

	Dry Density (kg/m^3)	E (MPa)	Poisson's Ratio	Friction Angle ϕ(∘)	Flow Stress Ratio	Dilation Angle ψ(∘)	UCS at Zero Strain(kPa)
Landslide Mass	1630	20.8	0.21	34.2	1	10	54.0
Slip Zone	1630	20.8	0.21	29.5	1	10	50.0
Bedrock	2000	61000	0.28	-	-	-	-

Table 5.6.2: Additional cohesion and friction angle weakening parameter

Landslide Region	Date	Friction Angle $\phi(\circ)$	Flow Stress Ratio	Dilation Angle $\psi(\circ)$	UCS at Zero Strain(kPa)
Slip Zone	Nov. 1st, 2009	29.5	1	10	50.0
	May 11th, 2011	28.2	1	10	35.0
	May 20th, 2012	27.0	1	10	30.0

Table 5.6.3: Yield stress ratio and equivalent plastic strain rate for landslide mass and slipe zone

Yield Stress Ratio	1.0	1.1	1.21	1.331	1.4641	1.61051
Equivalent Plastic Strain Rate (s^{-1})	0	1.16E-09	1.16E-08	1.16E-07	1.16E-06	1.16E-05

The location of the groundwater table at the toe of the landslide when the reservoir water level goes down and reaches the lowest level on June 20th, 2010 is shown in Figure 5.23. The location of the groundwater table at the toe of the landslide as the reservoir water level goes up and reaches the highest level on October 17th, 2010 is shown in Figure 5.24. In both figures, the boundary between the light color and the dark color in the landslide marks the groundwater table.

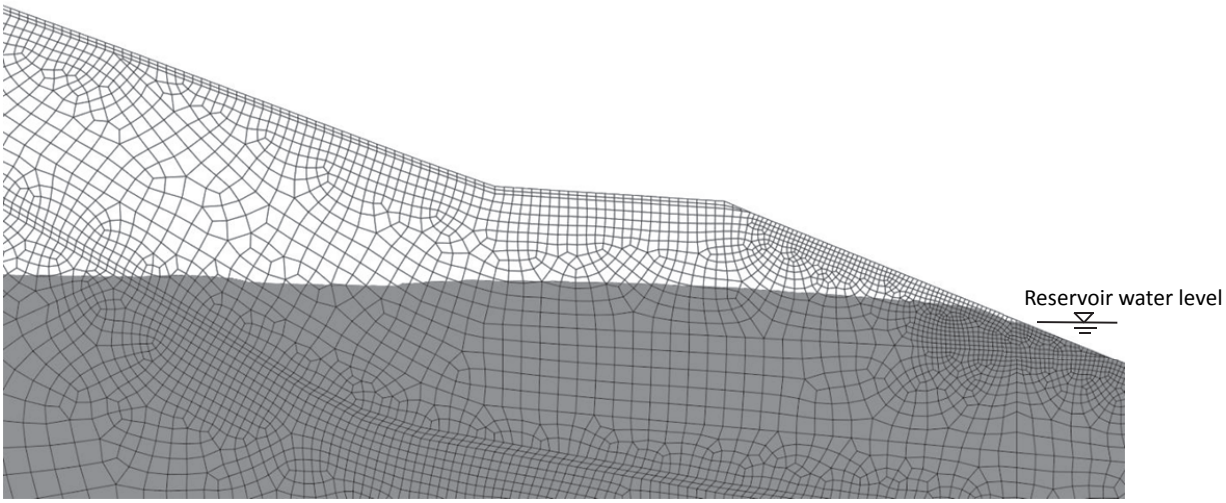

Figure 5.23: Location of groundwater table when reservoir water is at the lowest level

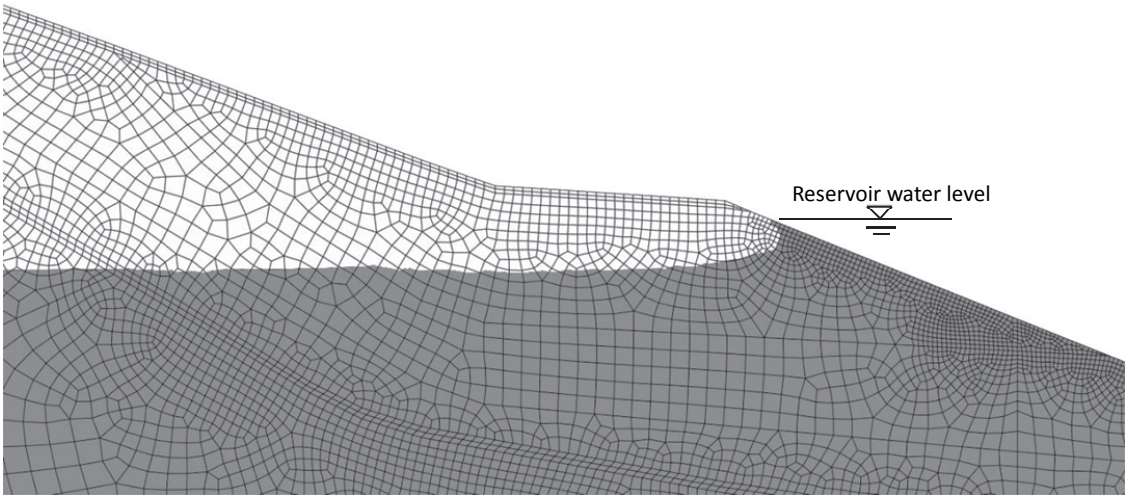

Figure 5.24: Location of groundwater table when reservoir water is at the highest level

In Figure 5.23, since the landslide material has a relatively low permeability, the groundwater table in the landslide lags behind the reservoir water level. The outward hydraulic gradient generates seepage forces which act towards the river channel. In addition, lower reservoir water level leads to less hydrostatic pressure at the toe of the landslide resulting in less stabilizing force. Thus, accelerated landslide movement is expected during reservoir drawdown.

In Figure 5.24, groundwater table in the landslide also lags behind the reservoir water level. The inward hydraulic gradient generates seepage forces which act in the opposite direction of the river channel. In addition, the increased hydrostatic pressure leads to larger stabilizing force at the toe of the landslide. Therefore, decelerated landslide movement is expected during rising of reservoir water level.

Contours of calculated horizontal movement for July 23rd, 2012 are plotted in Figure 5.25. It can be seen from this figure that most landslide movement is located at the toe. The amount of landslide movement decreases with increasing elevation towards the top of the landslide.

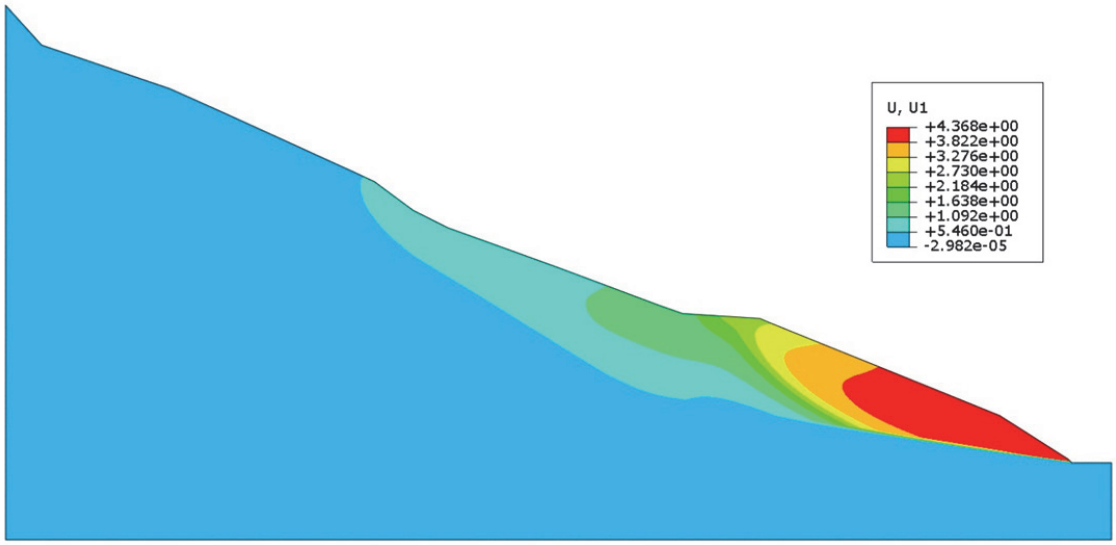

Figure 5.25: Contours of movement (July 23rd, 2012)

The relationship between the calculated horizontal movement at GPS station ZG 85 and time is plotted in Figure 5.26. The observed movement is also plotted for comparison.

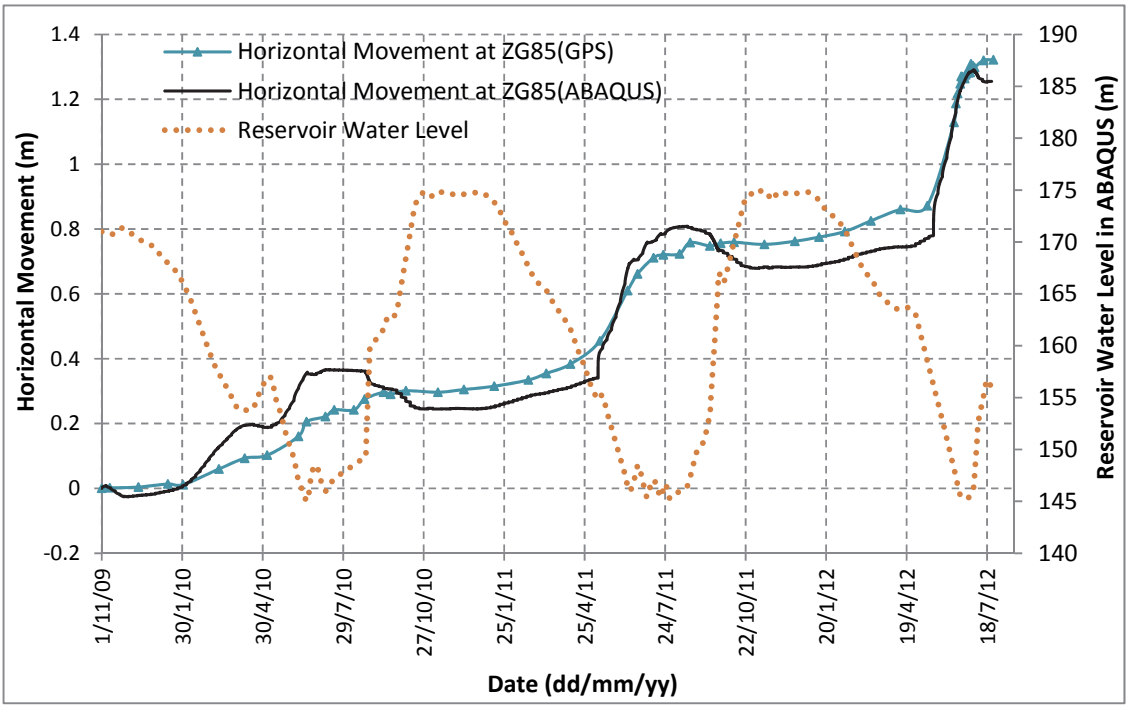

Figure 5.26: Horizontal movement at GPS station ZG 85 vs. time

In Figure 5.26, the calculated horizontal movements agree well with field observations. It

shows that accelerated movement occurs during lowering of the reservoir water level due to low permeability of the landslide material. When the reservoir water stays at its lowest level, the horizontal movement decelerates. This is because water has drained out of the soil and there is less seepage force at the toe of the landslide When reservoir water level goes up and stays high, there is also little movement towards the river channel. This verifies the assumption that Shuping landslide belongs to Mechanism 1: the landslide, which has low permeability, has higher rate of movement during drawdown of reservoir water level due to outward seepage force and less stabilizing force at the toe; the landslide moves slower when the rise of reservoir water level creates inward seepage force and larger stabilizing force at the toe.

Good agreement between calculated and observed movement implies that the soil in the slip zone has not reached residual strength yet. During previous cycles of reservoir water level fluctuation, both the friction angle and cohesion of the soil in the slip zone have decreased. In future cycles of reservoir water level fluctuation, it is expected that these strength parameters will continue to decrease until the residual values are reached. Direct shear test or ring shear test can be conducted in future research to analyze the softening characteristics and residual strength parameters of the slip zone soil.

Based on the results from the numerical model, it can be concluded that Shuping landslide belongs to Mechanism 1 and strain-rate dependent Drucker-Prager plasticity can be used to model the cyclic behavior of the material. A 10% hardening of the cohesion for every tenfold increase in strain rate is adequate for modeling the cyclic behavior of the material. Direct shear test and undrained triaxial test should be conducted in future research to verify the strain softening and strain rate hardening characteristic of the landslide soil.

Chapter 6 Case Study 2-Baishuihe Landslide-Based on Mechanism 1

Based on the GPS observation data, Baishuihe landslide was selected as another case for Mechanism 1. In this chapter, the plan view, cross sections, and geology backgrounds are covered in detail. Then the relationship between observed landslide movement and reservoir water level are discussed. Following is the discussion of the relationship between observed rainfall and landslide movement.

Seepage, stability, and coupled fluid/stress analysis were conducted based on the selected cross section and observed reservoir water level. The calculated pore pressure contours from seepage analysis are presented and discussed. The relationship between factor of safety and reservoir water level is analyzed following the seepage analysis. Then results from coupled fluid/stress finite element analysis are presented which show accelerated movement during the drawdown of reservoir water level.

6.1 Introduction to Baishuihe Landslide

The Baishuihe landslide is an old landslide which is located in the Three Gorges reservoir area in Shazhenxi Town, Zigui County, Hubei province, China. The landslide is located on the southern bank of the Yangtze River. It is located about 50 km upstream of the Three Gorges Dam. A plan view of the Baishuihe landslide is shown in Figure 6.1.

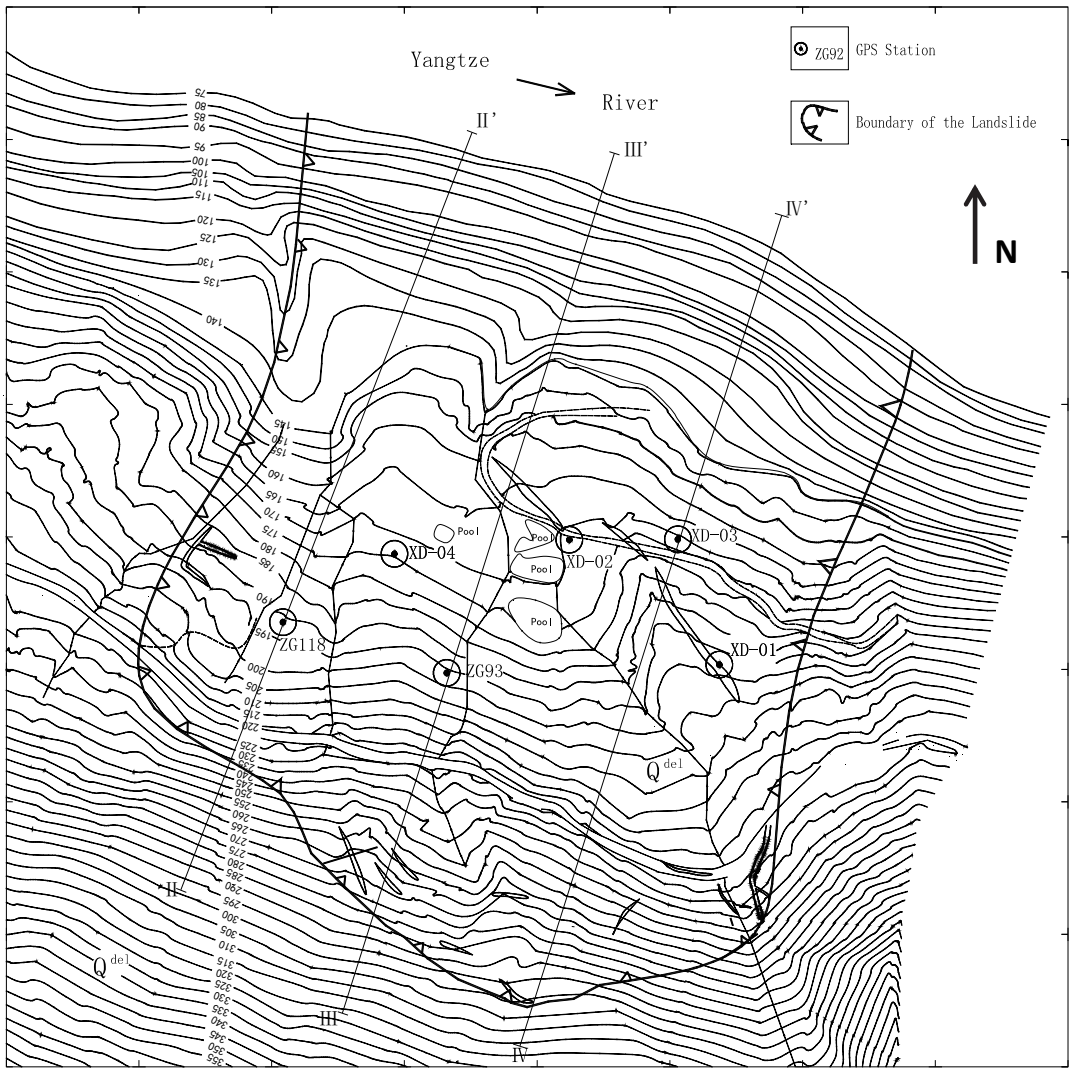

Figure 6.1: A plan view of Baishuihe landslide and location of GPS monitoring stations

The north-south length of the landslide is about 600 m and the east-west width is around 700 m. The average thickness of the landslide mass is about 30 meters with an estimated total volume of about 12.6 million m^3.

Three cross sections of the Baishuihe landslide: Section II-II', Section III-III' and Section IV-IV' are shown in Figures 6.2, 6.3 and 6.4 respectively. It is indicated in Figures 6.2 to 6.4 that the landslide mass becomes thicker from the west to the east and Section III-III' better reflects the average thickness of the landslide mass. Thus, Figure 6.3 is chosen for

the numerical analysis.

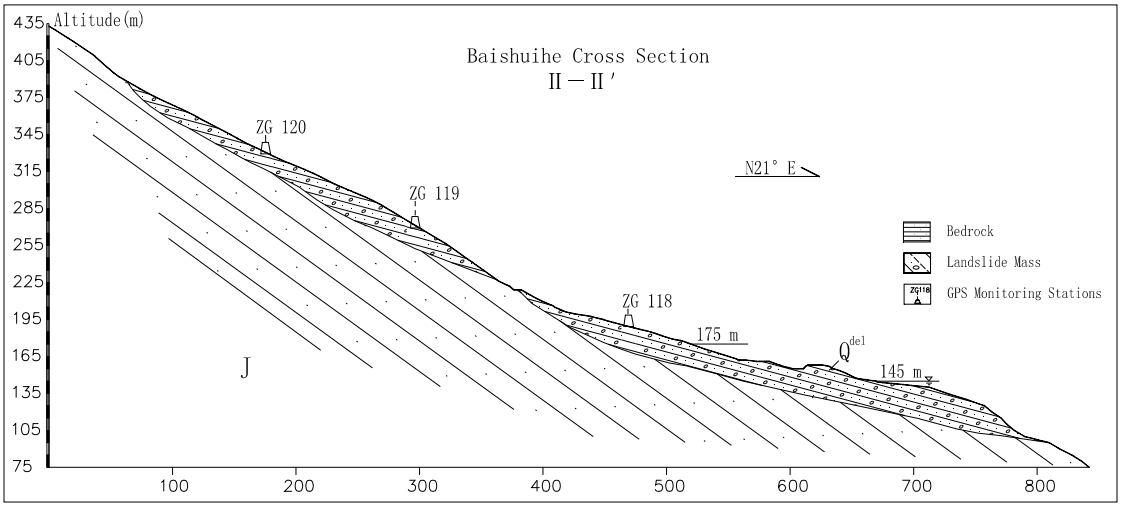

Figure 6.2: Section II-II’ of Baishuihe Landslide

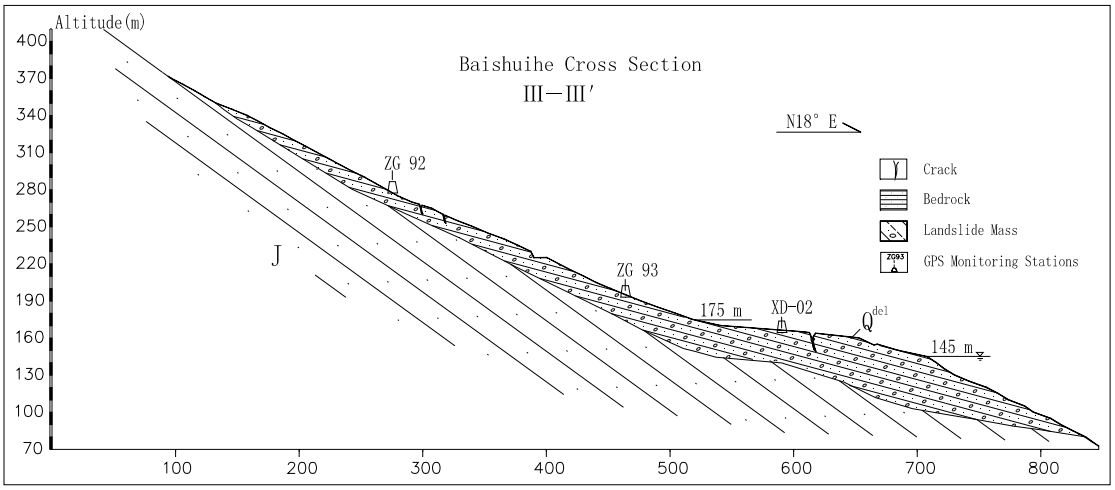

Figure 6.3: Section III-III’ of Baishuihe Landslide

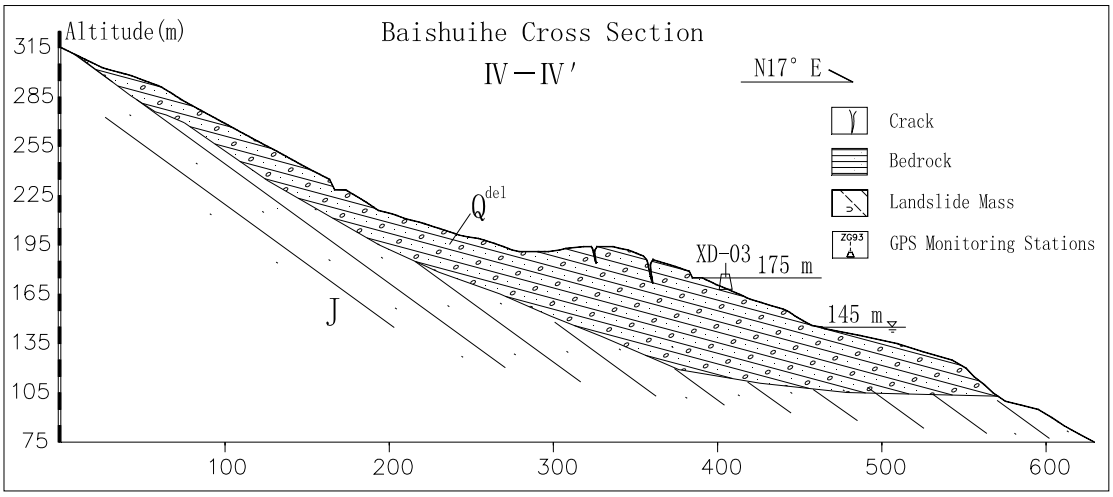

Figure 6.4: Section IV-IV’ of Baishuihe Landslide

The landslide mass is mainly quaternary colluvium (Q^{del}), which consists of silty clay, gravels and rock blocks. These gravels and rock blocks are mainly weathered sandstone and argillaceous siltstone. The size of the gravels ranges from 2 to 8 cm. The rock blocks are mainly within a diameter of 0.5 m. The mass ratio of silty clay to gravels and rocks for the colluvium ranges from 8:2 to 6:4.

Due to pervious sliding, there are two existing slip zones for this old landslide. The upper slip zone lies at the interface between the quaternary colluvium and the underlying weathered rock stratum. The weathered rock stratum is mainly composed of argillaceous siltstone. The thickness of the upper slip zone ranges from 0.9 to 3.1 m. The depth of the upper slip zone lies between 12 and 25 m. The lower slip zone lies at the interface between the weathered rock stratum and the underlying intact bedrock. The depth of the lower slip zone lies between 18.9 and 34.1 m. The lower slip zone is mainly composed of carbonaceous mudstone, which is in a muddy and schistose slate. The intact rock beneath the lower slip zone is mainly composed of interbeded siltstone and argillaceous siltstone. (The Ministry Of Education Key Laboratory of the Three Gorges Reservoir Geological Disasters, 2012)

6.2 Reservoir Water Level, Daily Rainfall and Landslide Movement

Before the impoundment of the Three Gorges dam, the water level of the Yangtze River at Baishuihe landslide was about 74 m. The Three Gorges dam started its first impoundment in May, 2003 and the reservoir water level at the dam was raised to 135 m.

GPS monitoring of the landslide movement started from July 2003 and landslide movement data are available from July 10, 2003 to July 25, 2012. Eleven GPS monitoring stations (ZG 91, 92, 93, 94, 118, 119, 120, XD-01, 02, 03, 04) were installed on the ground surface of the landslide. Among these GPS monitoring stations, six of them (ZG 93, ZG 118, XD-01, XD-02, XD-03 and XD-04) showed relatively large movement. Locations of these six GPS stations are plotted in Figure 6.1.

In Figure 6.1, the Section III-III' is chosen as the representative section for numerical analysis. GPS monitoring station ZG 93 is located on this section. The observed GPS horizontal movement at ZG 93 is corrected and the horizontal movement along the direction of Section III-III' is plotted in Figure 6.5. In this figure, the reservoir water level, which can be obtained from the website of China Three Gorges Corporation, reflects the water level at the location of the Three Gorges Dam. Since the direct distance from Baishuihe landslide to the Three Gorges Dam is only about 50 km, this water level is regarded as the actual reservoir water level at the location of the landslide. There is a gradient of water level towards the dam but the slope is very small.

Between June 2003 and August 2006, the reservoir water level fluctuated yearly between elevations 135 m and 140 m. During this period of time, GPS ZG 93 was moving in a regular step-like pattern of an average of 0.170 m/year. The accumulated horizontal movement at ZG 93 between June 2003 and August 2006 was about 0.60 m.

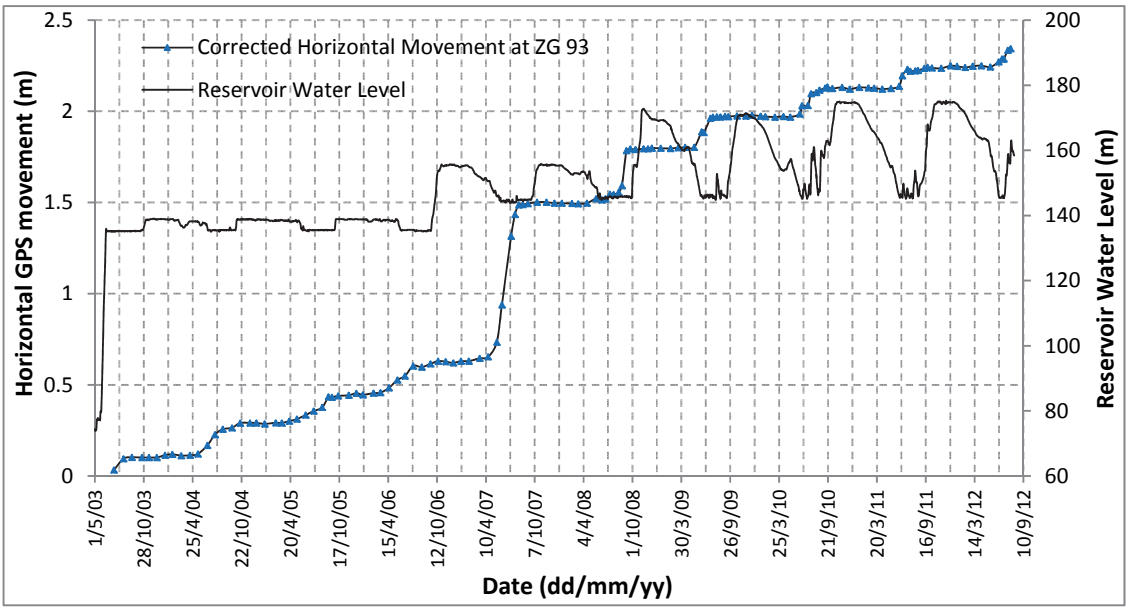

Figure 6.5: Corrected horizontal movement at GPS ZG 93 vs. reservoir water level

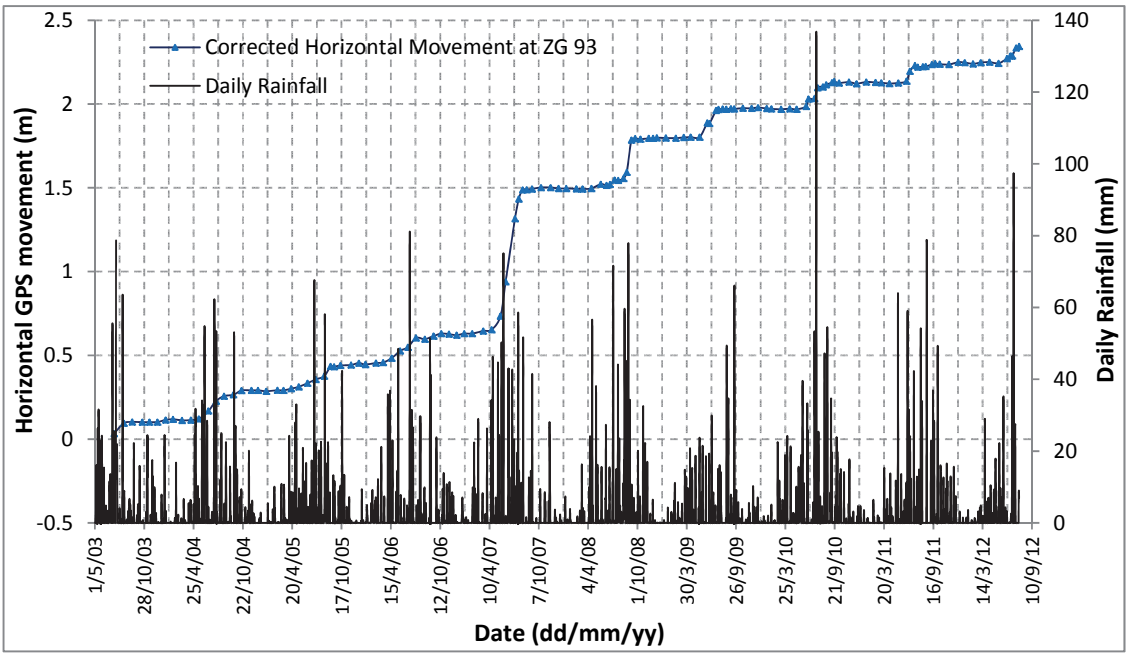

Figure 6.6: Corrected horizontal movement at GPS ZG 93 vs. daily rainfall

During September 2006 to October 2006, the reservoir water level at the dam was raised to 155 m. From October 2006 to September 2008, the reservoir water level fluctuated yearly between 155 m and 145 m. Accelerating horizontal movement of the

landslide was observed when the reservoir water level was dropped from 155 m to 145 m and remained at around 145 m level. The horizontal movement of the landslide slowed down during the period when the reservoir water level rose from 145 m to 155 m and remained high at 155 m.

In the year 2007, the landslide moved significantly during and after the first drawdown from 155 m reservoir water level. This fast and large movement started from April 18, 2007 and lasted until August 09, 2007, during which the horizontal movement along Section III-III' towards the river channel at ZG 93 was 0.834 meter. Because of the large movement in 2007, the accumulated horizontal movement at ZG 93 between August 2006 and September 2008 was about 1.197 meters.

During September 2008 and October 2008, the reservoir water level at the Three Gorges Dam was raised to 172 m. Since then, the reservoir water level started to fluctuate cyclically between 145 m and 175 m. The reservoir water level remained at 175 m during winter months in order to provide full hydro power generation. During rainy season in the summer, the reservoir water level was kept around 145 m for flood control.

Since September, 2008 the Baishuihe landslide had moved in a regular step-like pattern not like the large movement observed in 2007. The landslide moved faster when reservoir water level went down and stayed at around 145 m. There was little movement when the reservoir water level rose or remained high at around 175 m.

For accelerated horizontal movement at ZG 93 from September 2008 to July, 2012, the average horizontal movement rate was 2.31 mm/day. The average horizontal movement rate for the entire period of September 2008 to July, 2012 was 0.393 mm/day, which was 0.143 m/year. During this period of time, the cumulative horizontal movement at ZG 93 was 0.55 meter.

The relationship between horizontal movement and daily rainfall is presented in Figure 6.6. The rainfall data was obtained from Shazhenxi, a town where Baishuihe landslide is located. It is seen in this figure that rainy season occurs from May to September and there is no accelerated movement occurring beyond this period of time.

It should be noted that in the years 2008 and 2011, the horizontal movement of the landslide accelerated during the drawdown of the reservoir water level; however for these two years, the fastest movement rate occurred when the reservoir water level stayed at 145 m and after an intense rainfall. This means that movement of the landslide can be affected not only by the fluctuation of the reservoir water level, but also the intense rainfall from May to September each year.

6.3 Seepage Analysis of Baishuihe Landslide

Currently, there is no consistent groundwater information available for the Baishuihe landslide. Since soil properties and geology of Baishuihe landslide are similar to those of Shuping landslide, the material properties used for seepage analysis in Shuping landslide is adopted for Baishuihe landslide.

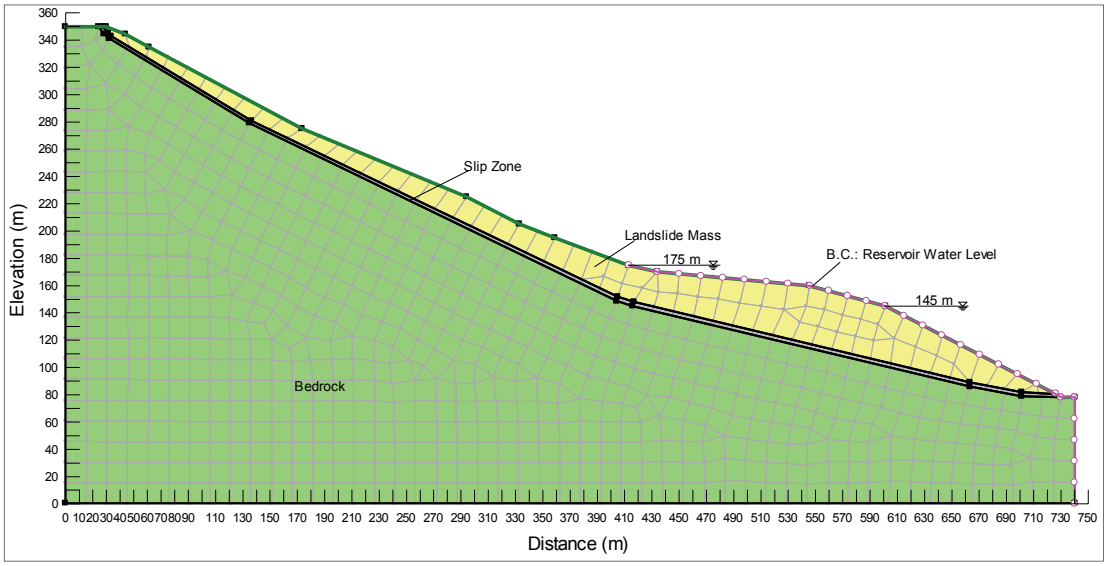

Figure 6.7: Seepage model for Baishuihe landslide (Section III-III')

Section III-III' in Figure 6.3 is selected for seepage analysis. Smoothing localized sharp angles on the ground surface and interface between different regions have been made to the original section III-III' in Figure 6.3. The seepage model for the Baishuihe landslide is shown in Figure 6.7. The seepage analysis is conducted with the following steps:

1. Steady-state seepage analysis. Steady-state seepage analysis is conducted first to generate the initial groundwater table and initial pore water pressure. Steady-state seepage analysis is the first step and lasts for 0 day. A constant total head of 146 m is applied to the toe of the landslide.

2. Transient seepage analysis. Transient seepage analysis is conducted to study the transient groundwater table in the landslide. The transient analysis has 1,140 steps and each step simulates 1 day. Therefore a complete transient seepage analysis simulates 1,140 days. Initial pore water pressure is based on previous steady-state seepage analysis. Variable total head vs. time, which is based on the observed daily reservoir water level at the Three Gorges Dam, is specified at the toe of the landslide. The total head vs. time is shown in Figure 6.8.

The saturated permeability for landslide mass, slip zone and bedrock regions of the Baishuihe transient seepage analysis is summarized in Table 6.3.1.

Table 6.3.1: Saturated permeability for transient seepage analysis

Seepage Model Region	k_H (m/day)	k_V (m/day)
Landslide Mass	0.1	0.01
Slip Zone	0.1	0.1
Bedrock	0.5	0.5

Currently there is no unsaturated laboratory permeability test conducted for the Baishuihe landslide. Unsaturated permeability tests have been conducted for soil samples from Sunjiazhuang landslide in Xingshan County, which is close to the Baishuihe

landslide. According to landslide observation reports from CTGU, geological history and composition of Baishuihe landslide and Sunjiazhuang landslide are quite similar. Baishuihe and Sunjiazhuang landslide are both colluvium landslides and their landslide masses are both quaternary colluvium materials. In addition, bedrock for both landslides belongs to Middle Triassic Period. Thus the saturated/unsaturated permeability test data of Sunjiazhuang landslide soil are used in seepage analysis of Baishuihe landslide. Detailed unsaturated permeability input for the seepage analysis is summarized in Appendix II.

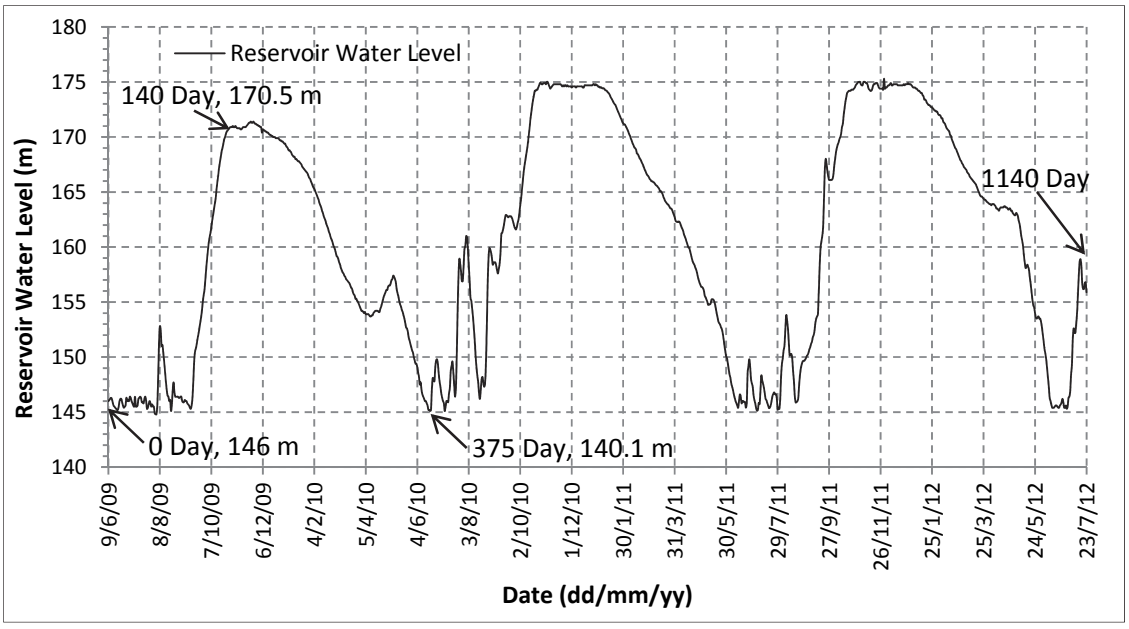

Figure 6.8: Variable total head vs. time for transient seepage analysis

The calculated pore pressure contours from transient seepage analysis on October 27, 2009 (140th Day) and June 19, 2010 (375th Day) are plotted in Figure 6.9 and Figure 6.10, respectively. Figure 6.9 shows the pore pressure contour when the reservoir just reached the highest level. The seepage velocity vectors show water mainly flows inward and upward during the rise of the reservoir water level. Because of relatively low permeability of the landslide soil, the time lag behind of the groundwater table in the Baishuihe landslide is very distinct. The groundwater table is consistent with the

reservoir water level near the ground surface. However for the area deep and close to the slip zone, the groundwater table is much lower than the reservoir water level. It is indicated in this figure that there is no significant increase of pore water pressure along the slip zone during the rise of reservoir water level.

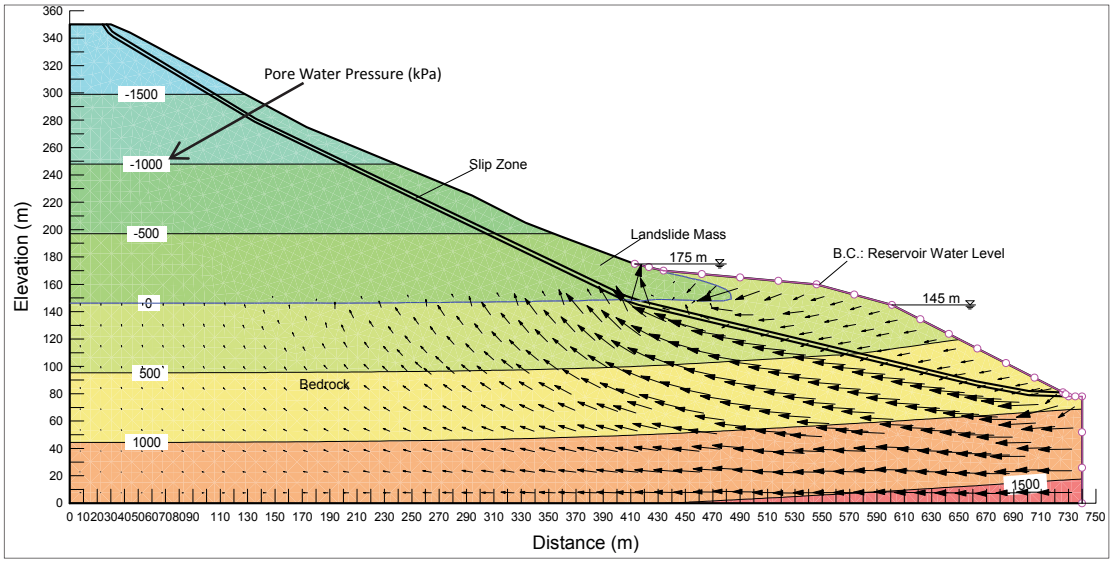

Figure 6.9: Pore pressure contour for Baishuihe on October 27, 2009 (140th Day)

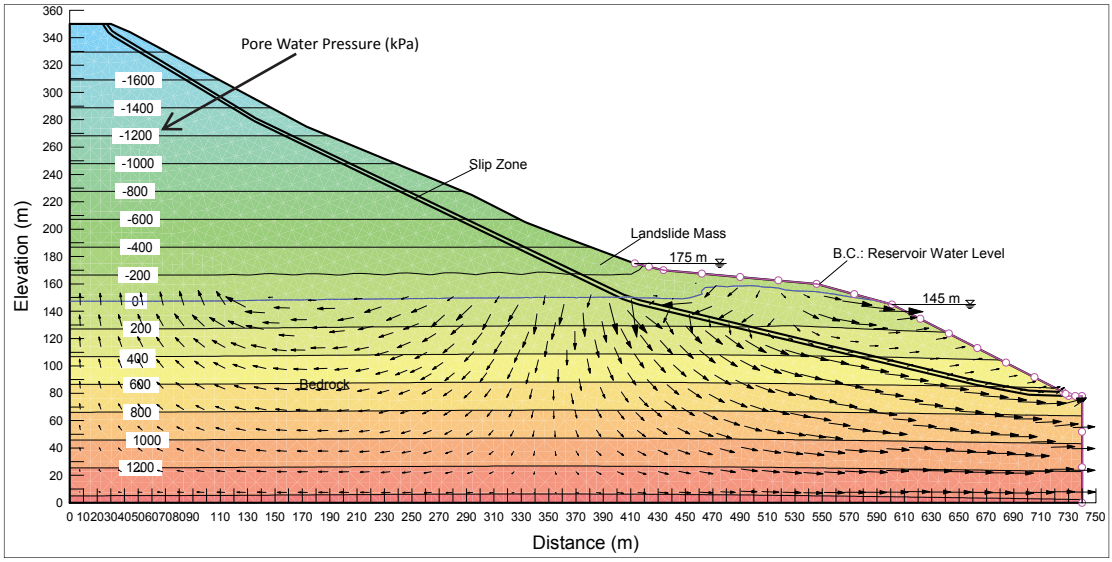

Figure 6.10: Pore pressure contour for Baishuihe on June 19, 2010 (375th Day)

Figure 6.10 presents the pore pressure contour when the reservoir just reached the

lowest level. The seepage velocity vectors show that in the landslide mass and bedrock, the groundwater flows both outward and inward. However, it should be noted that in both regions, the dominant seepage direction is outward towards the river channel. It is clear that the groundwater table lags behind the reservoir water level. The groundwater table is consistent with the reservoir water level near the ground surface. However for the area farther away from the ground surface, the groundwater table is higher than the reservoir water level. The pore pressure contour in this figure also indicates that there is no significant increase in pore water pressure along the slip zone when the reservoir water level drops. Seepage analysis of the Baishuihe landslide confirms the landslide belongs to Mechanism 1.

6.4 Stability Analysis of Baishuihe Landslide

Similar to Shuping landslide, SLOPE/W software is used for stability analysis of Baishuihe landslide. In SLOPE/W, the Morgenstern-Price method is adopted. The pore water pressure calculated from previous transient seepage analysis are imported to SLOPE/W. Since the landslide had slipped before, the slip surface for the stability analysis is fully specified which goes through the slip zone region. The stability model for the landslide is presented in Figure 6.11.

There is currently no laboratory test result available to determine the shear strength parameters of the soil in Baishuihe landslide. Since Shuping and Baishuihe landslides are located very close to each other and they have similar type of soil and geological history, the strength parameter for Shuping landslide are used in Baishuihe landslide analysis. The maximum, minimum and average values of cohesion and friction angle for Shuping landslide mass, slip zone and bedrock are summarized in Table 5.5.1.

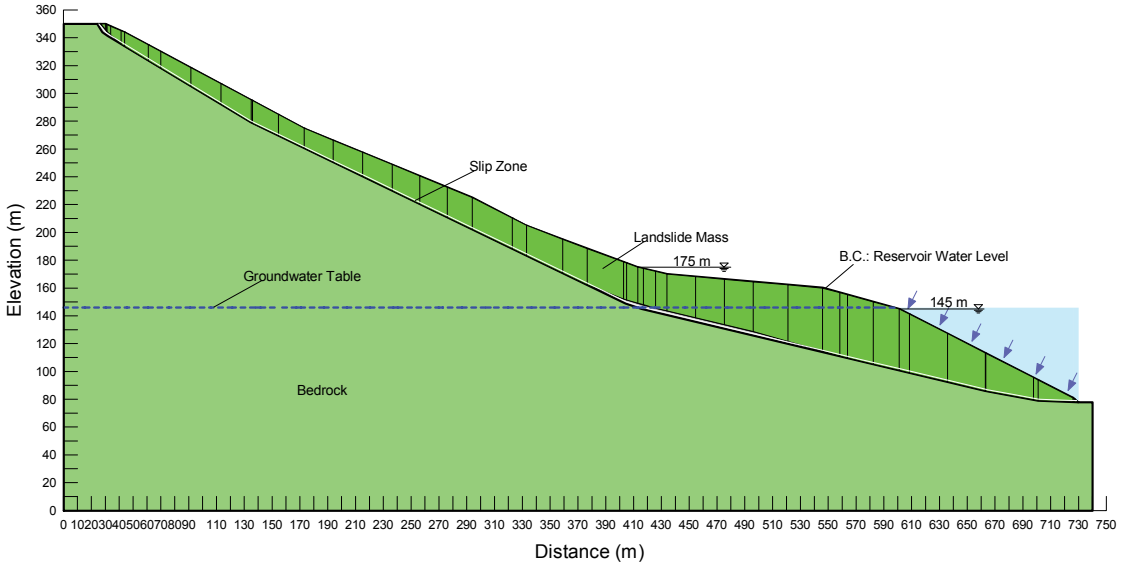

Figure 6.11: Stability model for Baishuihe landslide (Section III-III')

Table 6.4.1: Strength parameters used in stability analysis

Stability Model Region	Unit Weight (kN/m^3)	$c'(kPa)$	$\phi'(\circ)$
Landslide Mass	18	24.0	21.0
Slip Zone	18	20.0	19.0
		19.0	
		18.0	
		16.0	
		14.0	18.0
			17.0
			16.0
Bedrock	-	-	-

Based on the direct shear test results in Table 5.5.1, the strength parameters in Table 6.4.1 are selected for parameter stability study. The calculated factor of safety vs. time is plotted in Figures 6.12 and 6.13.

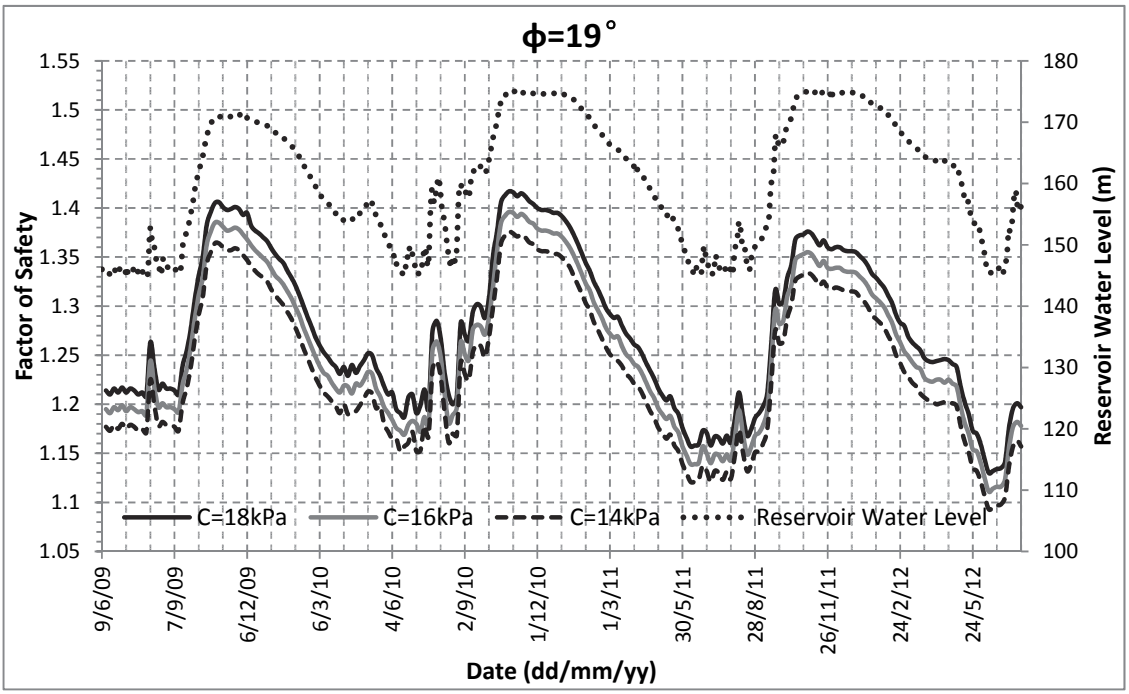

Figure 6.12: Factor of safety vs. time for Baishuihe landslide (ϕ=19°)

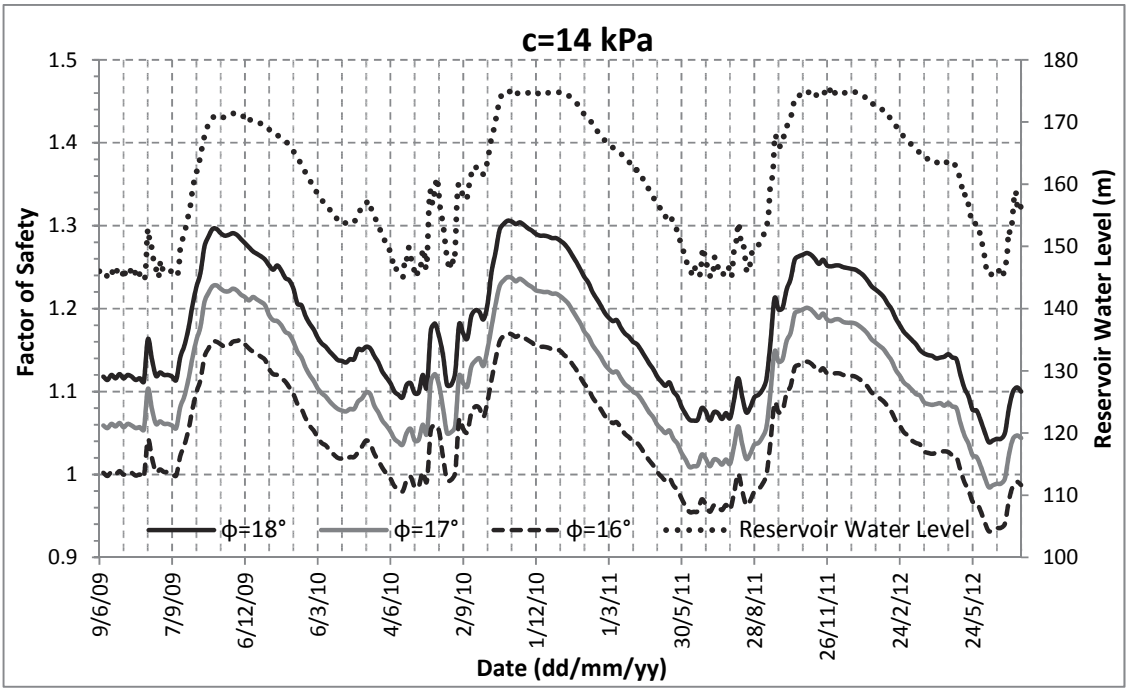

Figure 6.13: Factor of safety vs. time for Baishuihe landslide (c=14 kPa)

In Figure 6.12, the friction angle of the slip zone soil is fixed at 19° and cohesion is

decreased gradually. The trend of the factor of safety is consistent with the trend of the reservoir water level. The factor of safety increases when the reservoir water level rises. The factor of safety slightly drops when the reservoir water level remains at the highest level, and it decreases when the reservoir water level drops. The same pattern of factor of safety is found in Figure 6.13 where the cohesion of slip zone soil is fixed at 14 kPa and friction angle is decreased gradually.

The results of the stability analysis shown in Figure 6.12 and Figure 6.13 are consistent with Mechanism 1. On one hand, for Baishuihe landslide which has a low permeability, the rise of reservoir water level leads to higher factor of safety. When the landslide is more stable, its viscous movement rate becomes smaller. On the other hand, drawdown of the reservoir water level causes lower factor of safety. When the landslide is less stable, its viscous movement rate becomes larger, which means the landslide moves faster during the drawdown of the reservoir water level.

Comparing Figure 6.12 and Figure 6.13, the factor of safety for Baishuihe landslide is more sensitive to the changes in friction angle than the cohesion of the soil in the slip zone. By decreasing the cohesion from 18 kPa to 14 kPa, the factor of safety on June 9, 2009 drops from 1.214 to 1.177, which is only a 3.0 % decrease. However, by changing the friction angle from 18° to 17° only, the factor of safety on June 9, 2009 drops from 1.118 to 1.059, which is a 5.2 % decrease.

The factor of safety vs. time in Figure 6.12 and Figure 6.13 show the changing factor of safety for three years (three cycles). The maximum and minimum factor of safety for each cycle is summarized in Tables 6.4.2 and 6.4.3. The initial factor of safety on June 09, 2009 (0^{th} Day) is also included in these two tables for comparison. The maximum, minimum and initial factor of safety are also presented in Figures 6.14 and 6.15.

In Figures 6.14 and 6.15, the maximum factor of safety in Cycle 2 is higher than that in

Cycle 1. A reasonable explanation is that the peak reservoir water level in the Cycle 2 (174.9 m) is higher than that in Cycle 1 (171.4 m). The higher reservoir water level leads to higher hydrostatic pressure on the ground surface at the toe, which further stabilizes the landslide.

Table 6.4.2: Maximum and minimum factor of safety for each cycle (ϕ=19°)

c(kPa)	Initial FS	Max. FS			Min. FS		
		Cycle 1	Cycle 2	Cycle 3	Cycle 1	Cycle 2	Cycle 3
18	1.214	1.406	1.417	1.376	1.187	1.157	1.13
16	1.195	1.385	1.396	1.355	1.169	1.139	1.111
14	1.177	1.364	1.376	1.334	1.152	1.121	1.093
c(kPa)	Initial FS	Max. FS Increase (%)			Max. FS Decrease (%)		
		Cycle 1	Cycle 2	Cycle 3	Cycle 1	Cycle 2	Cycle 3
18	1.214	15.82	16.72	13.34	-2.22	-4.70	-6.92
16	1.195	15.90	16.82	13.39	-2.18	-4.69	-7.03
14	1.177	15.89	16.91	13.34	-2.12	-4.76	-7.14

Table 6.4.3: Maximum and minimum factor of safety for each cycle (c=14 kPa)

ϕ(°)	Initial FS	Max. FS			Min. FS		
		Cycle 1	Cycle 2	Cycle 3	Cycle 1	Cycle 2	Cycle 3
18	1.118	1.296	1.306	1.267	1.093	1.065	1.039
17	1.059	1.228	1.238	1.201	1.036	1.009	0.9847
16	1.002	1.162	1.170	1.136	0.980	0.955	0.932
ϕ(°)	Initial FS	Max. FS Increase (%)			Max. FS Decrease (%)		
		Cycle 1	Cycle 2	Cycle 3	Cycle 1	Cycle 2	Cycle 3
18	1.118	15.92	16.82	13.33	-2.24	-4.74	-7.07
17	1.059	15.96	16.90	13.41	-2.17	-4.72	-7.02
16	1.002	15.97	16.77	13.37	-2.24	-4.72	-7.03

In these two figures, the minimum factor of safety in Cycle 2 lies below that in Cycle 1. In addition, the maximum and minimum factor of safety in Cycle 3 are below those in Cycle 2. It is because the groundwater in landslide lags behind the reservoir level during drawdown in Cycle 2. The lagged-behind groundwater helps building higher pore pressure in the landslide which leads to lower stability.

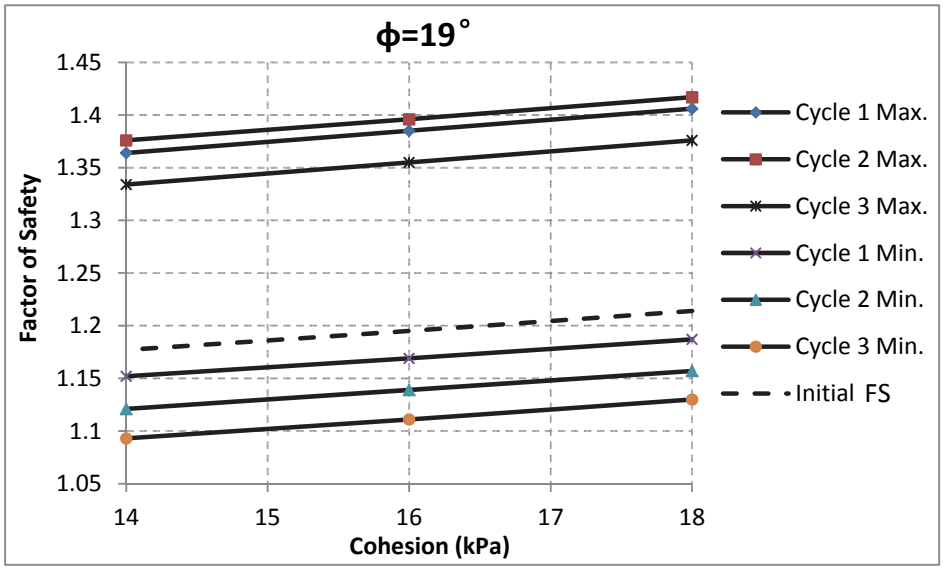

Figure 6.14: Maximum, minimum and initial factor of safety (ϕ=19°)

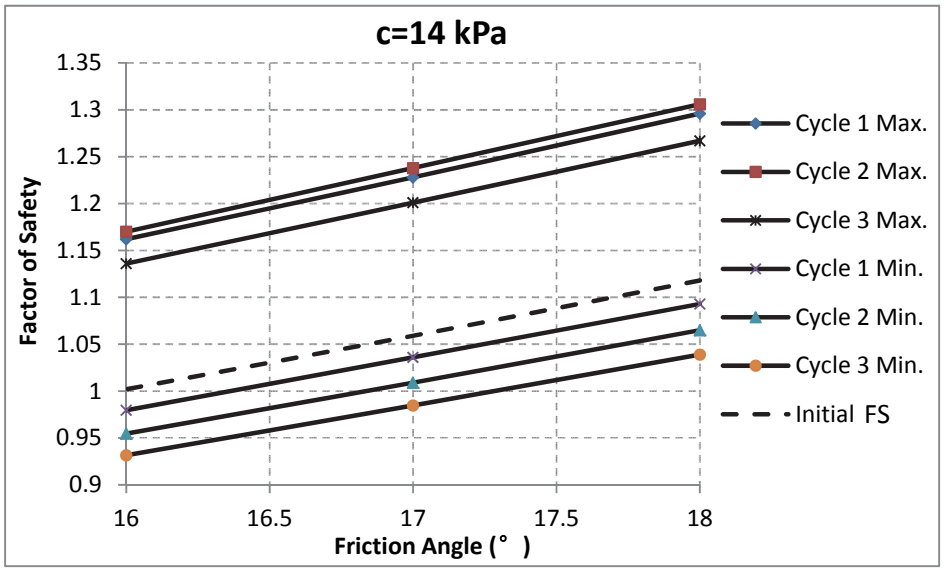

Figure 6.15: Maximum, minimum and initial factor of safety (c=14 kPa)

In addition, Figures 6.14 and 6.15 also indicate that the initial factor of safety, which corresponds to a reservoir water level of 146 m, is smaller than the maximum factor of safety and larger than the minimum factor of safety. Thus, the landslide is most stable when reservoir is rising and just before reaching the peak. The landslide is less stable at constant low reservoir water level. The least stable condition occurs during the drawdown of the reservoir water level.

The maximum percentage of increase and decrease from the initial factor of safety is calculated and summarized in Tables 6.4.2 and 6.4.3. It can be seen that during the three cycles of reservoir water level fluctuations, the stability of the landslide is increased by up to 17 % (FOS increased from 1.18 to 1.38) during rising of the reservoir water level. In addition, the stability of the landslide is lowered by up to 8 % (FOS deceased from 1.18 to 1.09) because of the reservoir water level drawdown. Thus, the fluctuation of reservoir water level can have a large impact on the stability of the landslide. Since the movement of the Baishuihe landslide is time dependent, its movement rate is much dependent on the stability of the landslide. The landslide moves slowly when its factor of safety is relatively high. When its stability is reduced by reservoir drawdown or other factors, accelerated movement may occur. In the back analysis of the friction angle and the cohesion of the slip zone, a criterion is set such that the landslide movement starts to accelerate when the factor of safety is close to one. The horizontal movement at GPS ZG 93 and the factor of safety for c=14 kPa and ϕ=16° of the slip zone soil are plotted in Figure 6.16. It can be seen that the landslide movement starts to increase significantly when the factor of safety drops below 1.0. Therefore cohesion and friction values of c=14 kPa and ϕ=16° are the most appropriate shear strength parameters for the slip zone soil based on back analysis. Compared with strength parameters from saturated drained direct shear test in Table 5.5.1, the back calculated strength parameters match well with laboratory test results.

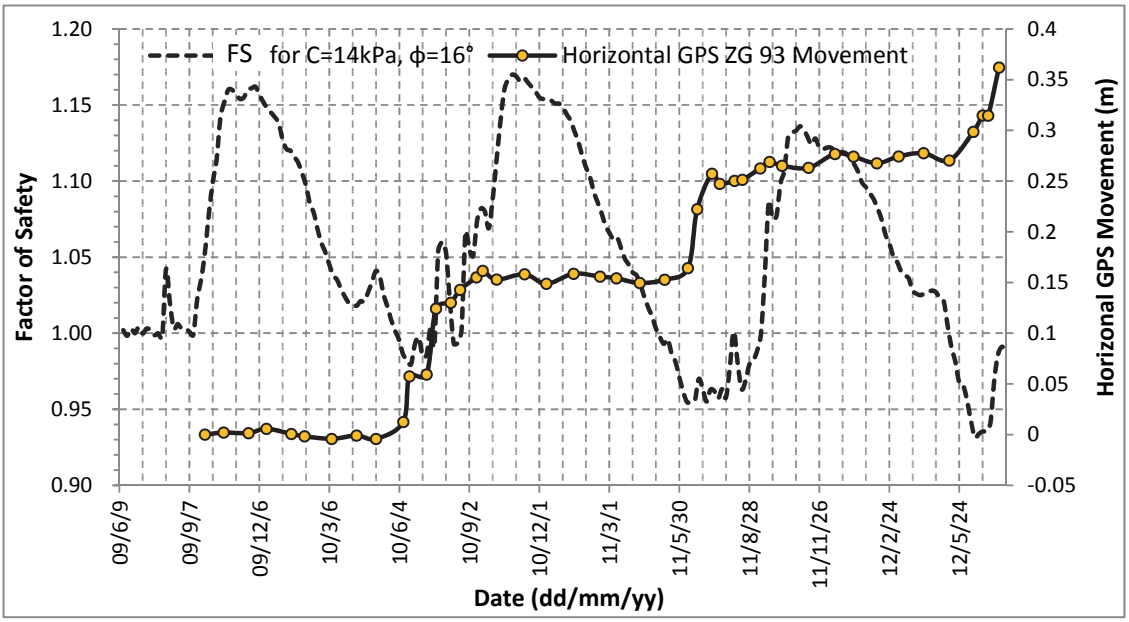

Figure 6.16: Movement and factor of safety of Baishuihe landslide

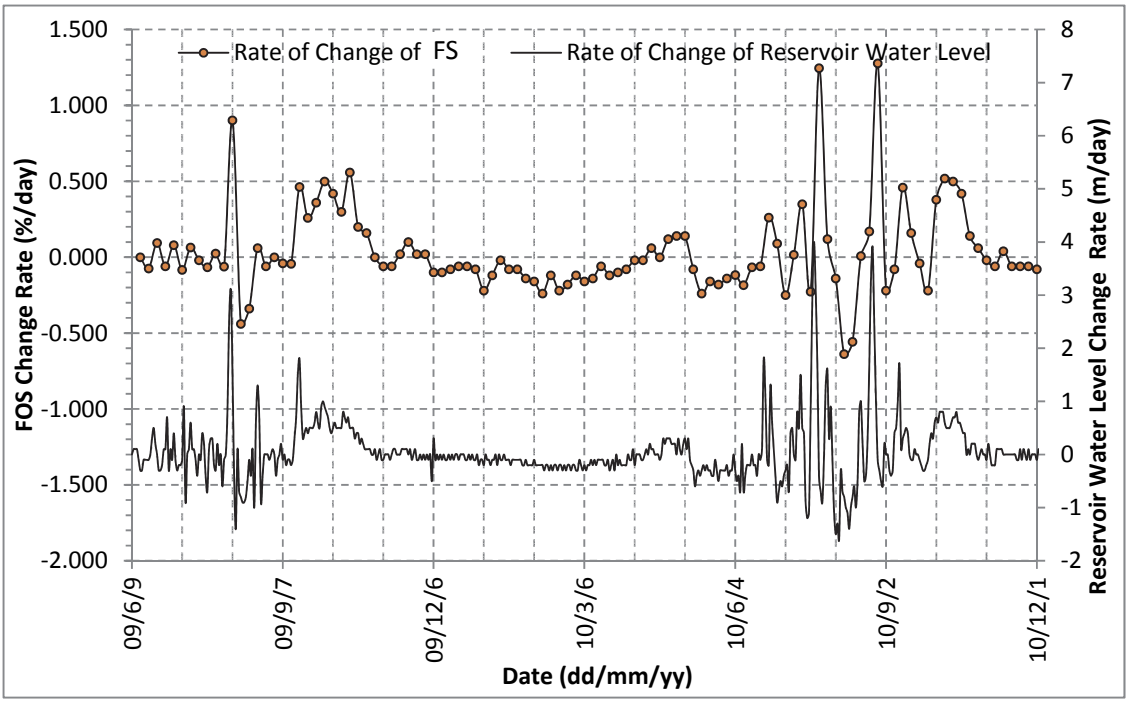

Figure 6.17: Rate of factor of safety and reservoir water level change for Baishuihe

More analyses have also been conducted on the rate of change of the factor of safety and the rate of change of the reservoir water level. It is clearly indicated in Figure 6.17

that the rate of change of the factor of safety is generally proportional to the rate of change of the reservoir water level. The highest rate of rising of reservoir water level is +3.9 m/day on August 25, 2010 and the corresponding rate of change of the factor of safety is +1.28 %/day. The highest rate of reservoir water level drawdown is -1.5 m/day on August 03, 2010 and the corresponding change in factor of safety is -0.64 %/day. This shows that the rate of change of the factor of safety is very sensitive to the rate of rate of change of the reservoir water level. Thus, the drawdown rate of the reservoir water level should be under very careful control to avoid sharp decrease of stability and landslide failure.

6.5 Movement Analysis of Baishuihe Landslide

ABAQUS 6.12 software is used to carry out 2D finite element modeling of the Baishuihe landslide. The analysis is based on Section III-III' in Figure 6.3. The configuration and mesh of the finite element model are shown in Figures 6.18 and 6.19, respectively.

In Figures 6.18 and 6.19, the horizontal length of the model is 740 m, and the vertical height is 350 m. The elevation at the bottom of both figures is equal to zero meter.

In Figure 6.19, the horizontal movement of the left and right boundaries of the landslide is fixed but they are free to move vertically. The bottom of the landslide is fixed in both horizontal and vertical directions. Coupled pore fluid/stress analyses were carried out using ABAQUS. The analysis started on November 1, 2009 as the beginning of time (0^{th} Day).

The first step in modeling is to conduct steady-state geostatic analysis. The initial reservoir water level at the toe of the landslide is set at an elevation of 171.0 m and gravity is activated during this step. When this geostatic step is completed, the initial stress field and initial pore pressure field are generated for the subsequent transient

pore fluid/stress analysis.

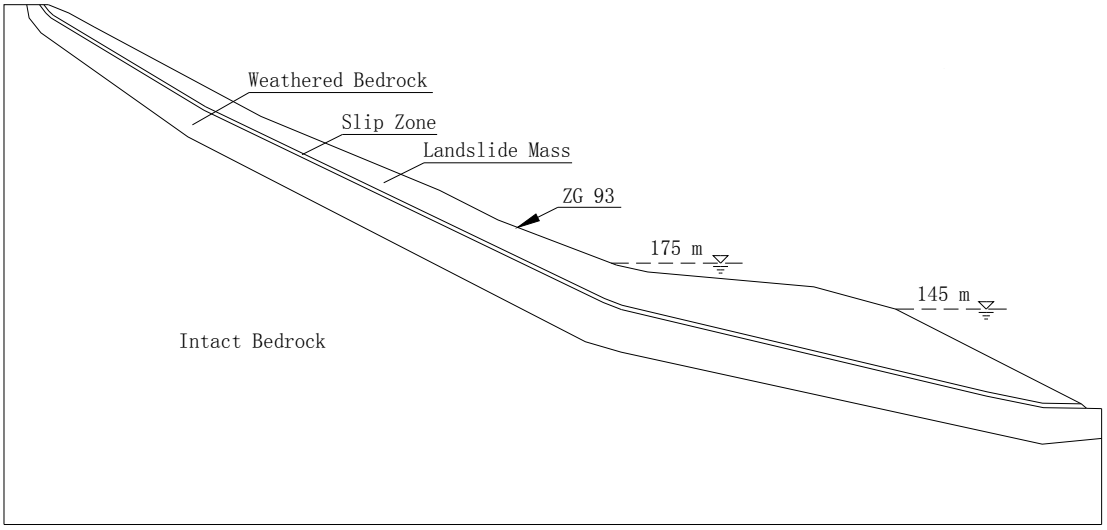

Figure 6.18: Configuration of the Baishuihe landslide model in ABAQUS

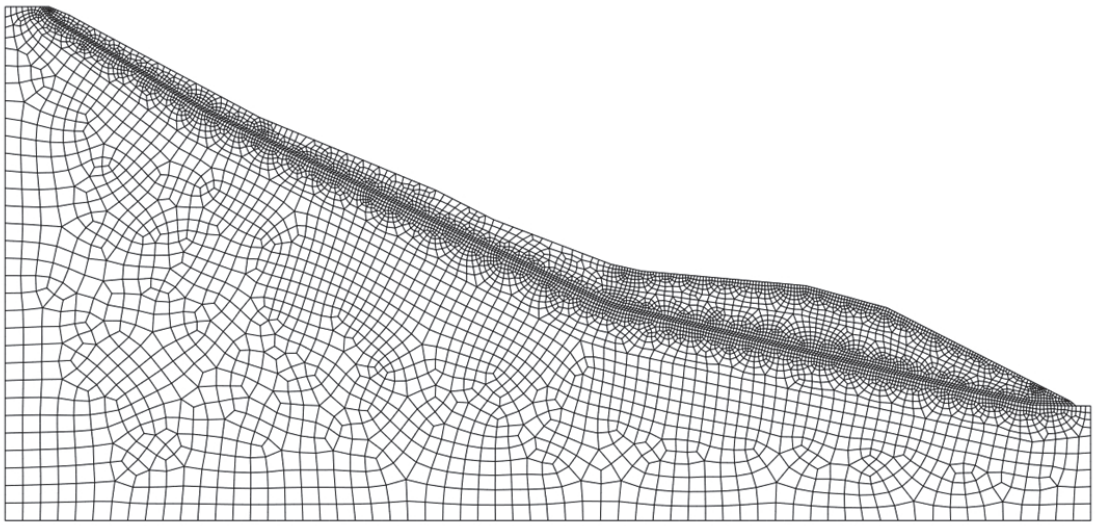

Figure 6.19: Finite element mesh of Baishuihe landslide using ABAQUS

Following the first step of the steady-state analysis, the boundary condition of pore water pressure and load condition of hydrostatic pressure at the toe of the landslide are changed to simulate reservoir water level fluctuation. The elevations of the reservoir water level are based on the recorded daily reservoir water level at the Three Gorges

Dam. Modifications such as smoothing short-term sharp changes or back-and-forth changes have been made to the original recorded water level data for better convergence of the finite element model. The reservoir water level between Nov 2009 and Jan 2011 is shown in Figure 6.20.

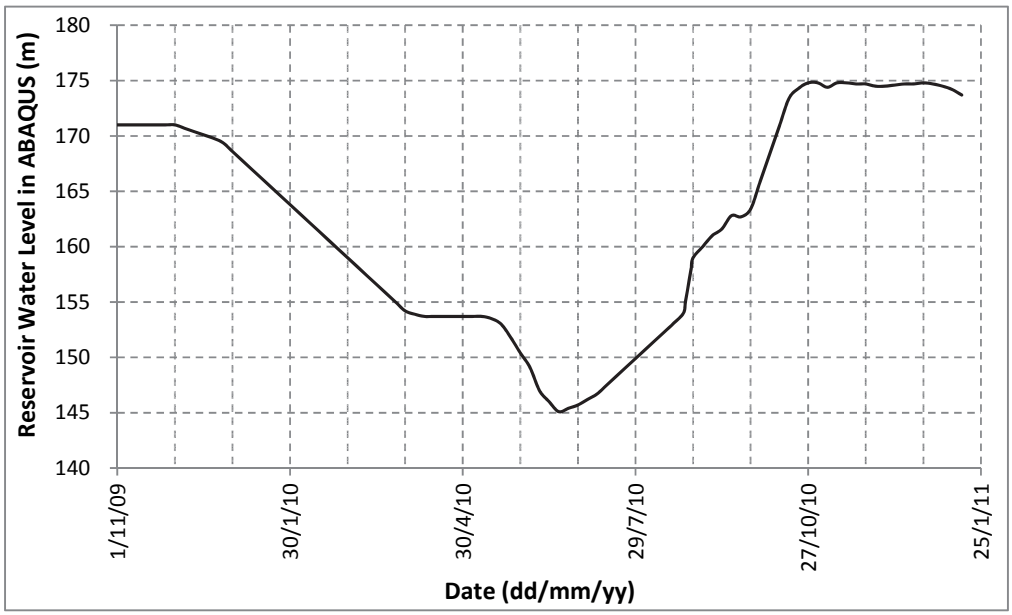

Figure 6.20: Reservoir water level boundary condition for the ABAQUS model (Baishuihe)

The landslide mass, slip zone and bedrock are assumed to be isotropic and homogeneous for the Baishuihe movement analysis. Based on the previous SEEP/W analysis, the saturated permeability is summarized in Table 6.5.1.

Table 6.5.1: Saturated permeability for Baishuihe movement analysis

Seepage Model Region	Landslide Mass	Slip Zone	Bedrock
$k_H=k_V$ (m/day)	0.1	0.1	0.5

In ABAQUS, the unsaturated hydraulic conductivity k_{usat} is defined by,

$$k_{usat} = k_s \times k \tag{6.1}$$

The k_s-Saturation and Saturation-Pore Pressure relationships for the ABAQUS modeling of Baishuihe landslide are summarized in Appendix II.

The rate-dependent Drucker-Prager constitutive model, which is developed in Chapter 4, has been implemented to model the slip zone. Similar to Shuping landslide, it is assumed that there is a 10% increase in cohesion for every tenfold increase in strain rate. Strain softening Drucker-Prager plasticity has been implemented to model the landslide mass and weathered bedrock. Linear elasticity is implemented for the intact bedrock.

The elastic and plastic soil parameters for each region of the finite element deformation model are listed in Table 6.5.2. Parameters in this table are selected based on laboratory tests and modeling results of the report from CTGU (The Ministry of Education Key Laboratory of the Three Gorges Reservoir Geological Disasters, 2012). Based on the report, the friction angle and UCS at zero strain presented in this table are back calculated from the finite element model for the best-fit movement curve. Similar to the Shuping landslide, for the strain-rate hardening of the slip zone material, the relationship between yield stress ratio and equivalent plastic strain rate is presented in Table 6.5.3.

Table 6.5.2: Elastic and plastic parameters for Baishuihe ABAQUS model

	Dry Density (kg/m^3)	E (MPa)	Poisson's Ratio	Friction Angle $\beta(\circ)$	Flow Stress Ratio	Dilation Angle $\psi(\circ)$	UCS at Strain=0 (kPa)
Landslide Mass	1650	20.8	0.28	32.0	1	10	60.0
Slip Zone	1650	20.8	0.30	29.0	1	10	40.0
Weathered Bedrock	1650	30.0	0.28	40.0	1	10	60.0
Intact Bedrock	2000	61000	0.21	-	-	-	-

Table 6.5.3: Yield stress ratio and equivalent plastic strain rate for Baishuihe

Yield Stress Ratio	1.0	1.1	1.21	1.331	1.4641	1.61051
Equivalent Plastic Strain Rate (s^{-1})	0	1.16E-09	1.16E-08	1.16E-07	1.16E-06	1.16E-05

In Figure 6.20, the reservoir water level went down and reached the lowest level (145.1 m) on June 19th, 2010. The reservoir then rised and reached the highest level (174.8 m) on October 27th, 2010. From coupled pore fluid/stress calculation, locations of groundwater table at the toe on June 19th, 2010 and October 27th, 2010 are shown in Figures 6.21 and 6.22, respectively. In both two figures, the boundary between the light grey color and the dark grey color marks the groundwater table.

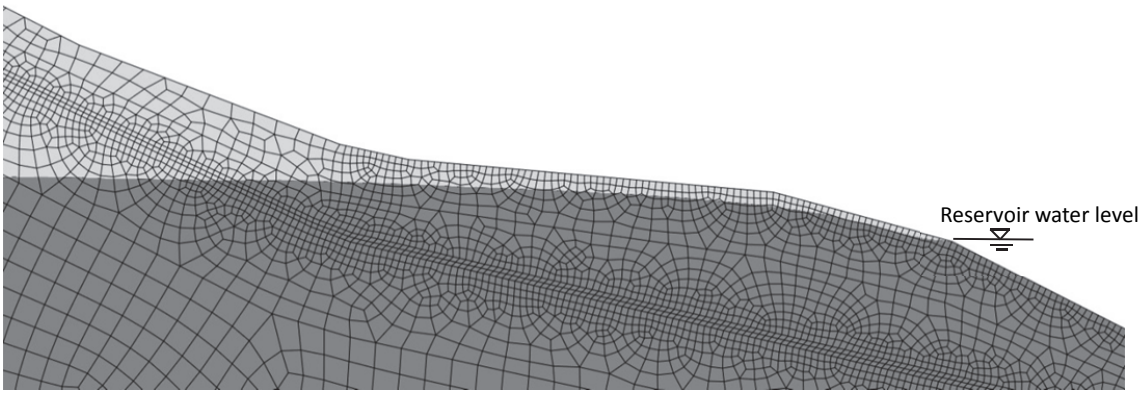

Figure 6.21: Location of groundwater table on June 19th, 2010 (lowest level 145.1 m)

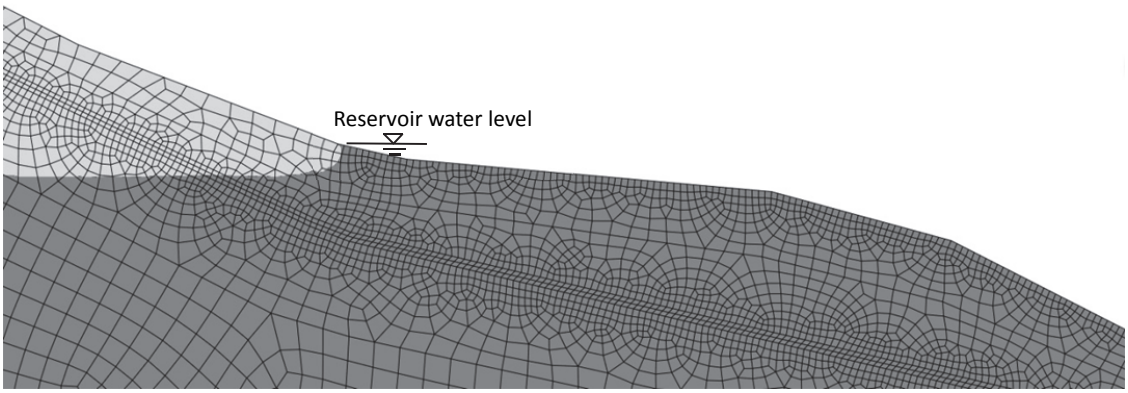

Figure 6.22: Location of groundwater table on October 27th, 2010 (highest level 174.8 m)

In Figure 6.21, since the permeability of the landslide is relatively low, the groundwater

table in the landslide lags behind the reservoir water level. The outward seepage force and less hydrostatic pressure at the toe make the landslide less stable and move faster during reservoir drawdown. In Figure 6.22, groundwater table in the landslide also lags behind the reservoir water level. The inward seepage force and increased hydrostatic pressure at the toe make the landslide more stable and move slower when reservoir water level is rising.

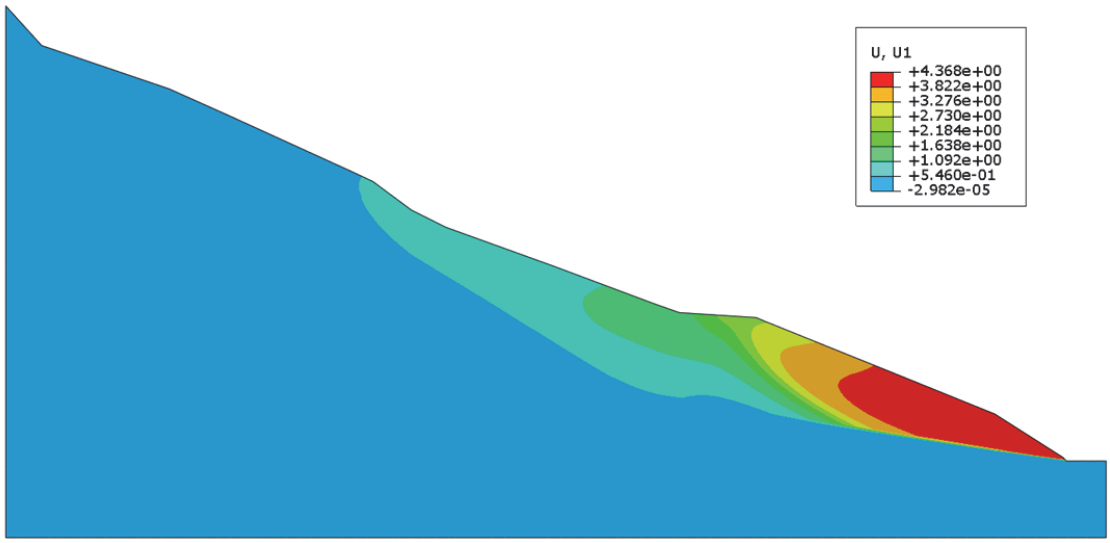

Figure 6.23: Contours of horizontal movement (January 23rd, 2011)

Contours of calculated horizontal movement for January 23rd, 2011 (the last step of the finite element analysis) are plotted in Figure 6.23. It is indicated in this figure that most horizontal movement is located at the toe. The amount of landslide movement decreases as the elevation increases uphill.

The calculated horizontal movement at ZG 93 from the pore fluid /stress analysis is plotted in Figure 6.24. The reservoir water level boundary condition in ABAQUS, monitored reservoir water level and monitored horizontal landslide movement at GPS station ZG 93 are also plotted in Figure 6.24 for comparison.

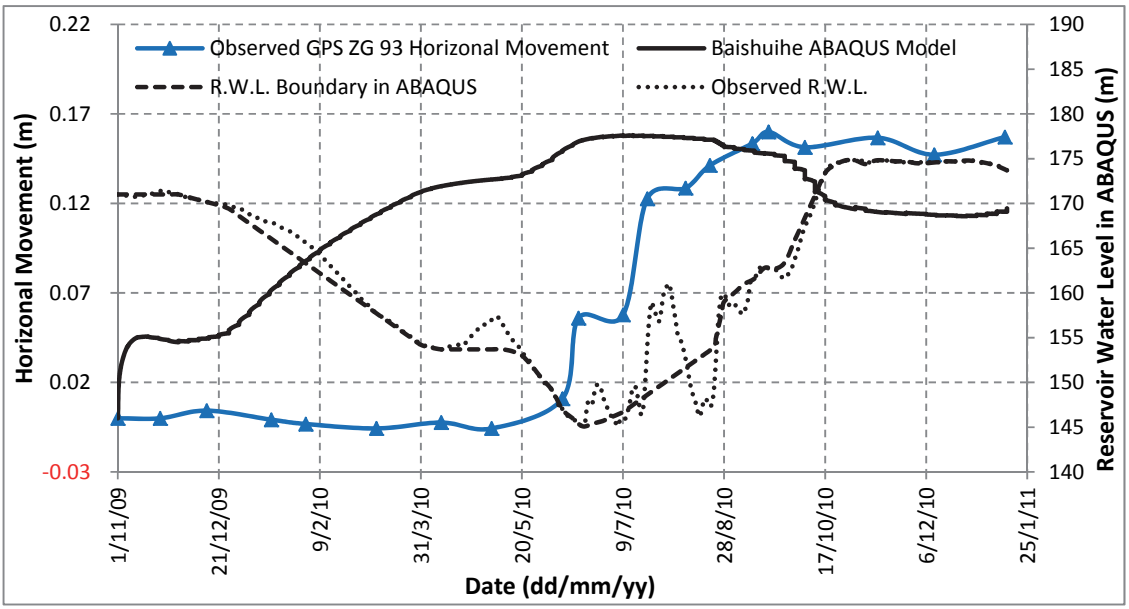

Figure 6.24: Horizontal movement at GPS station ZG 93 vs. time

In Figure 6.24, the reservoir water level boundary in ABAQUS is smoother than the observed reservoir water level for better numerical convergence. The horizontal movements from the finite element model and from the GPS station are close at the end of the analysis. However, the pattern of the movement from the finite element model is different from that of the field observations. The calculated movement increases steadily during the whole period of reservoir water level drawdown and then decreases a little bit during the rise of the reservoir water level. The observed movement from the GPS at ZG 93 remains almost constant during most part of the reservoir water level drawdown and then increases sharply at the end of drawdown. The observed landslide movement slows down when reservoir water level rises and remains at the highest level.

An explanation for the difference between movement pattern from the finite element model and GPS observation is the influence of steady and intense rainfall. In Figure 6.25, the recorded daily rainfall in the Shazhenxi Town is presented with the observed GPS horizontal movement at ZG 93. In this figure, the accelerated landslide movement is accompanied by steady and intense rainfall during May to August in 2010. The influence

of rainfall on landslide displacement will be studied and discussed in the future and not included in this research.

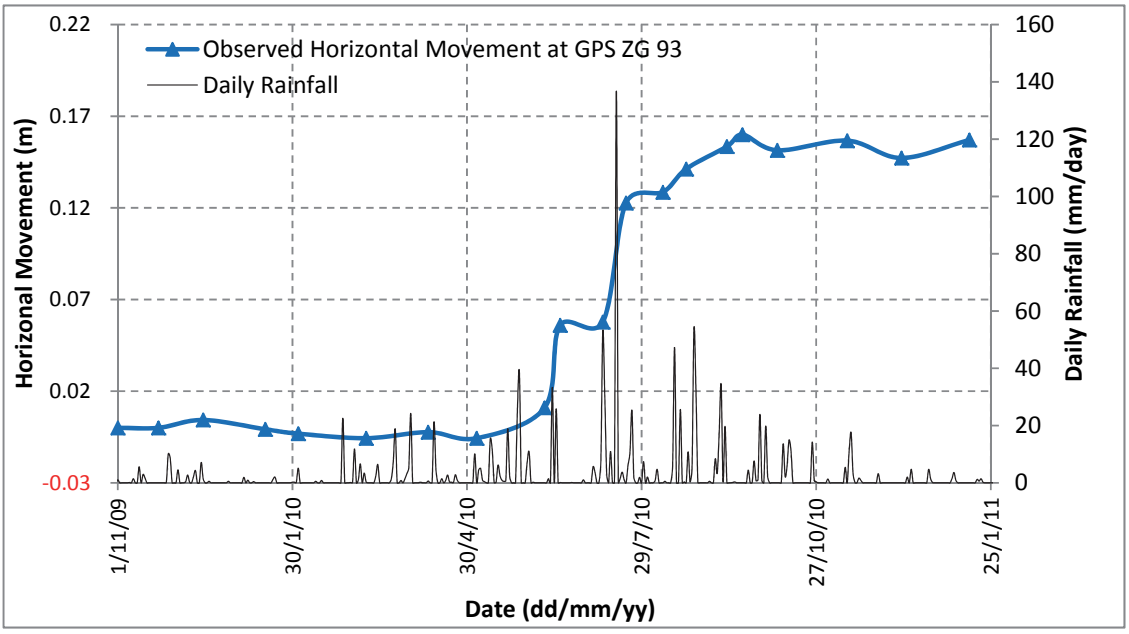

Figure 6.25: Observed horizontal movement and daily rainfall for Baishuihe

The above evidences from the finite element model and GPS records show that Baishuihe landslide also belongs to Mechanism 1. Because of the low permeability, the outward seepage force due to lagged-behind groundwater table and less hydrostatic pressure at the toe make the landslide less stable and tend to move faster during the reservoir drawdown.

In addition, the steady and intense rainfall at the end of reservoir drawdown and when reservoir stays at the lowest level increases the groundwater table and adds weight to the landslide mass, which further decreases the landslide stability and leads to the sharp increase of landslide movement.

One of the evidence of groundwater table rise due to rainfall is shown in Figure 6.1. There are four seasonal water pounds between elevations 165 m and 175 m near

Section III-III' during the rainy season when reservoir water level is around 145 m. Local residents have reported that these pounds are empty during dry seasons. The other evidence is that many small ground surface flows and small wet lands are found above the 175 m on the landslide on sunny days during the rainy season. Thus these ground surface flows and wet lands are indications of spring outcrop, which shows that the groundwater table is very close to the ground surface along the whole landslide during rainy seasons.

In the coupled pore fluid/stress analysis in this research, rainfall is not considered. Therefore the patterns of landslide movement from finite element modeling and GPS observation are different during the reservoir drawdown.

When the reservoir water level rises, inward seepage force due to lagged-behind groundwater table and larger hydrostatic pressure on the ground surface at the toe increase the stability and decelerate the landslide movement. It is shown in Table 6.4.2 and Table 6.4.3 that the maximum increase of factor of safety from the initial value can be as much as 17% during reservoir rising. The rise of reservoir water level is the controlling factor of landslide stability and movement during impoundment, which explains the deceleration of landslide movement in September, 2010 when there is still a lot of rain but the landslide movement decelerates.

For the Baishuihe landslide, experiments such as ring shear tests and direct shear tests should be conducted to further study the peak and residual strength parameters, as well as strain-rate hardening characteristics of the slip zone soil. Laboratory tests under different hydraulic pressure can be conducted to study the softening of slip zone soil under cyclic wetting and drying. In addition, unsaturated seepage tests can be conducted to get saturated/unsaturated p for the analysis of landslide movement under the effect of reservoir level fluctuation and precipitation.

Chapter 7 Case Study 3-Muyubao Landslide-Based on Mechanism 2

GPS observation data shows that Muyubao landslide moves faster when reservoir level rises and keeps at a high level. An introduction of the plan view, cross section as well as geology of Muyubao landslide is given in this chapter. The observed ground surface movement and reservoir water level are illustrated and discussed in detail. The relationship between observed movement and rainfall shows that rainfall has almost no impact on the landslide movement.

Seepage, stability and coupled fluid/stress were conducted based on the postulations of Mechanism 2. Analysis results are presented and discussed in this chapter. The calculated factor of safety decreases and movement accelerates when reservoir water level increases, which verifies the proposed Mechanism 2.

7.1 Introduction to Muyubao Landslide

The Muyubao landslide is an old landslide which slipped about 1.1 million years ago (The Ministry of Education Key Laboratory of the Three Gorges Reservoir Geological Disasters, 2012). The landslide is located on the southern bank of the Yangtze River in the Three Gorges reservoir area in Shazhenxi Town, Zigui County, Hubei province, China. It is located about 50 km upstream of the Three Gorges Dam. A plan view of the Muyubao landslide is shown in Figure 7.1.

The north-south length of the landslide is about 1300 m and the east-west width is around 1200 m. The average thickness of the landslide mass is about 50 meters with an estimated total volume of about 78.0 million m^3.

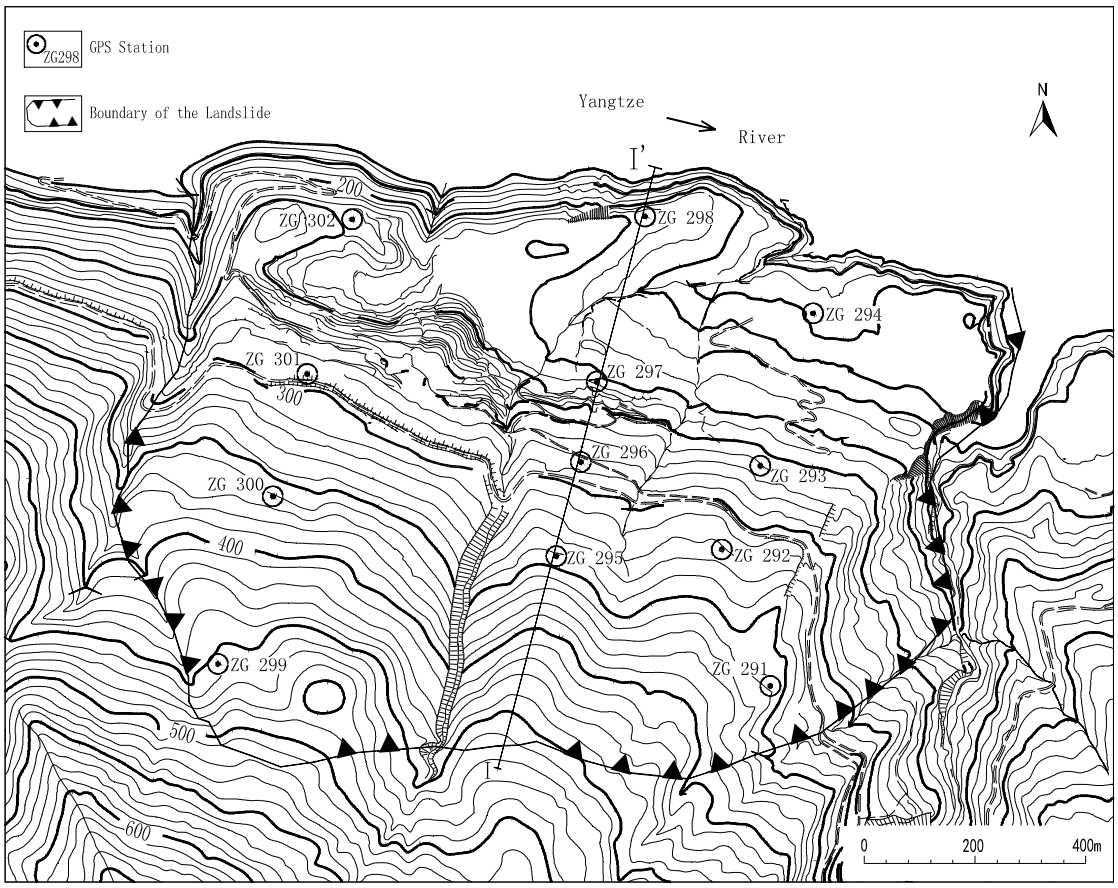

Figure 7.1: A plan view of Muyubao landslide

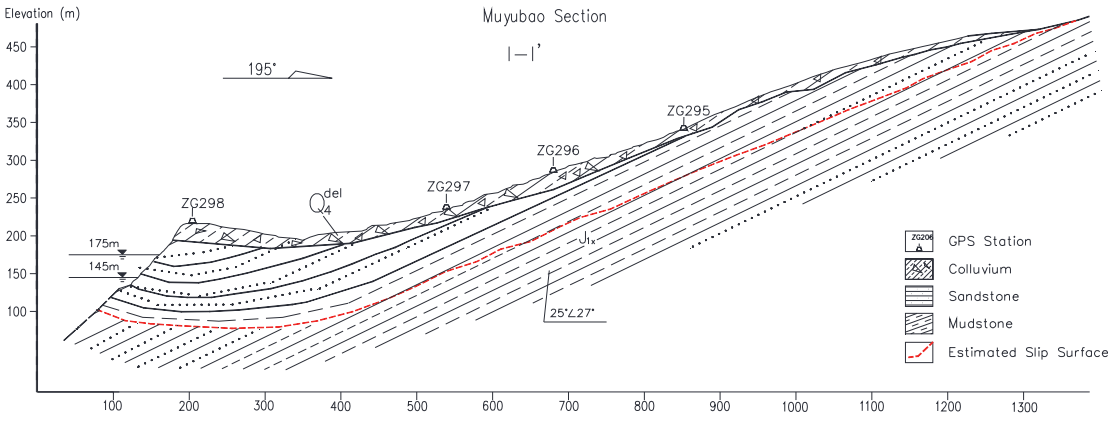

Figure 7.2: Section I-I' of Muyubao landslide

Cross section I-I' is taken in the middle of the Muyubao landslide, where four GPS stations are located along this section. Cross section I-I' is presented in Figure 7.2.

In Figure 7.2, the landslide mass consists of two layers. The upper layer of the landside mass is quaternary colluvium (Q^{del}), which mainly consists of clay and colluvial rock debris. The lower layer mainly consists of disturbed bedded quartz sandstone. The lower landslide mass is highly broken at the toe and it is relatively intact in the middle and at the top of the landslide.

The shape of the existing slip zone is circular at the toe and planar for the middle and top of the landside. The landslide mass slips along a weak silty mudstone layer in the middle and top of the landslide and the average thickness of the landslide mass is about 65 m. The slip surface shears through bedrock layers at the toe and its outcrop is around an elevation of 100 m. The maximum depth of the slip zone at the toe can reach as much as 135 m.

The bedrock underneath the slip zone at the middle and top of the landslide is mainly bedded mudstone. At the toe, the bedrock is mainly bedded sandstone and mudstone.

7.2 Reservoir Water Level, Daily Rainfall and Muyubao Landslide Movement

The water level of Yangtze River at Muyubao landslide before the impoundment of the Three Gorges Dam was about 74 m. The Three Gorges dam started its first impoundment in May, 2003 and the reservoir water level at the dam was raised to 135 m.

To record the movement of the landslide, twelve GPS stations were installed on the ground surface of the landslide in September 2006. Locations of the GPS stations are plotted in Figure 7.1. The landslide movement record is available from October 14, 2006 to July 25, 2012 and is plotted in Figure 7.3 to Figure 7.5. Until July 25, 2012, the average accumulated horizontal movement of GPS ZG 291, ZG 292, ZG 293 and ZG 294 is 1135.7 mm; the average accumulated horizontal movement of GPS ZG 295, ZG 296, ZG 297 and ZG 298 is 962.8 mm; the average accumulated horizontal movement of GPS ZG 299, ZG

300, ZG 301 and ZG 302 is 908.8 mm. It can be seen that the average accumulated horizontal movement decreases from east to west. Thus, Section I-I', which is almost on the center line of the Muyubao plan view, is chosen as the representative section for the subsequent 2D numerical analysis.

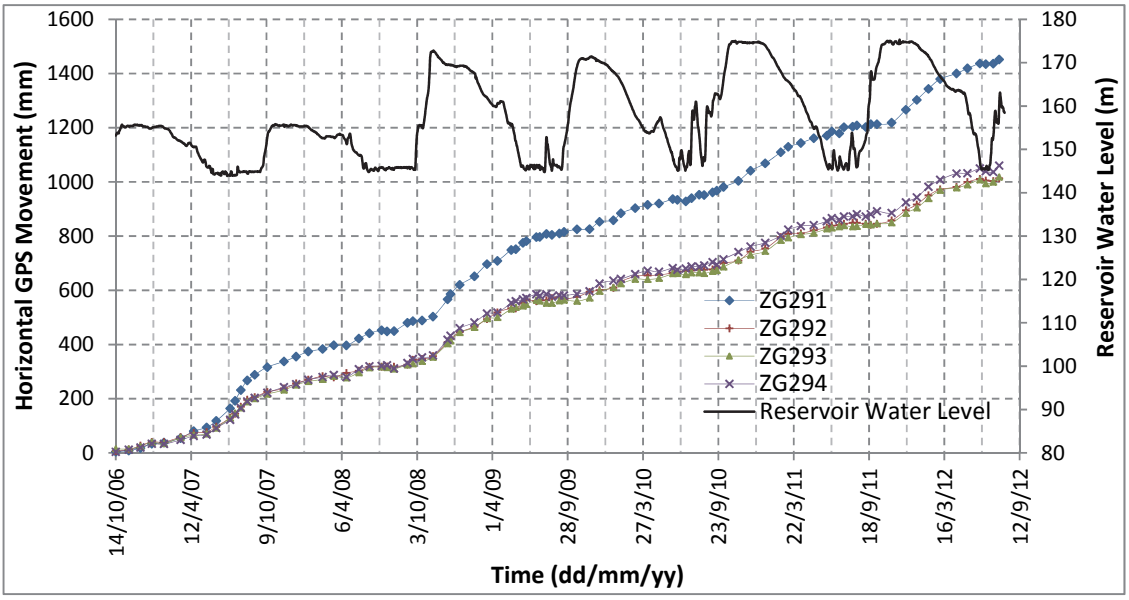

Figure 7.3: Horizontal movement of GPS stations (ZG 291 to ZG 294)

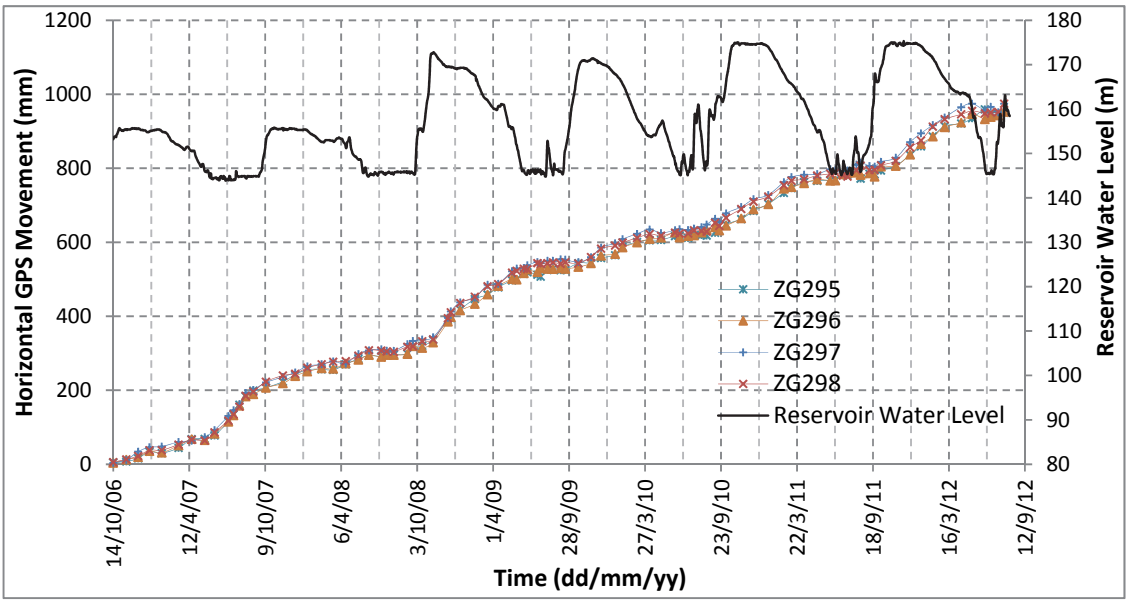

Figure 7.4: Horizontal movement of GPS stations (ZG 295 to ZG 298)

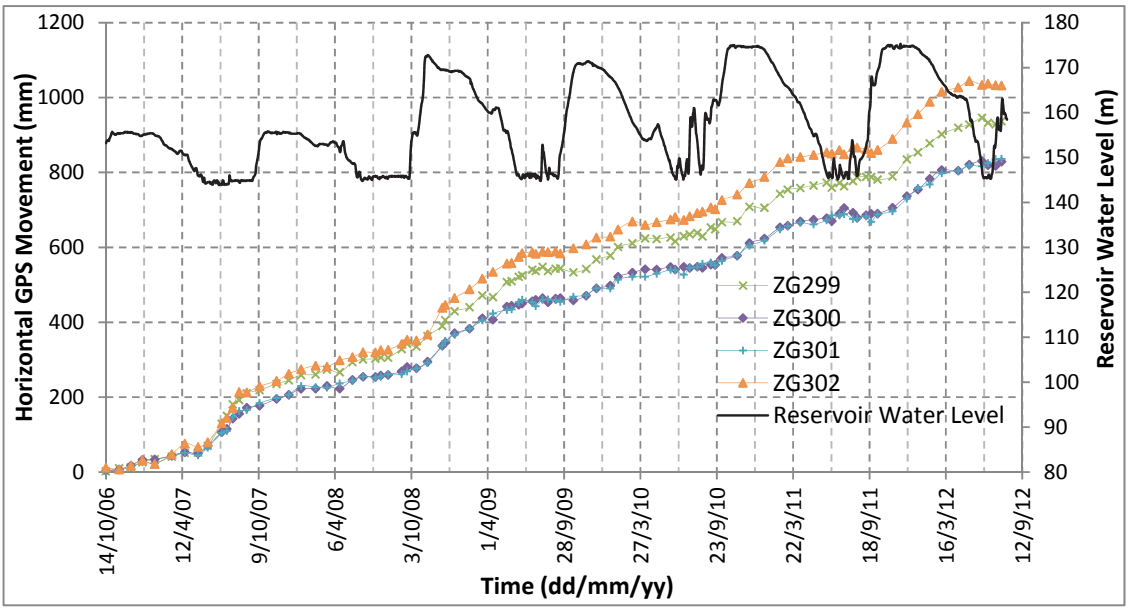

Figure 7.5: Horizontal movement of GPS stations (ZG 299 to ZG 302)

The observed reservoir water level is also plotted in Figure 7.3 to Figure 7.5 for comparison. It is indicated in these figures that, except for the year 2007, the horizontal landslide movement accelerates when reservoir rises and remains at the highest level. The landslide movement slows down when reservoir water level goes down and stays at the lowest level.

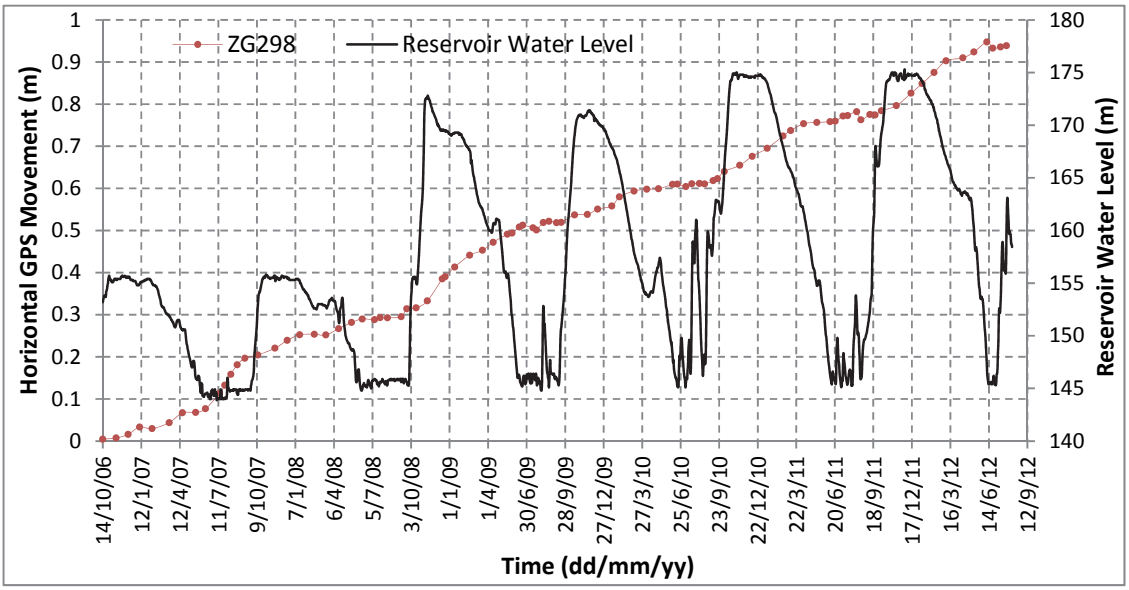

Figure 7.6: Horizontal GPS movement along Section I-I' and reservoir level for Muyubao

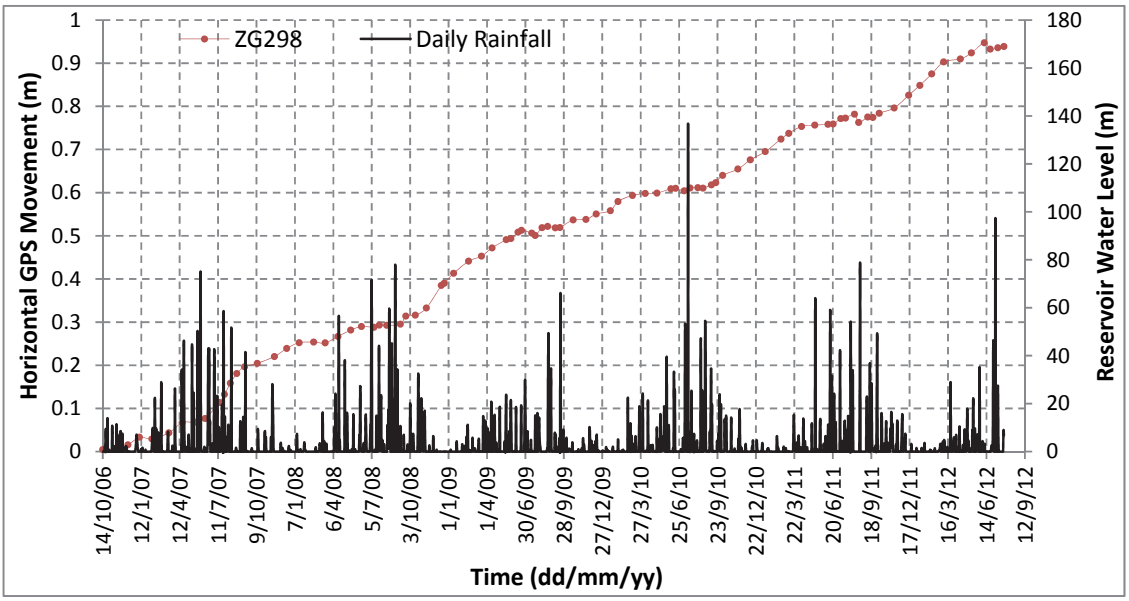

Figure 7.7: Horizontal GPS movement along Section I-I' and daily rainfall for Muyubao

In Figure 7.4, the observed movement at GPS ZG 295 to GPS ZG 298 is quite uniform. Thus, the observed horizontal movement at GPS ZG 295 is chosen for the analysis of Section I-I'. The component of the horizontal movement at GPS ZG 295 along the Section I-I' is calculated and plotted in Figure 7.6.

It is shown in Figure 7.6 that the horizontal GPS movement along Section I-I' at ZG 295 accelerates when reservoir level rises and remains at the peak. The movement slows down when reservoir level goes down and stays at the lowest level.

It is indicated in Figure 7.7 that the horizontal GPS movement decelerates during the rainy season for most of years except for 2007. In Figure 7.2 for Section I-I', the top colluvium layer has low permeability and prevents rainfall infiltration. In addition, the underneath disturbed and weathered quartz sandstone has large permeability and drains infiltrated rainfall very fast. Thus the groundwater table in the landslide is not affected much by the rainfall, which is not a key factor for the landslide analysis.

From July 2008 to July 2012 the reservoir water level fluctuated yearly between 145 m

and 175 m. During this period of time, the landslide was moving in a step-like pattern. The landslide moves faster when reservoir water level rises and remains at the highest water level.

Because it was the first time that the reservoir water level was raised from 145 m to over 170 m in the year 2008, the horizontal movement from 2008 to 2009 was larger than that in subsequent years. The accumulated horizontal movement along the Section I-I' from July 2008 to July 2009 was about 0.218 meter. The largest rate of movement during this period was 1.5 mm/day. From July 2009 to July 2012, the accumulated horizontal movement along Section I-I' was about 0.430 m, which was 0.143 m/year. The largest rate of movement during this period was 1.2 mm/day, which was observed in February 2010.

7.3 Seepage Analysis of Muyubao Landslide

Seepage analysis is carried out using SEEP/W (GEO-SLOPE International, Ltd., 2008). Section I-I' in Figure 7.2 is adopted for 2D seepage analysis. Smoothing localized sharp angles on the ground surface and interface between different regions have been made to the Section I-I' in Figure 7.2 to get better mesh. The seepage model for the landslide is presented in Figure 7.8.

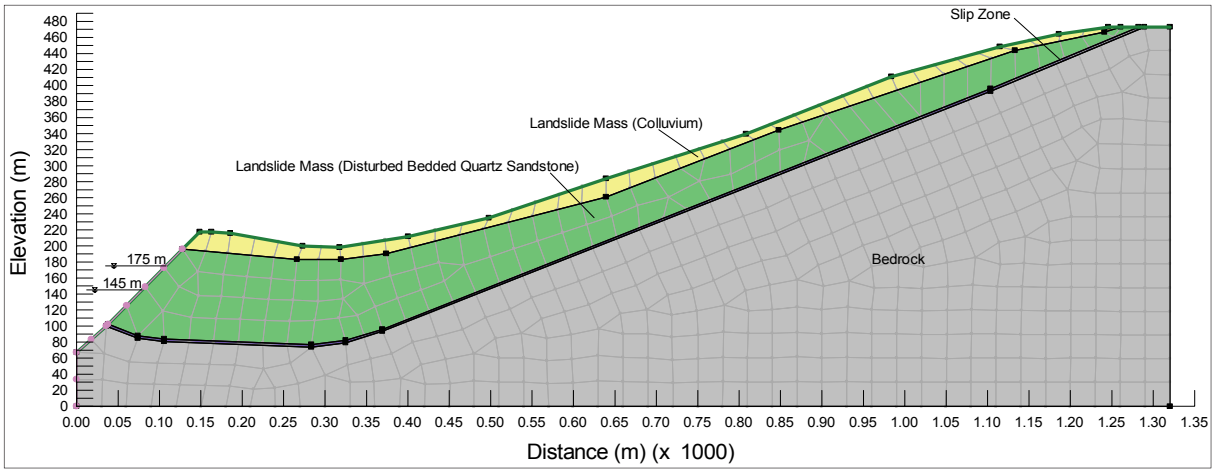

Figure 7.8: Seepage model for Muyubao landslide

The seepage analysis consists of steady-state and transient analysis. Steps for the seepage analysis are described as follows:

1. Steady-state seepage analysis. The steady-state seepage analysis is conducted first to generate the initial groundwater table and initial pore water pressure in the landslide. The steady-state seepage analysis lasts for 0 day. A constant total head of 146 m is applied at the toe of the landslide.

2. Transient seepage analysis. Transient seepage analysis is conducted to study the influence of reservoir water level fluctuation on the groundwater table in the landslide. The transient analysis has 1140 steps and each step simulates 1 day. Therefore a complete transient seepage analysis simulates 1140 days. Initial pore water pressure is based on previous steady-state seepage analysis. Variable total head vs. time, which is shown in Figure 7.8, is applied at the toe of the landslide.

Currently, there is no consistent groundwater monitoring data available for the landslide. There is also no field or laboratory test results of permeability. Thus, the permeability of Muyubao landslide is assumed based on permeability data of Sunjiazhuang landslide.

Sunjiazhuang landslide is located in Xingshan County, which is close to Muyubao landslide. According to landslide observation reports from CTGU, geological history and composition of Muyubao and Sunjiazhuang landslide are similar. Both landslides have colluvial landslide mass, which belongs to Q^{del}. In addition, bedrock for both landslides belongs to Middle Triassic Period.

The permeability of landslide mass, slip zone and bedrock regions of Muyubao landslide is considered to be homogeneous. Unsaturated permeability is calculated based on the permeability data of Sunjiazhuang landslide. Trails have been made to increase the permeability of the landslide material until the time lag behind of groundwater table

due to reservoir level fluctuation is negligible. The finally selected saturated permeability for each landslide material is summarized in Table 7.3.1. Unsaturated permeability input is summarized in Appendix III.

Table 7.3.1: Saturated permeability for transient seepage analysis

Seepage Model Region	$k_H=k_v$(m/day)
Landslide Mass (Colluvium)	0.1
Landslide Mass (Disturbed Bedded Quartz Sandstone)	864.0
Slip Zone	864.0
Bedrock	864.0

The calculated pore pressure contours from transient seepage analysis on October 27, 2009 (140th Day) and June 19, 2010 (375th Day) are plotted in Figures 7.9 and 7.10, respectively.

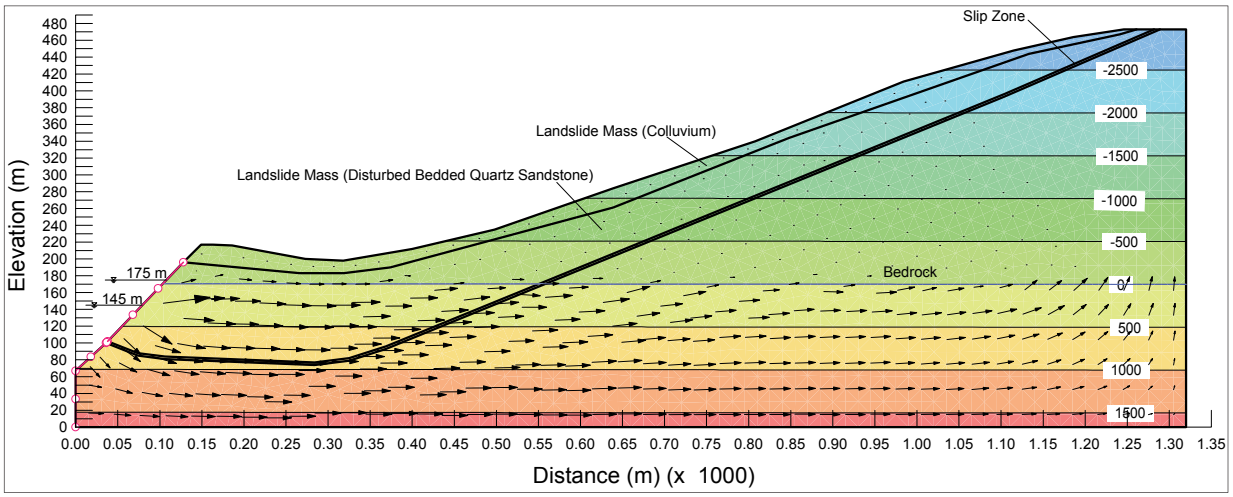

Figure 7.9: Pore pressure contour for Muyubao on October 27, 2009 (140th Day)

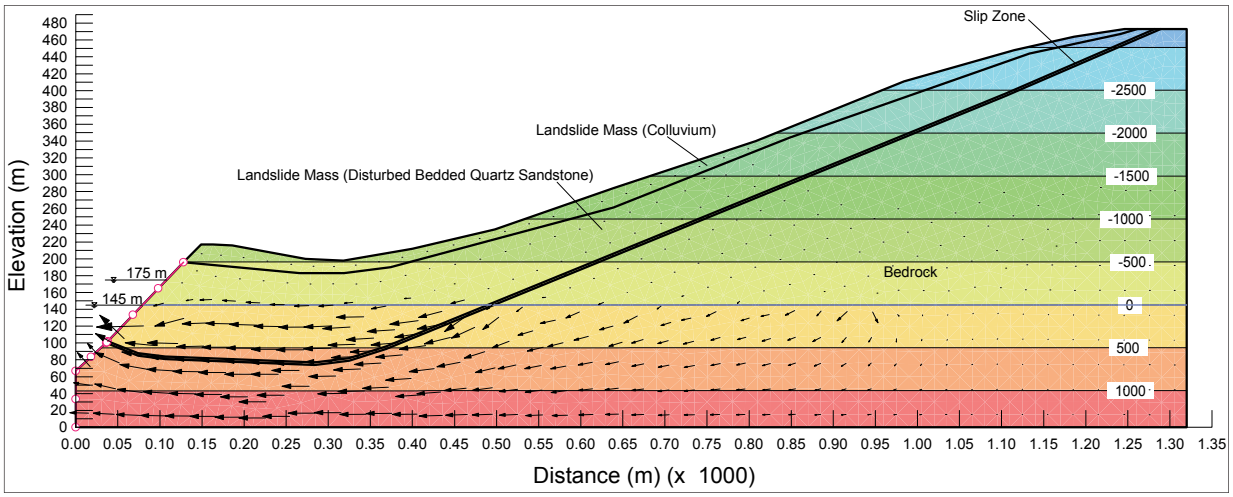

Figure 7.10: Pore pressure contour for Muyubao on June 19, 2010 (375th Day)

Figure 7.9 shows the pore pressure contour when the reservoir just reaches the high level at 170.5 m. The seepage velocity vectors show water mainly flows horizontally inward during the rise of reservoir water level. Because of high permeability of the landslide mass, slip zone and bedrock, there is hardly visible time lag of the groundwater table in the landslide. The pore pressure contours are horizontal and parallel to the groundwater table line. It is indicated in Figure 7.9 that the pore pressure along the slip zone increases quickly follows of the rise of the reservoir water level.

Figure 7.10 presents the pore pressure contour when the reservoir just reaches the lowest level at 145.1 m. The seepage velocity vectors show that the groundwater flows mainly horizontally outward in the landslide mass. In the bedrock underneath the slip zone, the ground water flows both outward and downward. The pore pressure contour are horizontal and parallel to the groundwater table. It is indicated in Figure 7.10 that the pore pressure along the slip zone decreases fast and follows closely with the decreasing reservoir level.

The seepage analysis results are consistent with Mechanism 2: For Muyubao landslide, which has high permeability, when the reservoir water level rises, water quickly seeps

into the landslide and pore pressure along the slip zone increases significantly and quickly. The increase of pore pressure along the slip zone leads to decrease of effective normal stress and shear strength and causes acceleration of landslide movement. During the drawdown of reservoir water level, groundwater quickly seeps out of the landslide and pore pressure along the slip zone decreases correspondingly. The decrease of pore pressure along the slip zone leads to larger normal stress and shear strength and causes the deceleration of landslide movement.

7.4 Stability Analysis of Muyubao Landslide

As for Shuping and Baishuihe landslide, SLOPE/W (GEO-SLOPE International, Ltd., 2008) is also used to analyze the stability of Muyubao landslide. The 2D stability analysis model, which is established based on Section I-I' in Figure 7.2, is presented in Figure 7.11.

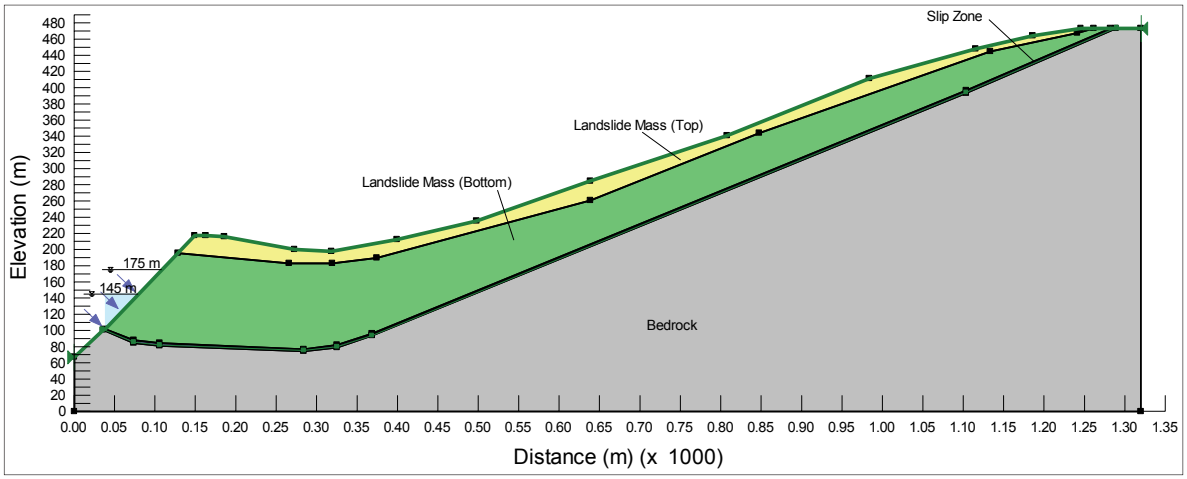

Figure 7.11: Stability model for Muyubao landslide

The Morgenstern-Price method is adopted and pore water pressure results from the previous transient seepage analysis is imported to the SLOPE/W model. Because the landslide is an old landslide which has slipped before, the slip surface is fully specified which goes through the slip zone region.

Table 7.4.1: Strength parameters for Muyubao stability analysis

Stability Model Region	Unit Weight (kN/m^3)	$c'(kPa)$	$\phi'(\circ)$
Landslide Mass (Top)	18	25.0	23.0
Landslide Mass (Bottom)	21	70.0	40.0
Slip Zone	18	18.0	19.0
		16.0	
		14.0	18.0
			17.0
			16.0
			15.0
			14.2
Bedrock	-	-	-

Based on the direct shear test results in Table 5.5.1, the strength parameters in Table 7.4.1 have been selected for sensitivity study and back calculation of strength parameters. The corresponding relationships between factor of safety and time are plotted in Figure 7.12 and Figure 7.13.

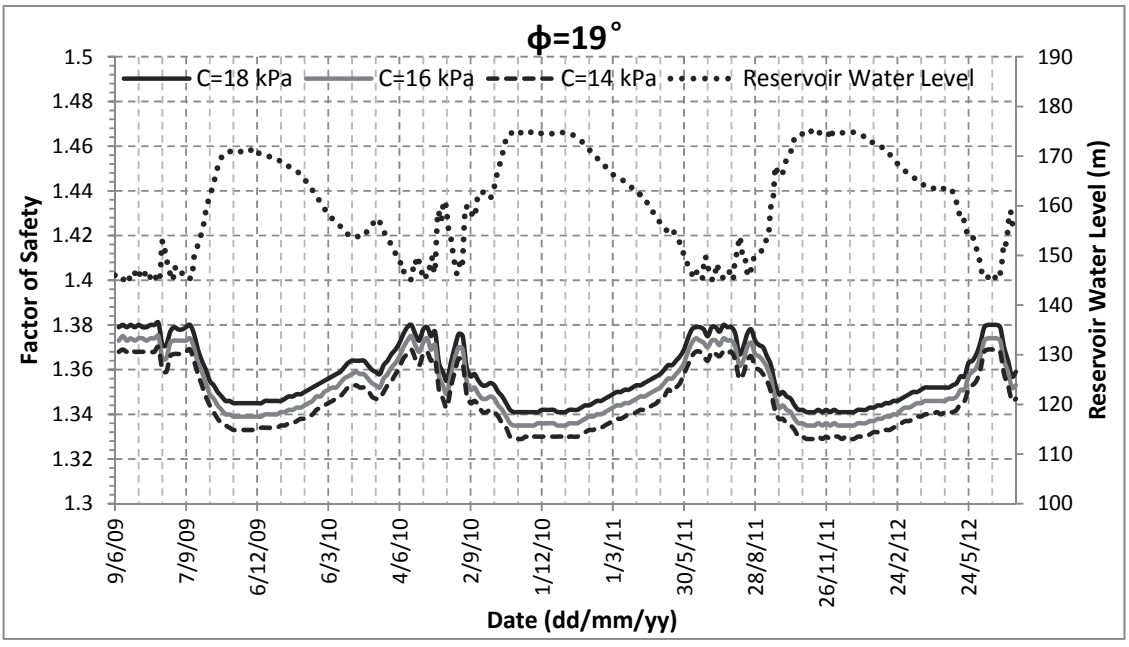

Figure 7.12: Factor of safety vs. time for Muyubao landslide (ϕ=19°)

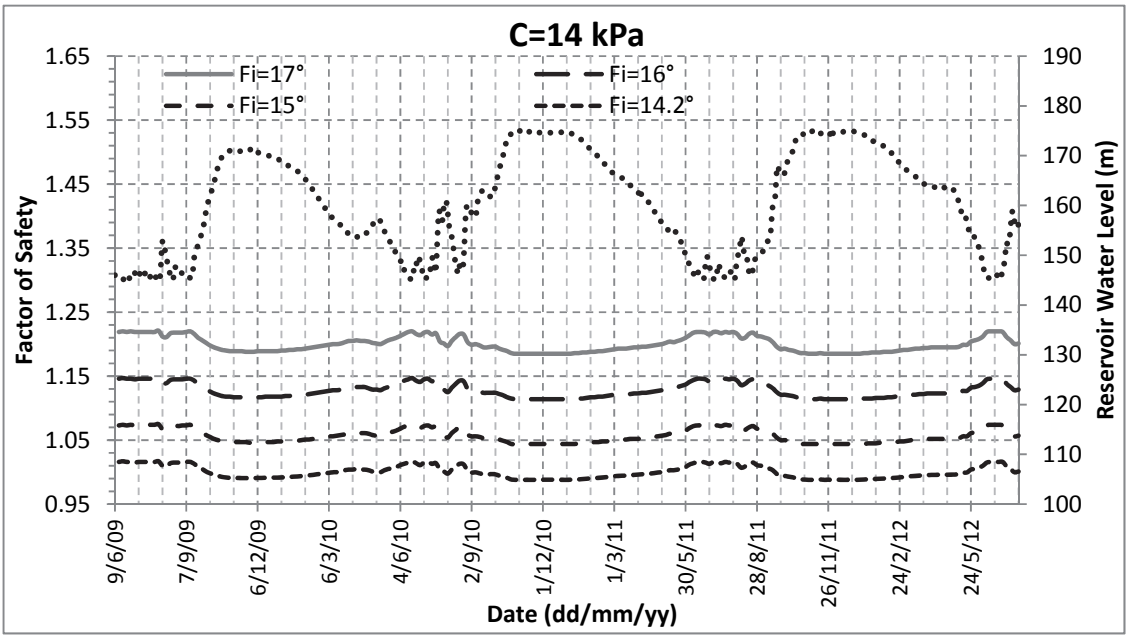

Figure 7.13: Factor of safety vs. time for Muyubao landslide (c=14 kPa)

In Figure 7.12, friction angle of the slip zone soil is fixed at 19° and cohesion is lowered gradually. The trend of the change of factor of safety is opposite to the trend of reservoir water level fluctuation. The factor of safety decreases when the reservoir water level rises and increases when the reservoir water level decreases. Similar pattern of factor of safety is found in Figure 7.13 where cohesion of the slip zone soil is fixed at 14 kPa and friction angle is decreased gradually.

The stability analysis results in Figure 7.12 and Figure 7.13 show that this landslide belongs to Mechanism 2. On one hand, for Muyubao landslide which has a high permeability, the factor of safety decreases when reservoir water level rises. When the landslide is less stable, the rate of time-dependent movement of the slip zone material tends to become higher which leads to the accelerated landslide movement. On the other hand, the factor of safety increases during the reservoir drawdown. When the landslide is more stable, the rate of time-dependent movement of the slip zone material tends to become lower, which leads to decelerated landslide movement..

Comparing Figure 7.12 and Figure 7.13, by changing the cohesion from 18 kPa to 14 kPa, the factor of safety on June 9, 2009 drops from 1.379 to 1.368, which is only a 0.8 % decrease. However, by changing the friction angle from 16° to 15° , the factor of safety on June 9, 2009 drops from 1.146 to 1.073, which is a 6.4 % decrease. Thus, the factor of safety is much more sensitive to the friction angle rather than the cohesion of the slip zone material.

Table 7.4.2: Maximum and minimum factor of safety for each cycle (ϕ=19°)

c(kPa)	Initial FS	Min. FS			Max. FS		
		Cycle 1	Cycle 2	Cycle 3	Cycle 1	Cycle 2	Cycle 3
18	1.379	1.345	1.341	1.341	1.380	1.380	1.380
16	1.373	1.339	1.335	1.335	1.375	1.374	1.374
14	1.368	1.333	1.329	1.329	1.369	1.368	1.369
c(kPa)	Initial FS	Max. FS Decrease (%)			Max. FS Increase (%)		
		Cycle 1	Cycle 2	Cycle 3	Cycle 1	Cycle 2	Cycle 3
18	1.379	-2.47	-2.76	-2.76	0.07	0.07	0.07
16	1.373	-2.48	-2.77	-2.77	0.15	0.07	0.07
14	1.368	-2.56	-2.85	-2.85	0.07	0.00	0.07

Table 7.4.3: Maximum and minimum factor of safety for each cycle (c=14 kPa)

ϕ(°)	Initial FS	Min. FS			Max. FS		
		Cycle 1	Cycle 2	Cycle 3	Cycle 1	Cycle 2	Cycle 3
16	1.146	1.117	1.114	1.114	1.147	1.146	1.146
15	1.073	1.046	1.044	1.044	1.074	1.074	1.074
14.2	1.016	0.991	0.988	0.988	1.017	1.016	1.016
ϕ(°)	Initial FS	Max. FS Decrease (%)			Max. FS Increase (%)		
		Cycle 1	Cycle 2	Cycle 3	Cycle 1	Cycle 2	Cycle 3
16	1.146	-2.53	-2.79	-2.79	0.09	0.00	0.00
15	1.073	-2.52	-2.70	-2.70	0.09	0.09	0.09
14.2	1.016	-2.51	-2.76	-2.77	0.10	0.00	0.00

The maximum and minimum factor of safety in Figure 7.12 and Figure 7.13 for each cycle is summarized in Table 7.4.2 and Table 7.4.3. The initial factor of safety on June 09, 2009 (0^{th} Day) is also included in these two tables for comparison. The maximum,

minimum and initial factor of safety are plotted in Figure 7.14 and Figure 7.15.

In Figure 7.14 and Figure 7.15, the minimum factor of safety in Cycle 1 is larger than that in Cycle 2. A possible explanation is that the peak reservoir water level in Cycle 1 (171.4 m) is lower than that in Cycle 2 (174.9 m). Since the permeability of the landslide is high, the groundwater table follows closely with the reservoir water level and reaches 171.4 m in Cycle 1 and 174.9 m in Cycle 2. The higher the groundwater table, the higher the pore pressure is along the slip zone. Higher pore pressure leads to lower effective normal stress and smaller shear strength of the slip zone. Thus the minimum factor of safety in Cycle 2 is lower than that in Cycle 1.

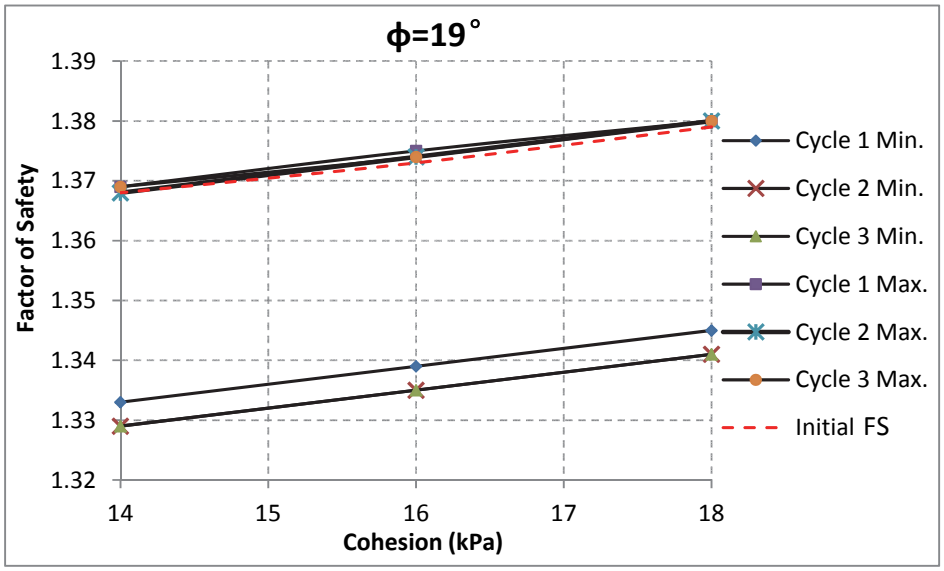

Figure 7.14: Maximum, minimum and initial factor of safety (ϕ=19°)

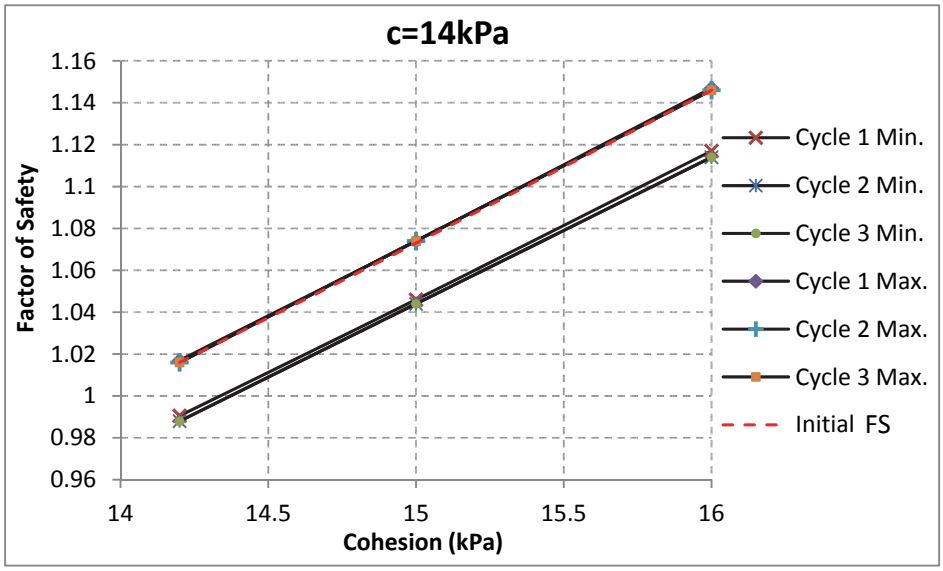

Figure 7.15: Maximum, minimum and initial factor of safety (c=14 kPa)

In addition, in Figures 7.14 and 7.15 the minimum factor of safety in Cycle 2 and Cycle 3 overlap. The reason is that peak reservoir levels in Cycle 2 (174.9 m) and Cycle 3 (175.0 m) are almost the same. Because the landslide has high permeability, groundwater in the former cycles can drain freely and has little cumulative effect on subsequent cycles. Thus, the peak groundwater table is almost the same in Cycle 2 and Cycle 3, which leads to the overlapped minimum factor of safety.

It is also indicated in Figures 7.14 and 7.15 that the maximum factor of safety in Cycle 1, Cycle 2 and Cycle 3 also almost overlap. Because the lowest reservoir water level in Cycle 1 (145.1 m), Cycle 2 (145.1 m) and Cycle 3 (145.4 m) are almost the same, and the high permeability which leads to little cumulative effect between different cycles, the lowest groundwater table is almost the same in Cycle 1, Cycle 2 and Cycle 3. Thus, curves for the maximum factor of safety overlap each other.

In addition, Figures 7.14 and 7.15 also indicate that the initial factor of safety, which corresponds to a reservoir water level of 146 m, is very close to the maximum factor of safety obtained at the lowest reservoir water level. Thus, the landslide is most stable

when the reservoir remains at the lowest level. The landslide is less stable when reservoir water level goes up or down. The landslide is the least stable when the reservoir remains at the peak level.

The maximum percentage of increase and decrease from the initial factor of safety for the landslide is calculated and summarized in Table 7.4.2 and Table 7.4.3. During the three cycles of reservoir water level fluctuation, the stability of the landslide only increases up to 0.2 % (FOS increases from 1.373 to 1.375) when reservoir level goes down and remains at the lowest level. The stability decreases by up to 2.9 % (FOS decreases from 1.368 to 1.329) when the reservoir water level just reaches the peak. This indicates that the landslide movement is very sensitive to the change of stability.

The landslide is now in the time-dependent movement stage. To back calculate friction angle and cohesion of the soil in the slip zone, the criterion is set such that the landslide movement starts to accelerate when the factor of safety is close to one.

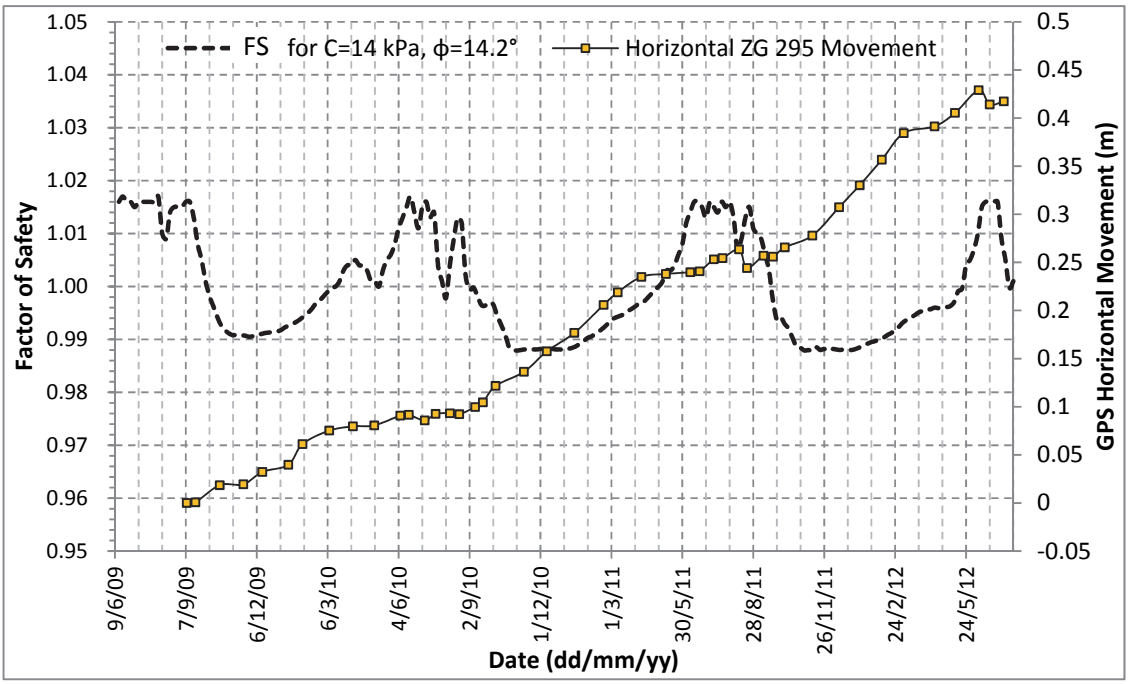

Figure 7.16: Movement and factor of safety of Muyubao landslide

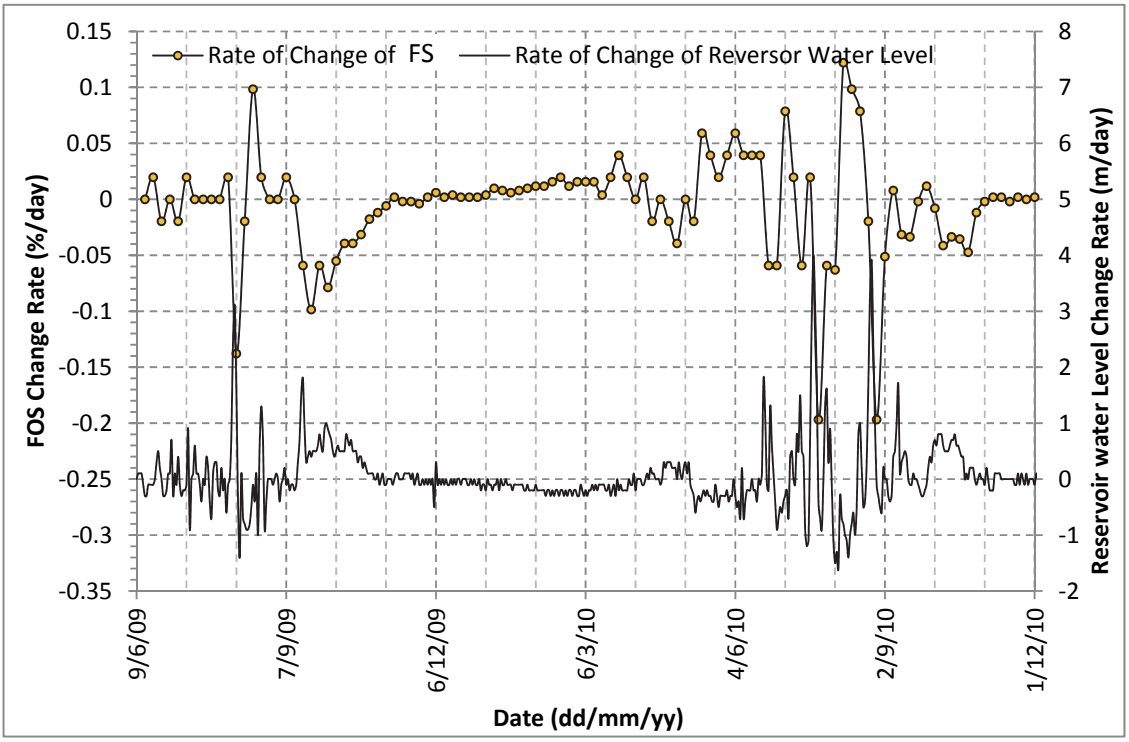

Figure 7.17: Rate of change of factor of safety and reservoir water level for Muyubao

The observed horizontal movement at GPS ZG 295 along Section I-I' and calculated factor of safety for c=14 kPa and ϕ=14.2° of the soil in the slip zone are plotted in Figure 7.16. It is shown that the landslide movement starts to accelerate every time when the factor of safety drops below 1.0. Thus, c=14 and ϕ=14.2° are chosen as the back calculated strength parameters for the soil in the slip zone. These back calculated strength parameters lie within the range of saturated drained direct shear test results in Table 5.5.1. The rate of change of factor of safety and the rate of change of reservoir water level are plotted in Figure 7.17, which indicates that the rate of change of factor of safety is roughly proportional to the rate of change of reservoir water level. The highest rate of reservoir drawdown is -1.5 m/day on August 03, 2010 and the corresponding change in factor of safety is +0.12 %/day. The highest rate of rising of the reservoir water level is +3.9 m/day on August 25, 2010 and the corresponding change in factor of safety is -0.20 %/day. This shows that the rate of change of the factor of safety is very sensitive

to the rate of change of reservoir water level. Because the reservoir fluctuation has a critical impact on the change of landslide stability and thus the landslide movement, the rate of change of reservoir level and the peak reservoir level need to be under very careful control to avoid failure of Muyubao landslide.

7.5 Movement Analysis of Muyubao Landslide

ABAQUS 6.12 software is used to carry out 2D finite element modeling of the Muyubao landslide. The analysis is based on Section I-I' in Figure 7.2. The configuration and mesh of the finite element model are shown in Figure 7.18 and Figure 7.19, respectively.

In Figure 7.18 and 7.19, the horizontal length of the model is 1320 m, and the vertical height is 473 m. The elevation at the bottom of both figures is equal to zero meter.

In Figure 7.19, movement of the left and right boundaries of the landslide is fixed in the horizontal direction but they are free to move vertically. The bottom of the landslide model is fixed in both horizontal and vertical directions.

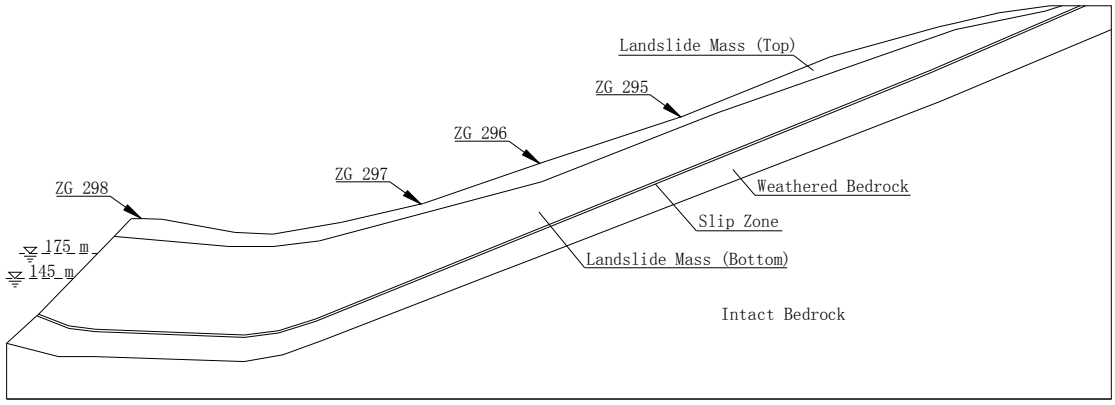

Figure 7.18: Configuration of the Muyubao ABAQUS model

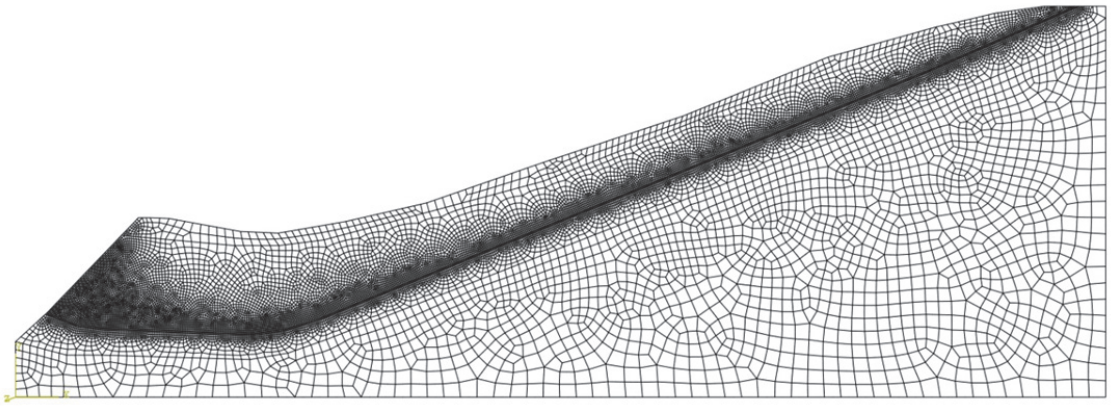

Figure 7.19: Mesh of the Muyubao ABAQUS model

Coupled pore fluid/stress analysis is used in the finite element model. The model is established to simulate the landslide movement since September 7, 2009, when reservoir level started to rise from the lowest level.

A steady-state geostatic analysis step is created at first to establish initial conditions for the landslide modeling. The initial reservoir water level is set at an elevation of 146.0 m and gravity is activated during this step. When the calculation is completed, the initial stress field and pore pressure are generated for the subsequent transient pore fluid/stress analysis.

Following the steady-state geostatic analysis are the steps for transient analysis of landslide movement under fluctuating reservoir water level. Pore pressure boundary conditions and load conditions in the finite element model are based on the recorded daily reservoir water level at the Three Gorges Dam. Some modifications such as smoothing short-term sharp changes or back-and-forth changes have been made to the original recorded reservoir water level for better convergence of the finite element model. The reservoir water level between September 2009 and November 2011 is presented in Figure 7.20.

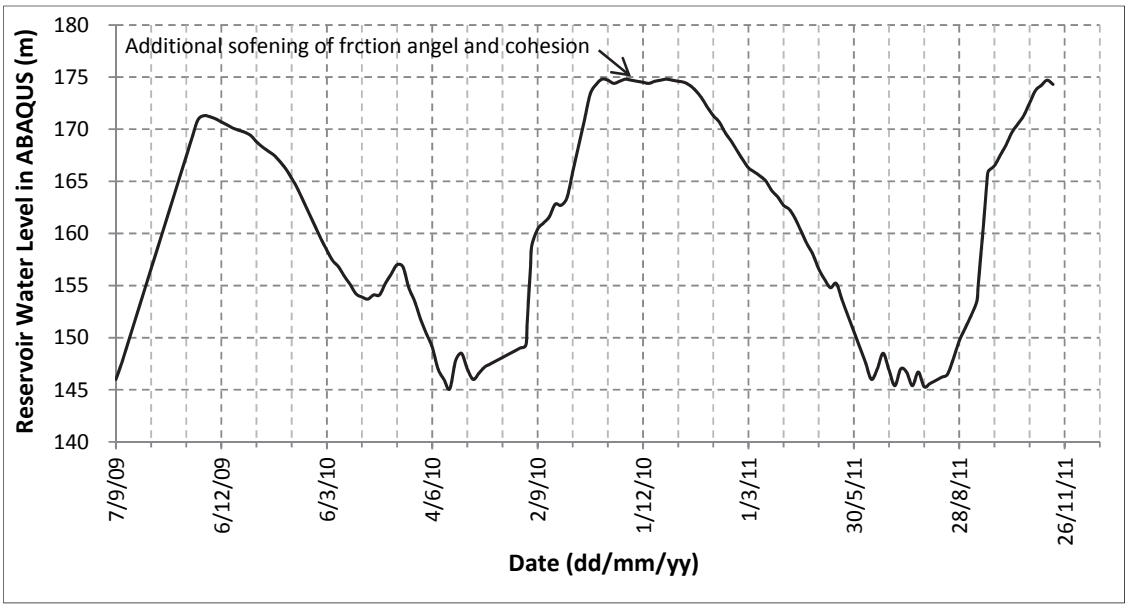

Figure 7.20: Reservoir water level in the Muyubao ABAQUS model

The landslide mass, slip zone and bedrock are assumed to be isotropic and homogeneous. Based on the previous seepage analysis of the landslide, the saturated permeability for the finite element model is summarized in Table 7.5.1.

Table 7.5.1: Saturated permeability of Muyubao ABAQUS model

Seepage Model Region	Landslide Mass (Top)	Landslide Mass (Bottom)	Slip Zone	Bedrock
$k_H=k_V$ (m/day)	0.1	864.0	864.0	864.0

In ABAQUS, the unsaturated permeability k_{usat} is defined by,

$$k_{usat} = k_s \times k \tag{7.1}$$

where

k is the saturated permeability.

k_s is a factor which is related to saturation. The k_s-Saturation relationship for the finite

element model is defined by $k_s = (S_r)^3$.

Saturation-Pore Pressure relationships for the analysis of landslide movement are summarized in Appendix III.

In the model, the strain-rate hardening strain softening Drucker-Prager constitutive model which is developed in Chapter 4, is implemented to model the slip zone. Similar to Shuping and Baishuihe landslide, it is assumed that there is 10% increase in cohesion for every tenfold increase in strain rate. Strain softening Drucker-Prager plasticity is implemented to model the landslide mass regions (both Top and Bottom) and the weathered bedrock. Linear elasticity is adopted for the intact bedrock.

The elastic and plastic parameters at zero plastic strain for the finite element model are summarized in Table 7.5.2. For the soil in the slip zone, the strain-rate hardening relationship between yield stress ratio and equivalent plastic strain rate is presented in Table 7.5.3.

Table 7.5.2: Elastic and plastic parameters for Muyubao ABAQUS model

	Dry Density (kg/m^3)	E (MPa)	Poisson's Ratio	Friction Angle β(∘)	Flow Stress Ratio	Dilation Angle ψ(∘)	UCS at Strain=0 (kPa)
Landslide Mass (Top)	1630	18.5	0.30	40.0	1	10	70.0
Landslide Mass (Bottom)	1800	200.0	0.24	48.0	1	10	150.0
Slip Zone	1800	18.5	0.32	26.0	1	10	40.0
Weathered Bedrock	1800	200.0	0.24	48.0	1	10	150.0
Intact Bedrock	2000	61000	0.21	-	-	-	-

Table 7.5.3: Yield stress ratio and equivalent plastic strain rate for Muyubao

Yield Stress Ratio	1.0	1.1	1.21	1.331	1.4641	1.61051
Equivalent Plastic Strain Rate (s^{-1})	0	1.16E-09	1.16E-08	1.16E-07	1.16E-06	1.16E-05

Besides strain softening of cohesion for landslide mass, slip zone and weathered bedrock regions, some additional softening of friction angle and cohesion for the slip zone is added on November 16, 2010 and summarized in Table 7.5.4. This additional softening takes into account the softening casued by wetting and drying.

Table 7.5.4: Additional softening for the slip zone region of Muyubao

Landslide Region	Date	Friction Angle β(∘)	Flow Stress Ratio	Dilation Angle ψ(∘)	UCS at Zero Strain(kPa)
Slip Zone	Sep. 07, 2009	26.0	1	10	40.0
	Nov. 16, 2010	24.7	1	10	35.0

Two typical views of groundwater table of the finite element model are shown in Figures 7.21 and 7.22. Figure 7.21 shows the groundwater table when reservoir level goes down and reaches the lowest level (145.1 m) on June 19, 2010. The Figure 7.22 shows the groundwater table when reservoir rises and reaches the highest level (174.8 m) on October 27, 2010. In both figures, the boundary between light and darker colors is the groundwater table line.

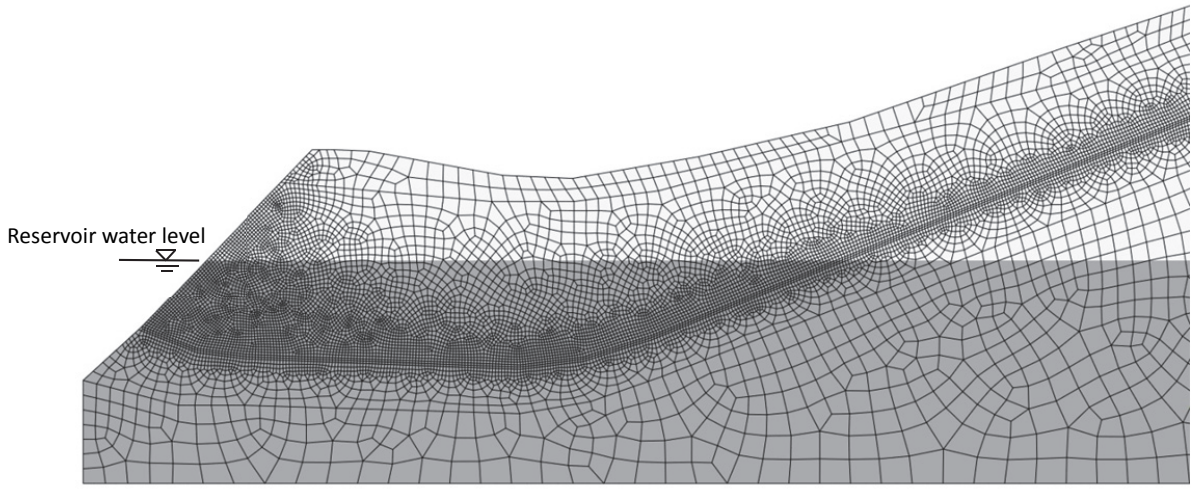

Figure 7.21: Location of groundwater table on June 19, 2010 (lowest level 145.1 m)

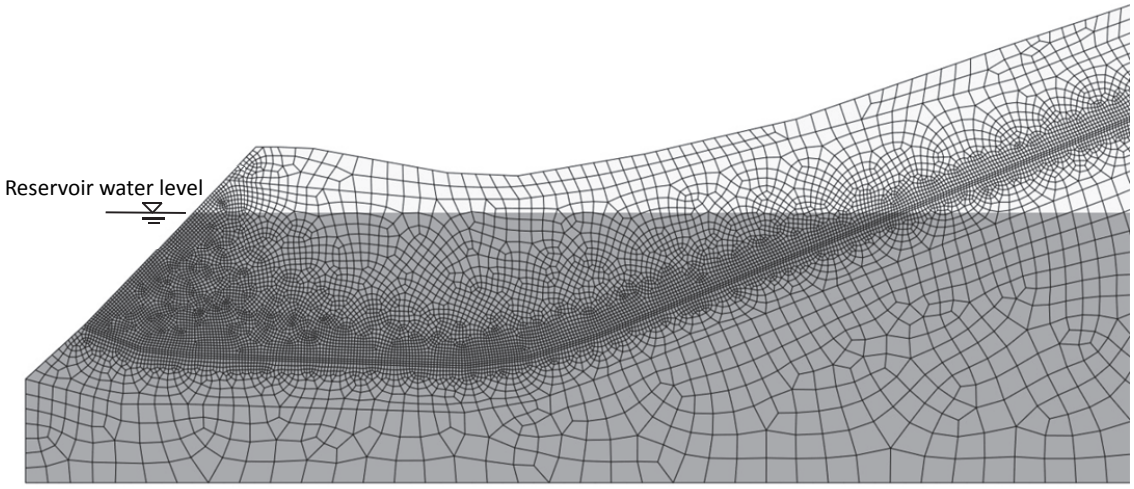

Figure 7.22: Location of groundwater table on October 27, 2010 (highest level 174.8 m)

In Figures 7.21 and 7.22, since the permeability of the landslide is high, the groundwater table follows the reservoir level closely and there is no identifiable time lag. When the reservoir level goes down, the pore pressure along the slip surface decreases correspondingly with the reservoir level, leading to higher landslide stability and slower landslide movement. When the reservoir level goes up, the pore pressure along the slip surface correspondingly increases, causing lower landslide stability and faster movement.

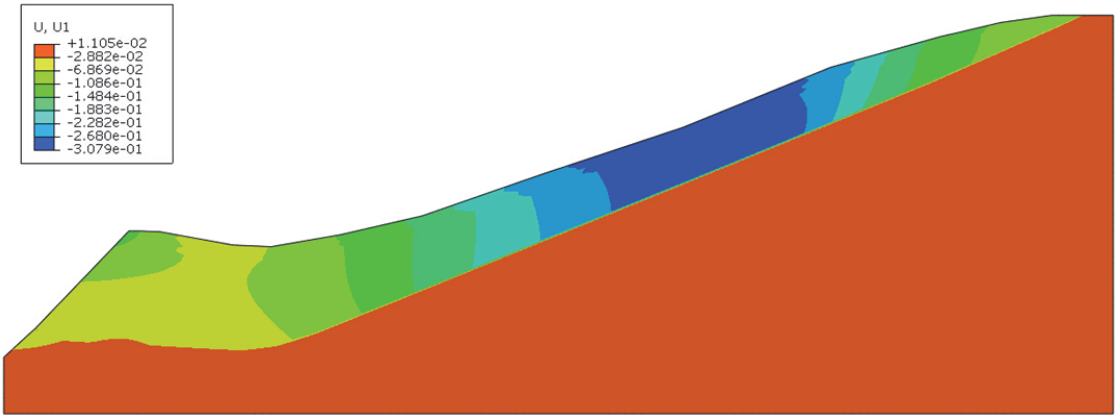

Figure 7.23: Contours of horizontal movement (December 6th, 2011)

Contours of calculated horizontal movement for November 16, 2011 are plotted in Figure 7.23. In this figure, most horizontal movement is located at the middle part of the landslide. The horizontal movement is smaller at the toe and top of the landslide.

The calculated horizontal movement at the location of GPS station ZG 295 is plotted in Figure 7.24. The reservoir water level boundary condition in ABAQUS, observed reservoir water level and observed horizontal movement at GPS station ZG 295 are also plotted in Figure 7.24 for comparison.

In Figure 7.24, the reservoir water level boundary in ABAQUS is modified to be smoother than real monitored reservoir water level for better convergence. The pattern and magnitude of horizontal movement from the finite element modeling generally matches the real observed movement.

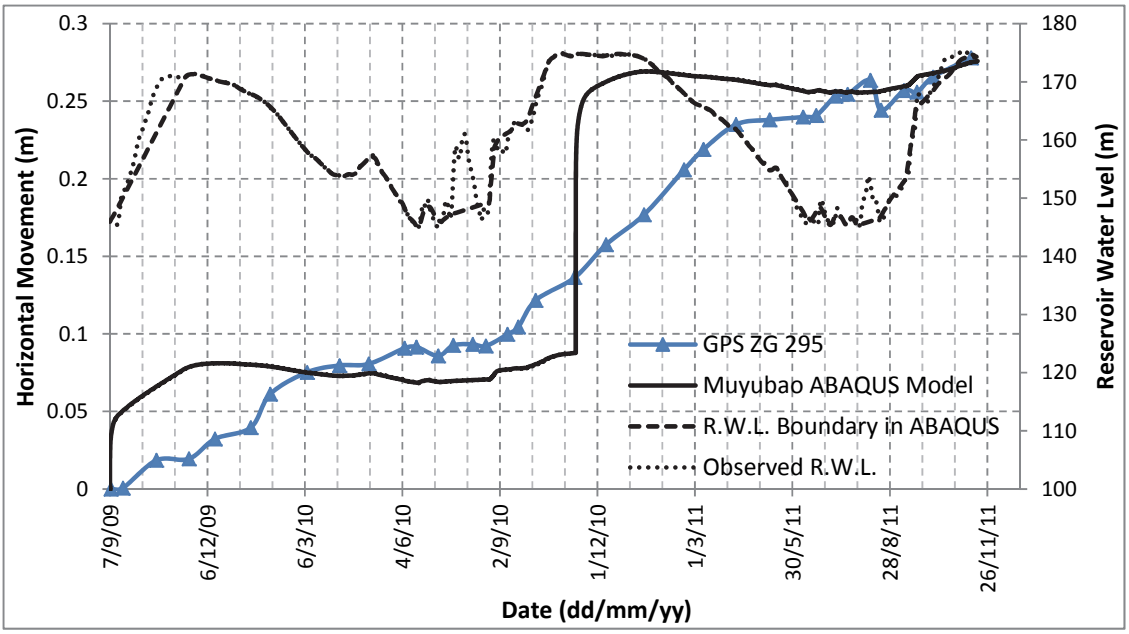

Figure 7.24: Horizontal movement at GPS station ZG 295 vs. time

It is indicated in Figure 7.24 that the calculated movement accelerates when reservoir water level goes up. The additional softening of friction angle and cohesion of the soil in the slip zone on November 16, 2010 leads to sharp increase of landslide movement.

Comparing the observed and calculated horizontal movement in Figure 7.24, the horizontal movement from finite element modeling only accelerates when reservoir water level goes up. However, the horizontal movement from GPS record shows acceleration when reservoir water level rises, remains at the peak, and at the beginning of drawdown. This indicates that in the finite element model, the landside moves faster when reservoir water level goes up, and becomes stable when reservoir stops rising. In the real case, the landslide moves at a faster rate when pore pressure along the slip zone is high and the effective normal stress is low, even when reservoir water level stops rising.

A reasonable explanation for the above difference is that in the strain softening Drucker-Prager constitutive model in ABAQUS, only cohesion is decreased with

increasing plastic strain while friction angle is a constant except for the additional softening on November 16, 2010. For the real landslide, both the cohesion and friction angel gradually decreases with increasing plastic strain and these parameters can further decrease because of the wetting and drying effect from the fluctuating reservoir level. Because of the limitation of ABAQUS software, these softening details of the real landslide are not completely included and reflected in the finite element model model. Thus there is some difference between modeled and observed landslide movement.

A close up view of the observed horizontal movement at GPS station ZG 295 and the recorded daily rainfall is plotted in Figure 7.25. It can be seen in this figure that the rainy season is mainly in the months of May to September. Although there is a lot of rain during this period, the landslide movement does not accelerate until reservoir level starts to rise. It can also be seen that although there is not much rain from October to March, the landslide still moves at a higher rate. Thus, rainfall is not an important factor for the movement analysis.

The above evidences from the finite element modeling and GPS observation show that the landslide belongs to Mechanism 2. Because of high permeability, the groundwater table follows closely with the reservoir water level. The increased pore pressure along the slip zone makes the landslide less stable and moves faster. When the reservoir level goes down, the groundwater level lowers correspondingly, which leads to the decrease of pore pressure along the slip zone and the decelerated movement of the landslide.

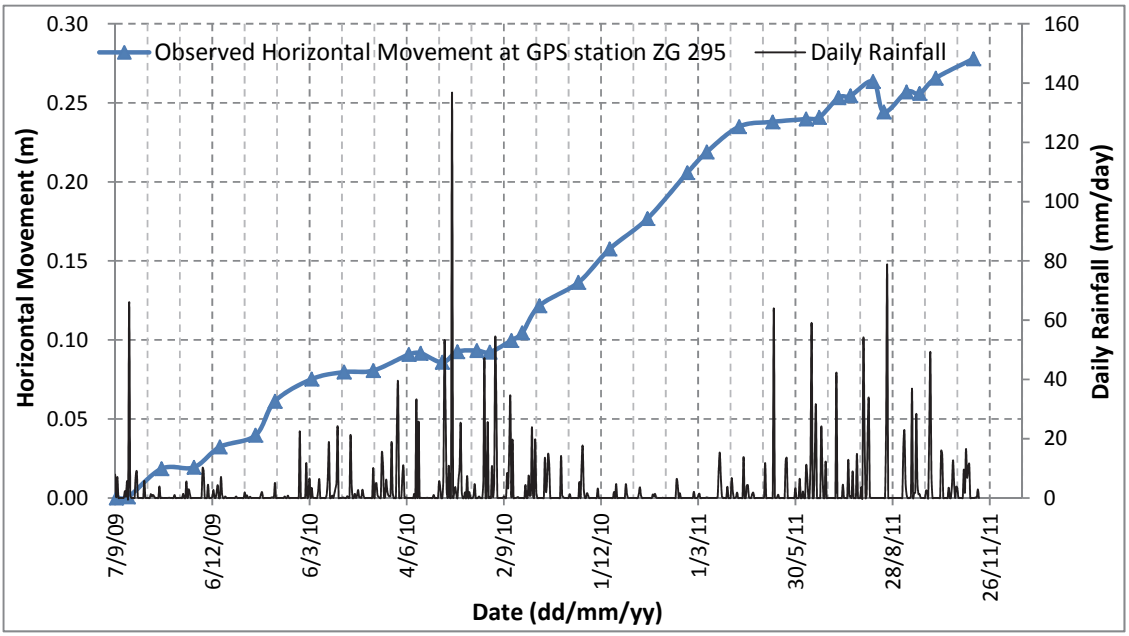

Figure 7.25: Observed horizontal movement and daily rainfall

For Muyubao landslide, piezometers can be installed to monitor the groundwater reaction to the fluctuating reservoir level. The observed groundwater table can be used to back calculate the permeability of landslide mass, slip zone and bedrock. Besides, ring shear or direct shear test can be conducted to study the strain-rate hardening and strain softening characteristics of the soil in the slip zone. In addition, some further experiments can be conducted to study the softening of landslide soil/rock under cyclic wetting and drying caused by reservoir water level fluctuation. A user-defined material model (UMAT) in ABAQUS, which is more flexible to include various kinds of softening characteristics, can be developed in the future to better model the landslide movement.

Chapter 8 Factors Affecting the Mechanism of Movement

At the beginning of this chapter, an introduction of four factors affecting the mechanism of landslide movement is given. The reservoir water level fluctuation is divided into four scenarios and the impact of four factors in each scenario is discussed. Then, for each factor, a stability model was established and boundary/load conditions were changed to study the impact of the affecting factor on landslide stability.

8.1 Introduction to Factors Affecting the Mechanism of Movement

Generally, there are four factors that affect the mechanism of movement in a landslide. The influence of these parameters on factor of safety of a landslide are denoted as: water pressure at the toe (FS 1), effective stress at the slip surface (FS 2), seepage force at the toe (FS 3) and weight of water at the toe (FS 4). During the fluctuation of reservoir water level, these four effects will compete with each other and the dominant effect will have decisive influence on the movement of the landslide.

During one cycle (lasts about one year) of reservoir water level fluctuation, a landslide will undergo the following four scenarios.

Scenario 1. This scenario is shown in Figure 8.1. The reservoir decreases from high to low water level. In this scenario, FS 1 will decrease and FS 2 will increase. FS 3 will decrease because of the outward seepage force and FS 4 will decrease because of less weight at the toe caused by reduced saturation. Generally, the neutral point is above the toe of the landslide, thus less weight at the toe produces less stabilizing force.

Scenario 2. This scenario is shown in Figure 8.2. The reservoir remains at low water level and there is little change in the groundwater level in the slope. In this scenario, FS 1 and FS 2 remain constant with different values. The influence of FS 3 and FS 4 are negligible.

Scenario 3. This scenario is shown in Figure 8.3. The reservoir increases from low to high water level. In this scenario, FS 1 will increase, FS 2 will decrease. FS 3 will increase because of the inward seepage force and FS 4 will increase because of more weight at the toe caused by increased saturation.

Scenario 4. This scenario is shown in Figure 8.4. The reservoir remains at high water level and there is little change in the groundwater level in the slope. In this scenario, FS 1 and FS 2 remain constant with different values. The influence of FS 3 and FS 4 are negligible.

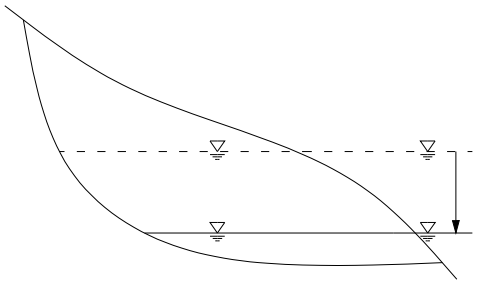

Figure 8.1: Scenario 1 water level decreases

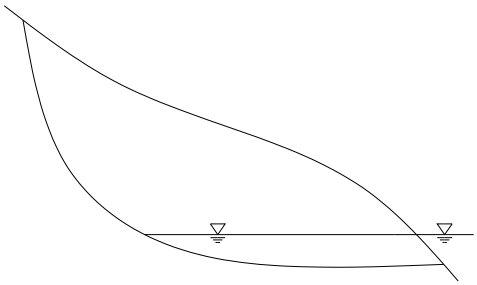

Figure 8.2: Scenario 2 water level remains low

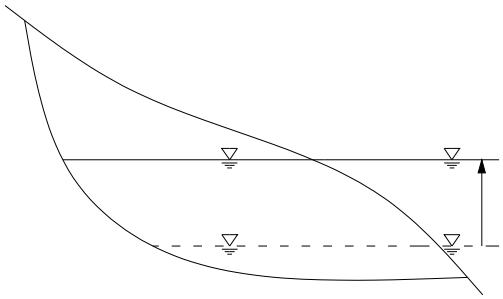

Figure 8.3: Scenario 3 water level increases

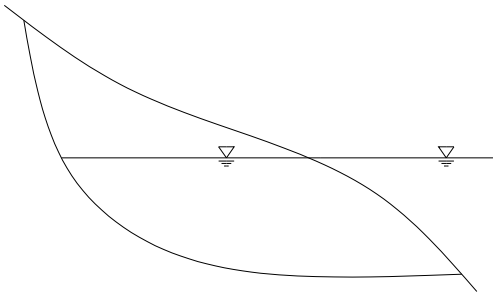

Figure 8.4: Scenario 4 water level remains high

Because factor of safety in Scenario 2 and Scenario 4 do not change much and Scenario 1 and Scenario 3 are just two reverse processes, the Scenario 1 is chosen and numerical models are established to further study these four factors that affect the mechanism of movement.

8.2 Factor of Hydrostatic Water Pressure at the Toe

The configuration in Figure 5.8 is selected for the analysis of influence of water pressure at the toe. To study the influence of water pressure on the stability of the landslide, SIGMA/W (GEO-SLOPE International, Ltd., 2008) is used to calculate the change of stress field during reservoir drawdown and the calculated stress results are imported to SLOPE/W for the corresponding stability analysis.

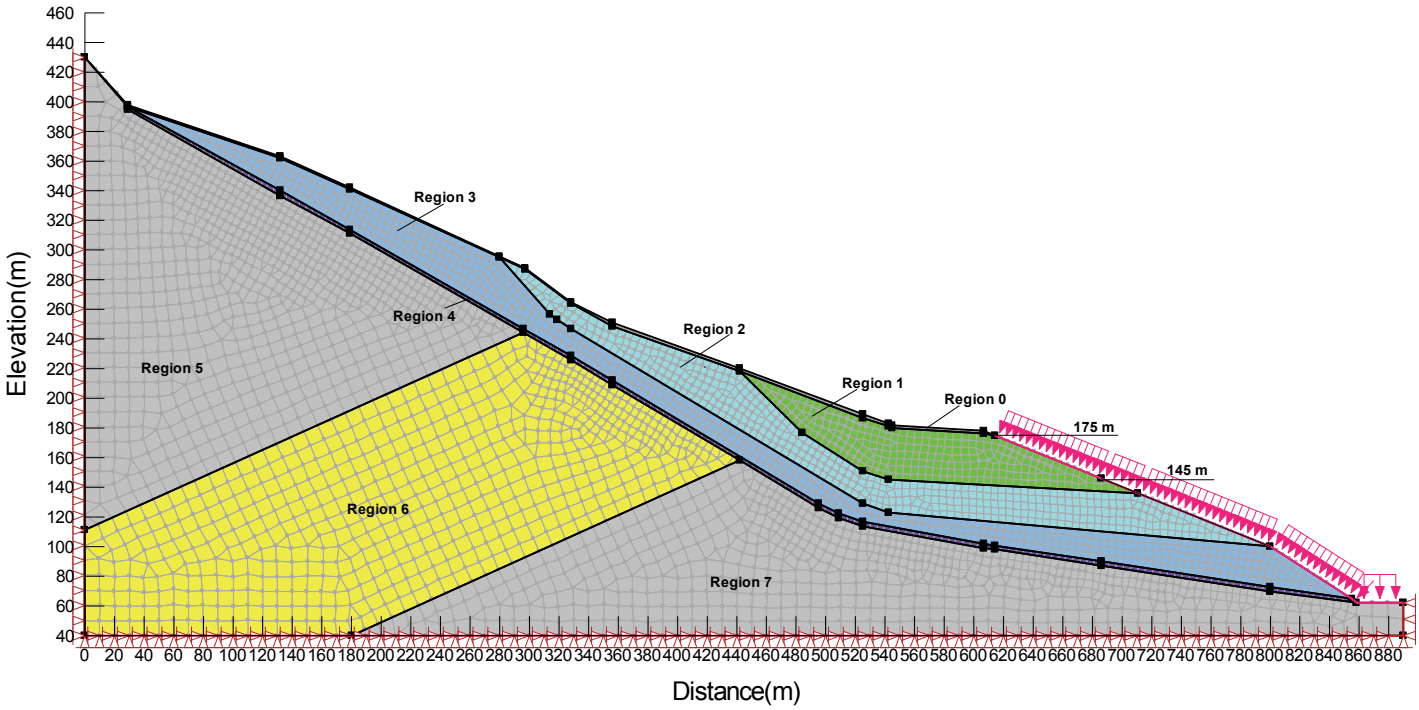

Figure 8.5: SIGMA/W model for the analysis of hydrostatic pressure at the toe

The SIGMA/W model for the analysis of hydrostatic pressure at the toe is presented in Figure 8.5. In this figure, Region 0 represents the top soil. The landslide mass consists of Regions 1 to 3. The slip zone is represented by Region 4. The bedrock consists of Regions 5 to 7.

In the SIGMA/W, Elastic-Plastic constitutive model is selected to model top soil, landslide mass, and slip zone materials. The bedrock is assumed to be elastic and impenetrable.

The mechanical properties of the materials in each region are summarized in Table 8.2.1.

In the model, left and right boundaries are fixed horizontally but free to move vertically. The bottom is fixed in both horizontal and vertical directions. The hydrostatic pressure boundary at the toe is decreased from 175 m to 145 m within 150 days. The corresponding rate is 0.2 m/day. Calculated stress field from the SIGMA/W is then imported to SLOPE/W to calculate factor of safety. The relationship between hydrostatic pressure head and factor of safety is plotted in Figure 8.6.

Table 8.2.1: Mechanical properties for the SIGMA/W model

Region #	Unit Weight (kN/m^3)	E' (MPa)	ν	c' (kPa)	ϕ' $(\circ)$
Region 0 (Top Soil)	20.0	20.8	0.28	26.6	23.4
Region 0, 1, 2, 3 (Landslide Mass)	20.0	20.8	0.28	26.6	23.4
Region 4 (Slip Zone)	20.0	20.8	0.28	25.1	19.3
Region 5, 6, 7 (Bedrock)	21.9	61000	0.21	-	-

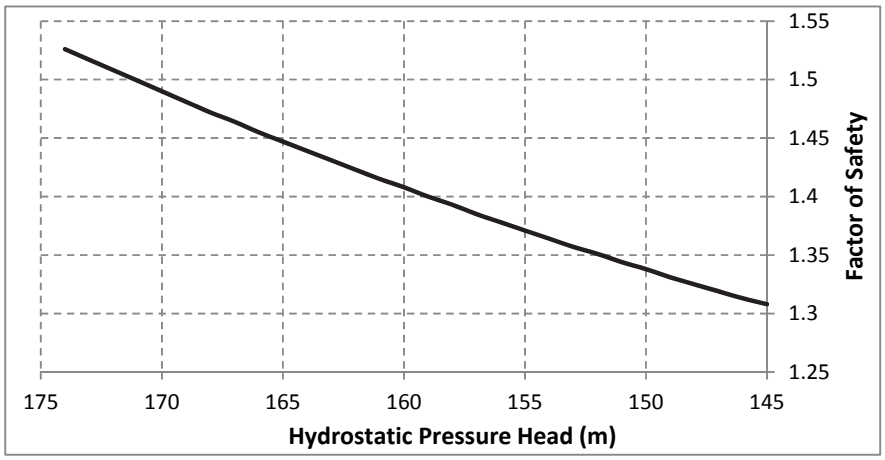

Figure 8.6: Hydrostatic pressure head and factor of safety

It is indicated in this figure that the factor of safety decreases almost linearly with the hydrostatic pressure at the toe. The factor of safety is 1.526 when hydrostatic pressure head equals to 174 m. It drops to 1.308 when hydrostatic pressure head equals to 145 m. In this case, there is 14.3% decrease of factor of safety when the hydrostatic pressure is deceased from 174 m to 145 m.

8.3 Factor of Effective Stress at the Slip Surface

Similarly, SIGMA/W and SLOPE/W are used to study the influence of effective stress at the slip surface on the factor of safety. The configuration of the SIGMA/W model for this analysis is the same as that in Figure 8.5. The boundary conditions in the model are shown in Figure 8.7.

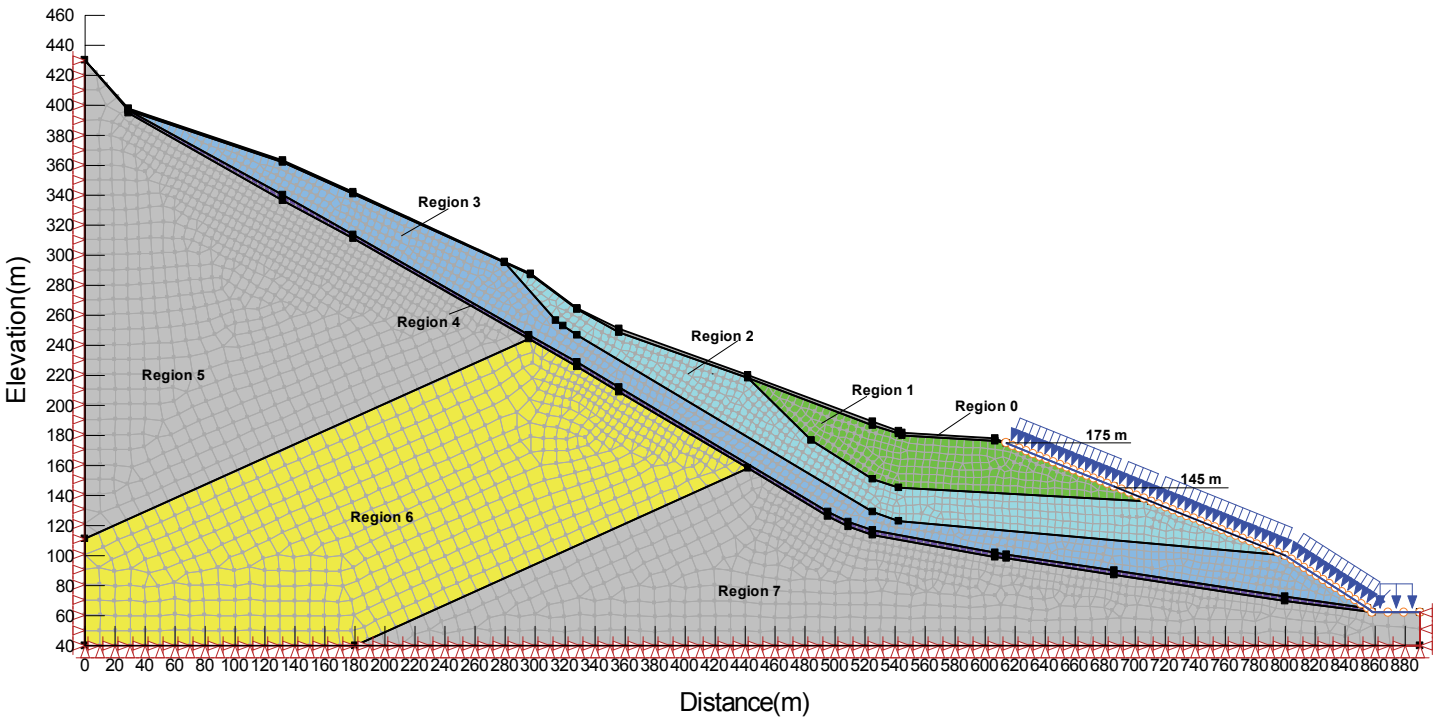

Figure 8.7: SIGMA/W model for the analysis of effective stress at the slip surface

The left and right boundaries are horizontally fixed but free to move vertically. The bottom is fixed both in the horizontal and vertical directions. The arrows pointing at the

ground surface at the toe are the hydrostatic pressure boundary which is a constant (175 m) throughout the analysis. Small circles along the ground surface at the toe represent the total head boundary for the seepage. The total head boundary is decreased from 175 m to 145 m within 150 days.

Elastic-Plastic constitutive model is selected to model top soil, landslide mass, and slip zone regions. The bedrock is assumed to be elastic and impenetrable. The mechanical properties of the materials in each region are the same as those summarized in Table 8.2.1. Permeability of the landslide is assumed to be homogeneous and isotropic. Saturated/unsaturated permeability selected for the model is summarized in Table 8.3.2.

Table 8.3.2: Saturated/unsaturated permeability in the SIMGA/W model

Matric Suction (kPa)	1	10	20	40	60	80	100
Permeability (m/day)	851.4	800.9	210.8	25.3	10.1	8	7.4

The contours of vertical effective stress when total head boundaries are at 175 m and 145 m are plotted in Figures 8.8 and 8.9.

Comparing Figures 8.8 and 8.9, vertical effective stress along the slip zone in Figure 8.8 is smaller than that in Figure 8.9. This indicates that the normal effective stress along the slip zone increases with the decreasing total head at the boundary, which leads to higher shear strength at the toe and larger factor of safety.

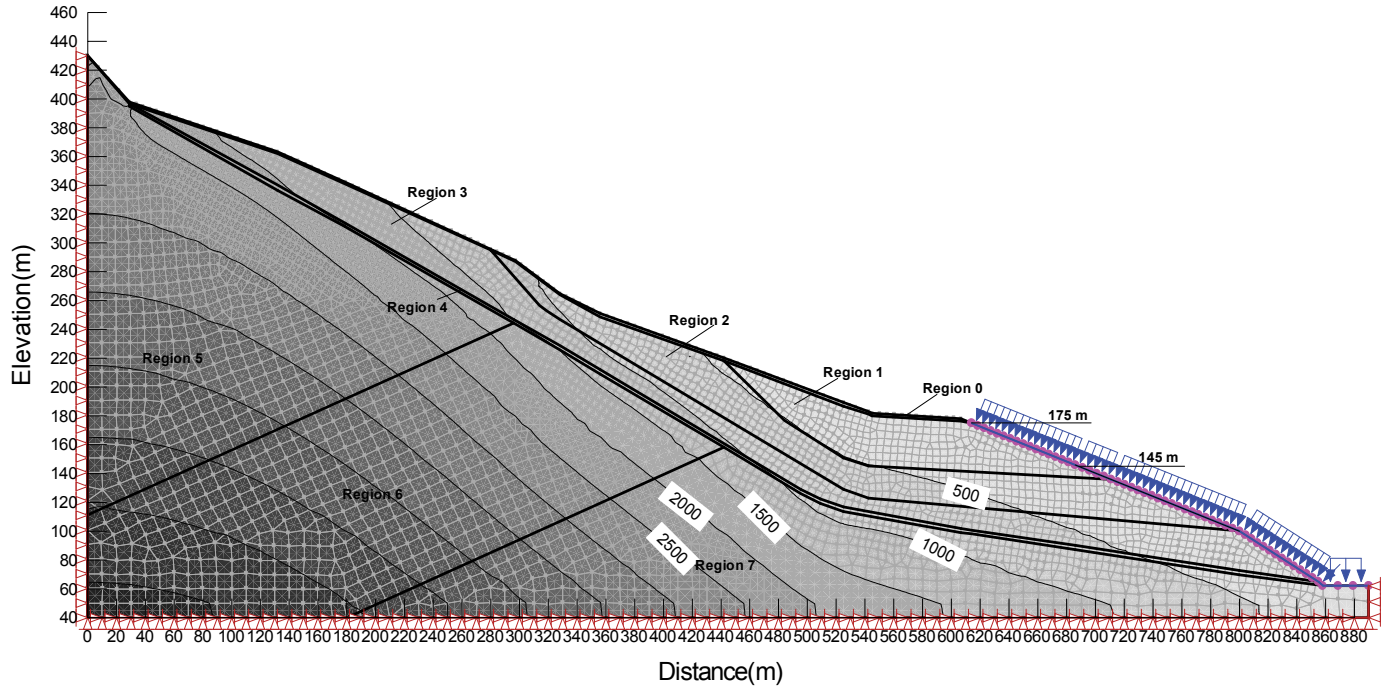

Figure 8.8: Vertical effective stress when total head boundary is at 175 m (unit: kPa)

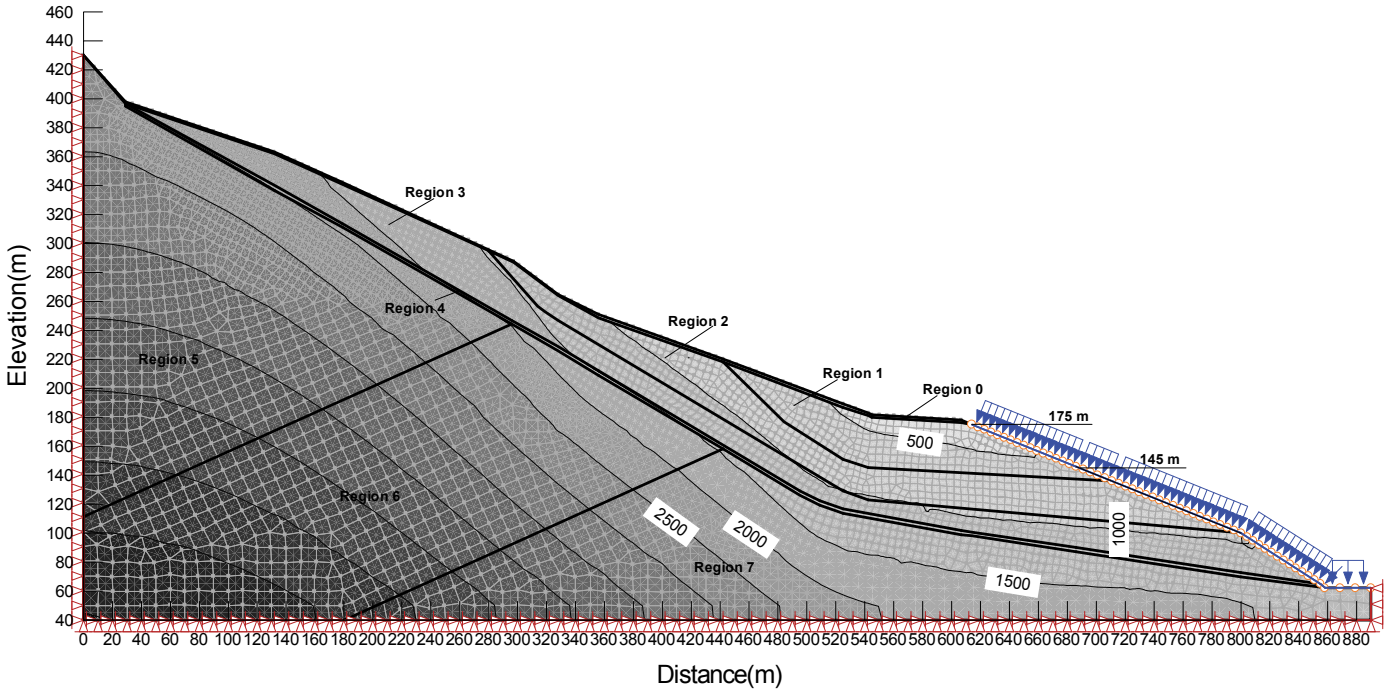

Figure 8.9: Vertical effective stress when total head boundary is at 145 m (unit: kPa)

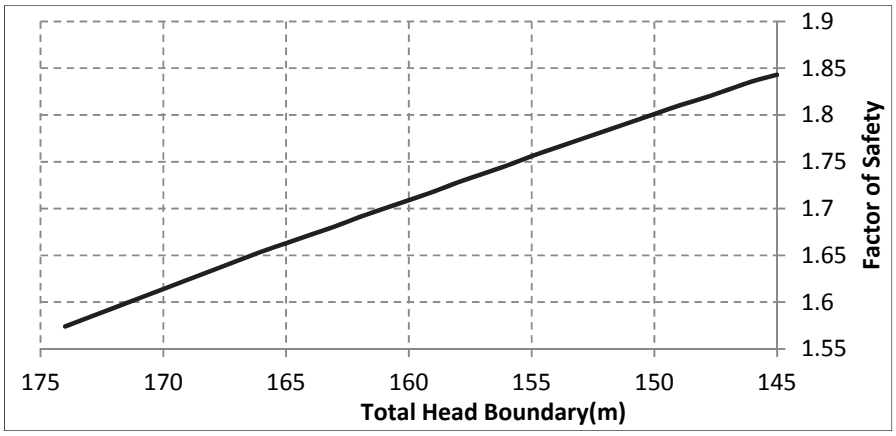

Figure 8.10: Total head boundary and factor of safety

The relationship between total head boundary and factor of safety is plotted in Figure 8.10. In this figure, the factor of safety increases almost linearly with the decrease of total head. The factor of safety is 1.574 when total head is at 174 m. It becomes 1.843 when total head is decreased to 145 m. Thus, there is 17.1% increase of factor of safety when the total head is decreased from 174 m to 145 m.

8.4 Factor of Seepage Force at the Toe

SIGMA/W and SLOPE/W software are used to study the influence of seepage force at the toe on the factor of safety. The configuration of the landslide model is presented in Figure 8.11.

The resultant seepage force in the landslide can be calculated by,

$$T = \gamma_w \cdot i \cdot A \tag{8.1}$$

where

γ_w is the unit weight of pore fluid;

$i = \sin\alpha$ is the hydraulic gradient, and α is the average inclination of the slip zone;

A is the area where seepage happens.

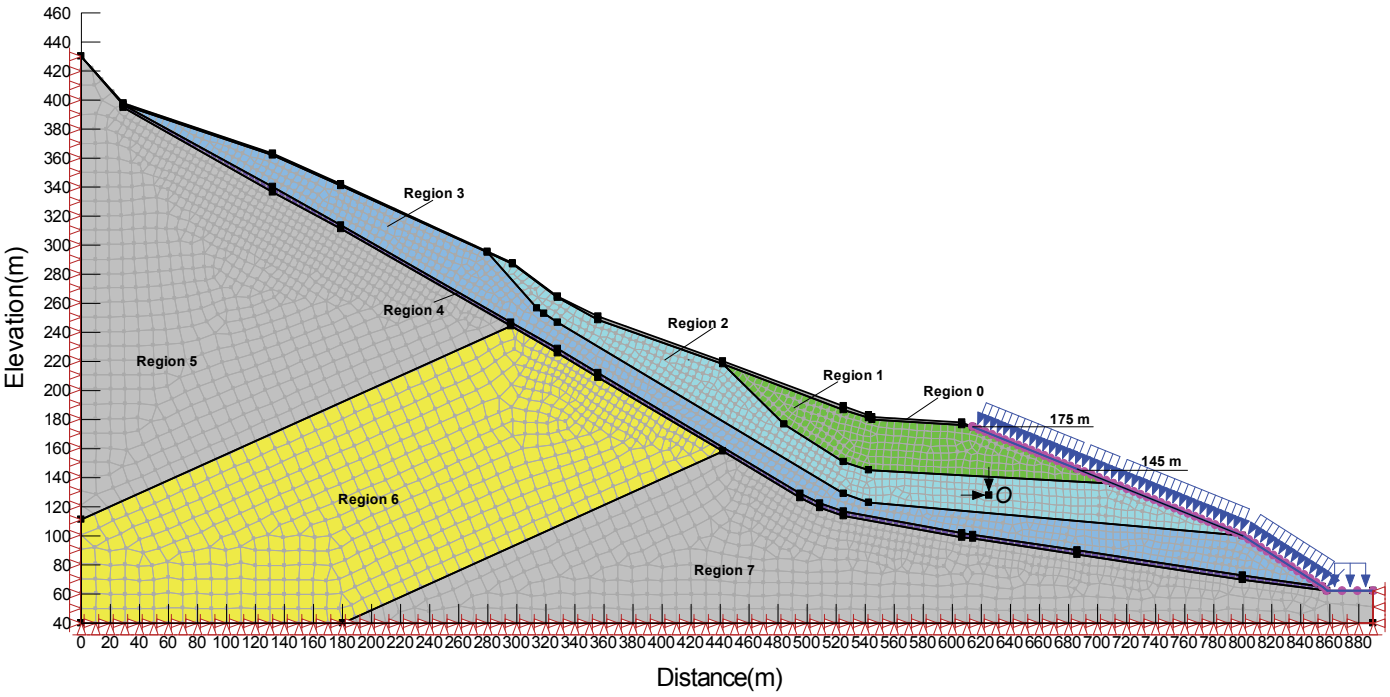

Figure 8.11: SIGMA/W model for the analysis of seepage force at the toe

For this research, it is assumed that $\alpha = 20^\circ$, thus $i = \sin 20^\circ = 0.342$. It is assumed that the area of the landslide mass, which is below the 175 m level, is the area where seepage happens and seepage force exists. This area is plotted in Figure 8.12. Thus, A=20611 m^2.

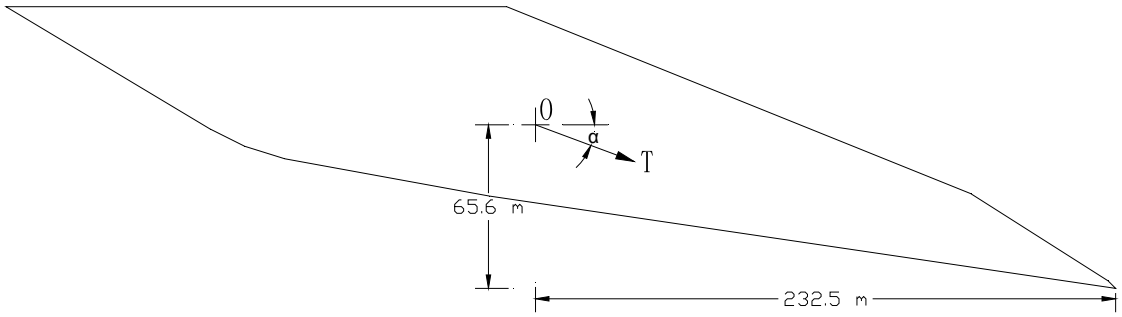

Figure 8.12: The area where seepage happens

The resultant seepage force $T = 9.8 \times 20611 \times 0.342 = 69{,}080\ kN$

It is assumed that the resultant seepage force acts at the barycenter (Point O) of the seepage area in Figure 8.12. This point is also plotted in Figure 8.11.

In Figure 8.11, left and right boundaries are horizontally fixed but free to move vertically. The bottom is fixed in both horizontal and vertical directions. Arrows pointing to the ground surface at the toe represent load of 175 m hydrostatic pressure. The small circles at the toe represent total head boundary at 175 m. The vertical and horizontal arrows at Point O are the vertical and horizontal components of seepage force.

Elastic-Plastic constitutive model is selected to model top soil, landslide mass, and slip zone. Bedrock is assumed to be elastic and impenetrable.

Stress fields with and without considering seepage force are calculated in SIGMA/W and then imported to SLOPE/W to calculate factor of safety. The calculated factor of safety is summarized in Table 8.4.1.

Table 8.4.1: Factor of safety for the study of influence of seepage force

	Factor of Safety
Without Seepage Force	0.994
With Seepage Force	0.810

It can be seen in Table 8.4.1 that the factor of safety is decreased from 0.994 to 0.810, which is 18.5%, after adding seepage force to the landslide mass. This indicates that the seepage force has a very huge impact on the stability of the landslide. Thus the drawdown rate should be under very careful control in order to mitigate the adverse effect of seepage force.

8.5 Factor of Weight of Water at the Toe

SLOPE/W is used to study the influence of weight of water at the toe on the factor of safety. The 145 m – 175 m area of the landslide mass is horizontally divided into three sections. Different unit weight can be assigned to different sections to model the change of weight of landslide mass due to the absorption or exsorption process. The reservoir drawdown (exsorption process) is studied in this research. Configurations of the landslide model when the top of the saturated area is at 175 m, 165 m, 155 m and 145 m are presented in Figures 8.13 to 8.16. The unit weight of the landslide mass in light gray and dark gray color are 17 kN/m^3 and 20 kN/m^3, respectively.

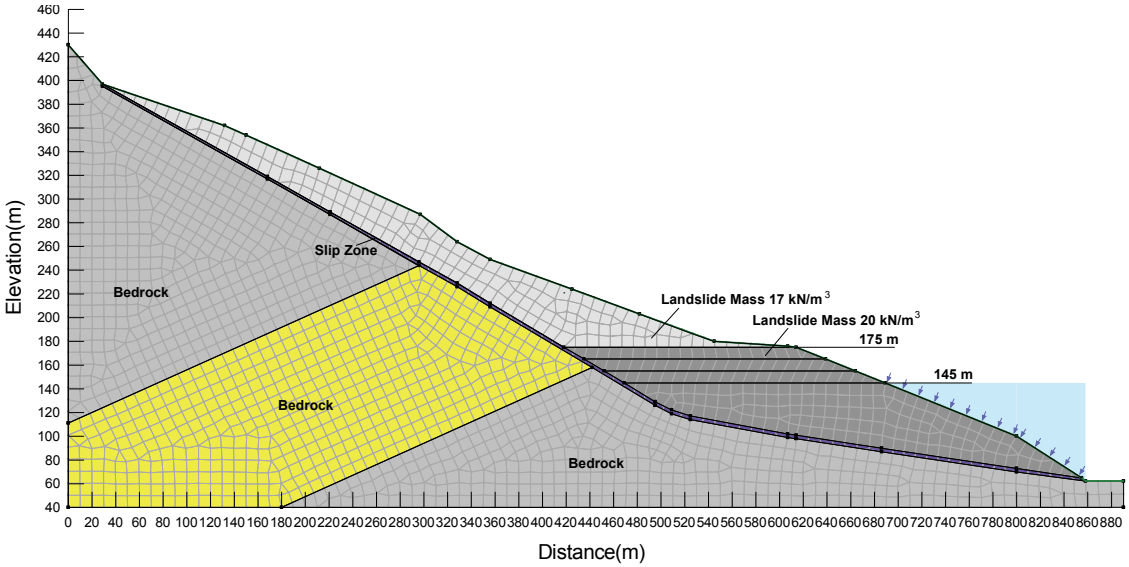

Figure 8.13: SLOPE/W model for the analysis of weight of water (175 m)

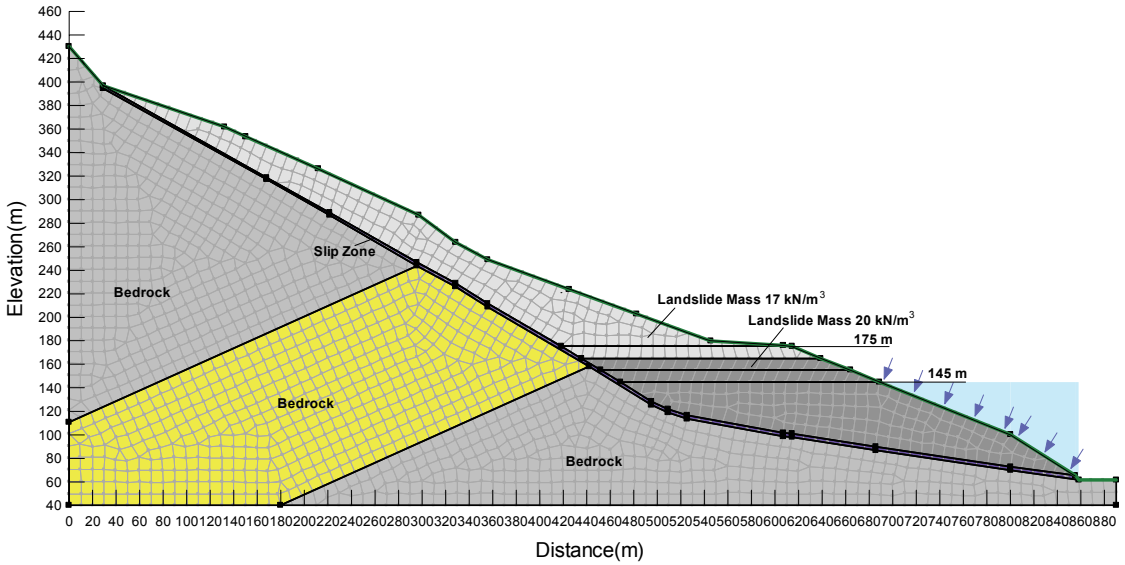

Figure 8.14: SLOPE/W model for the analysis of weight of water (165 m)

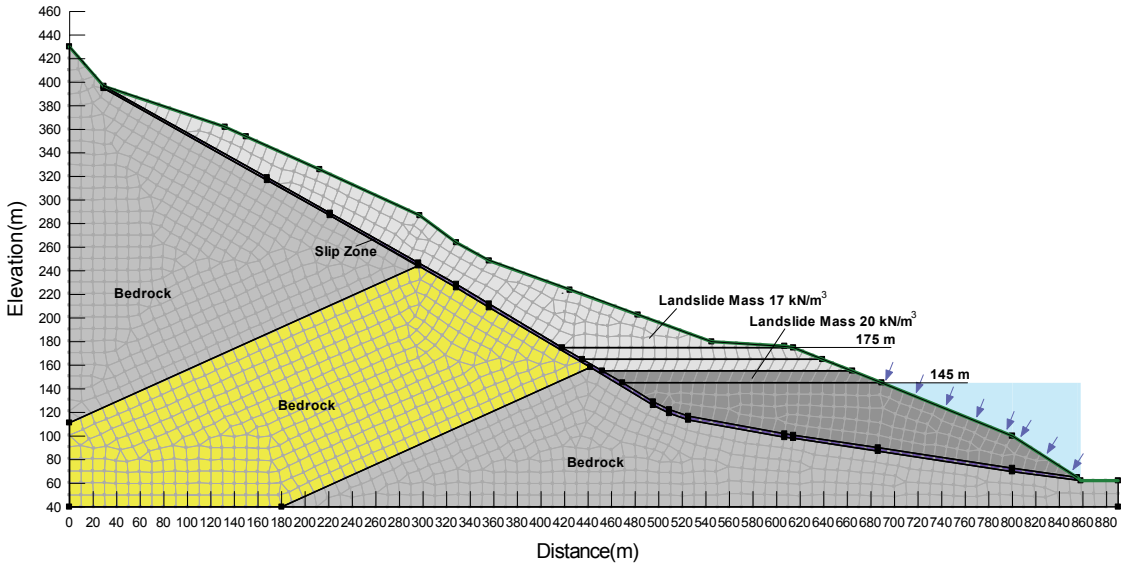

Figure 8.15: SLOPE/W model for the analysis of weight of water (155 m)

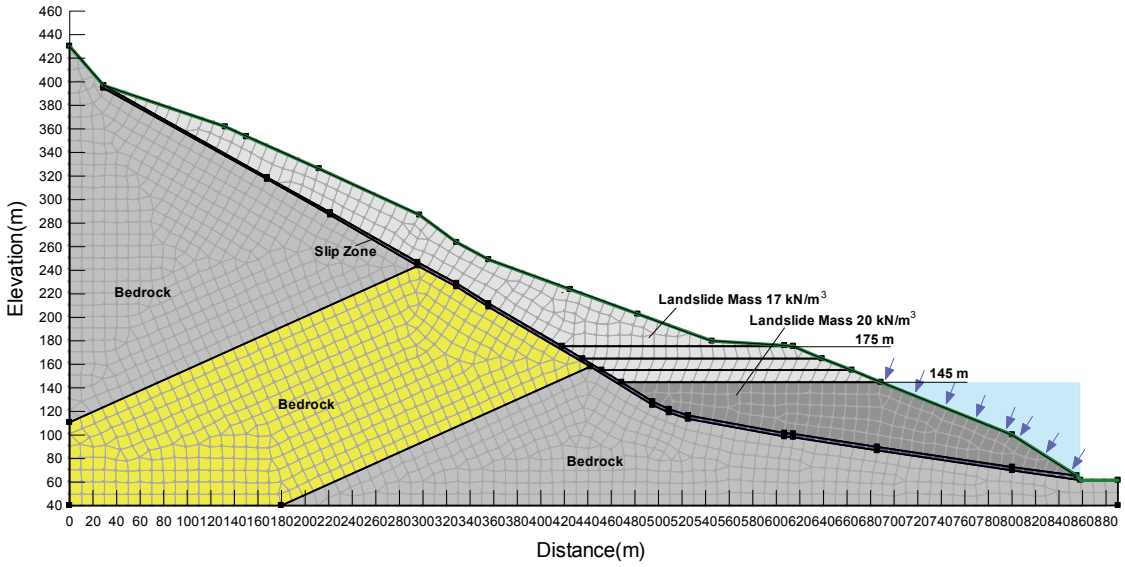

Figure 8.16: SLOPE/W model for the analysis of weight of water (145 m)

Figures 8.13 to 8.16 show the change of unit weight of the landslide mass in order to model the exsorption process during reservoir drawdown. The groundwater table is maintained at 145 m to keep the same pore water pressure condition throughout the analysis. Morgenstern-Price method with fully specified slip surface though the slip zone is selected for the analysis.

Elastic-Plastic constitutive model is selected to model landslide mass and slip zone. Bedrock is assumed to be elastic and impenetrable. Mechanical properties used in the model are summarized in Table 8.5.1.

The relationship between calculated factor of safety and top of the saturated area is presented in Figure 8.17.

It can be seen in Figure 8.17 that the factor of safety tends to decrease as the elevation of the top of the saturated area decreases. This verifies the assumption that the decreased weight of landslide mass at the toe can lead to lower stability. In this case, the factor of safety decreases from 1.107 to 1.104 when the top of the saturated area is decreased from 175 m to 145 m. This 0.27% decrease of factor of safety is relatively

negligible compared to the influence of other factors studied in this chapter earlier.

Table 8.5.1: Mechanical properties in the SLOPE/W model

Region #	Unit Weight (kN/m^3)	E' (MPa)	ν	c' (kPa)	ϕ' $(\circ)$
Landslide Mass (Light Gray)	17.0	20.8	0.28	26.6	23.4
Landslide Mass (Dark Gray)	20.0	20.8	0.28	26.6	23.4
Slip Zone	20.0	20.8	0.28	25.1	19.3
Bedrock	21.9	61000	0.21	-	-

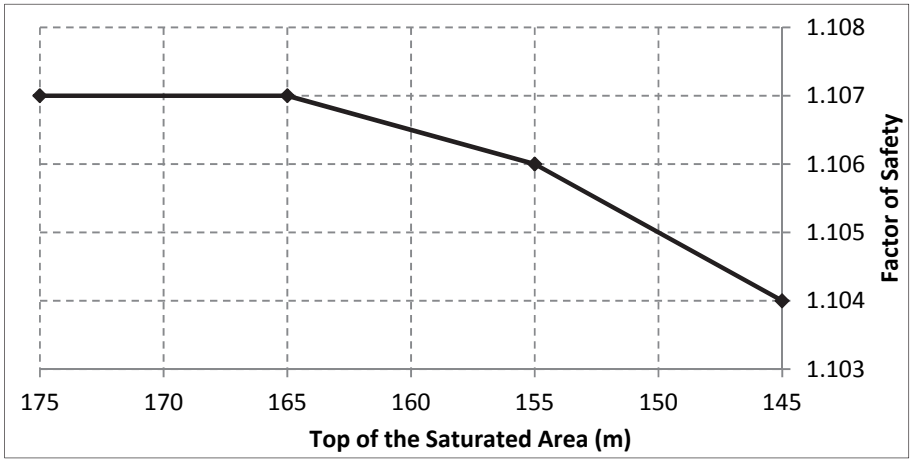

Figure 8.17: Factor of safety and top of the saturated area

Chapter 9 Conclusions and Recommendations for Further Research

Landslides in the Three Gorges reservoir area can be classified into two main types based on their movement patterns: one type of landslide moves when the reservoir water level drops, while the other type of landslide moves when reservoir water level rises.

Two corresponding mechanisms are proposed for these two types of landslides. Mechanism 1, for landslide which moves when reservoir water level drops, assumes that the landslide body has low permeability. When water level of the Three Gorges reservoir drops from an elevation of 175 m to 145 m, the groundwater table in the low-permeable landslide lags behind the reservoir level, which leads to large hydraulic gradient and outward seepage force at the toe of the landslide. The decreasing reservoir water level also means smaller resistant hydrostatic pressure on the slope surface at the toe. As a result the stability of the landslide decreases and the movement accelerates when reservoir water level drops. When the reservoir water level rises, the groundwater table also lags behind the reservoir level and the seepage forces are acting towards the landslide which helps stabilize it. In addition, the higher reservoir level means larger hydrostatic pressure on the slope surface at the toe. Thus, the landslide is more stable and the movement is slower when the reservoir water level rises.

Mechanism 2, for landslide which moves when reservoir water level rises, assumes that the landslide mass has high permeability. When the water level of the Three Gorges reservoir rises from elevation of 145 m to 175 m, the changes in the groundwater table in the highly permeable landslide body follows closely with the reservoir level. This leads to an increase of pore water pressure and decrease of normal effective stress along the slip zone. Consequently the shearing resistance of the soil in the slip zone decreases resulting in more unstable condition and the landslide movement accelerates. When the reservoir water level drops, the groundwater table in the landslide follows closely with

the reservoir level because of the high permeability of the soil. The decrease of pore pressure leads to higher effective normal stress and increase in shearing resistance of soil in the slip zone. Thus, the landslide is more stable and the movement is slower during the drawdown of reservoir level.

Permeability field tests were conducted for Shuping and Baishuihe landslides. Field test results show that the permeability of the soil at Shuping landslide ranges from 2.2 m/day to 13.8 m/day, and the permeability of the soil at Baishuihe landslide ranges from 4.4 m/day to 12.7 m/day.

Laboratory tests show that the soils in both Shuping and Baishuihe landslides consist of silty clay with gravel. In addition, Atterberg limits tests show that the soils have low liquid limit and plasticity index.

Transient seepage and stability analysis of Shuping, Baishuihe and Muyubao landslides have been carried out using SEEP/W and SLOPE/W software based on field and laboratory test results. For Shuping and Baishuihe landslides, whose soils have low permeability, the analysis results show that the changes in groundwater table lag behind the reservoir water level. In addition, for both landslides, the factor of safety increases when the reservoir level rises, and it drops slightly when the reservoir level remains at the highest level, but decreases when the reservoir level drops. For Muyubao landslide, whose soils have high permeability, the analysis results show that the changes in groundwater table follow closely with the reservoir water level. In addition, the factor of safety decreases when the reservoir level rises and increases when the reservoir level drops. For both types of landslides, the rate of change of the factor of safety is generally proportional to the rate of change of the reservoir water level.

Coupled pore fluid/stress analysis using ABAQUS software also shows that the change in groundwater table lags behind the reservoir level for low permeability landslide, while

the groundwater table follows closely with the reservoir level for the high permeability landslide. In addition, the model shows that landslide moves faster during the reservoir drawdown when the permeability is low, while the modeled landslide moves faster during the rise of the reservoir water level when permeability is high, which verifies the two mechanisms proposed here. Case studies in analyzing the movement of Shuping and Baishuihe landslides verify that both landslides belong to Mechanism 1. The results also show that the soils at the slip zone in both landslides have not reached the residual strength yet. The models shows that both cohesion and friction angle of the soil in the slip zone continue to decrease under cyclic landslide movement. The calculated movements at the Shuping landslide agree well with the observed GPS movement without considering the effect of rainfall. This suggests that strain softening and strain-rate hardening Drucker-Prager plasticity constitutive model is appropriate in modeling cyclic landslide movement due to reservoir fluctuation. The case study for Baishuihe landslide shows that rainfall has greater influence on landslide movement and rainfall should be taken into consideration for the better matching between modeled and observed landslide movement.

The results from the case study of Muyubao landslide conclude that this landslide belongs to Mechanism 2. The results also suggest that strain softening and strain-rate hardening Drucker-Prager plasticity constitutive model can be used to model cyclic movement of type 2 landslide. Moreover the case of Muyubao landslide also shows that the softening characteristics of both cohesion and friction angle in the constitutive model are crucial in modeling landslide movement. Rainfall does not have much influence on the movement in this case.

In the three case studies, the coupled pore fluid/stress analysis was only conducted and compared with the observation during the past years and not extended to predict the trend of future displacement of the landslide. Models can be adjusted with further strain

softening and boundary conditions to study the possible failure after a certain number of reservoir fluctuation cycles.

In the displacement analysis of case studies, landslides were modeled to move mainly by the deformation of a thin weak slip zone. One of the limitations for this technic is that there is a limit for the deformation of the slip zone mesh and there will be numerical convergence problem when mesh distortion exceeds a certain amount. An interface can be added between bedrock and landslide mass in the future research to model large landslide displacement and the influence of interface element can be further studied.

Direct shear or ring shear test is recommended to further study the strain softening and strain-rate characteristics of the soil in the slip zone. Moreover unsaturated permeability of landslide mass and slip zone soil can be further studied by conducting unsaturated seepage tests. In addition, a more flexible UMAT subroutine for ABAQUS should be developed to include different kinds of softening characteristics of the slip zone soil.

Four factors have been identified for the landslides in the Three Gorges reservoir that affect their movements: (1) the effect of water pressure at the toe, (2) the effective stress at the slip surface, (3) the seepage force, and (4) the weight of water at the toe. It can be concluded that for these landslide cases, the effect of water pressure due to the reservoir level fluctuation at the toe can cause as much as 14.3 % change in the factor of safety of the landslide. The effect of effective stress at the slip surface can change the factor of safety by up to 17.1%. The seepage force at the toe can lead to a maximum of 18.5% change in the factor of safety. The weight of water at the toe can cause 0.27% change in the factor of safety. Therefore the water pressure at the toe, the effective stress at the slip surface and the seepage force have important effects on the stability and movement of the landslides while the effect of the weight of water at the toe is quite limited.

References

Alonso, E. E., Pinyol, N. M., and Olivella S. (2008). "Rapid drawdown in slopes and embankments." Water Resources Research, 44(5).

Alonso, E. E., and Pinyol, N. M. (2011). "Landslides in reservoirs and dam operation." 2nd International Congress on Dam Maintenance and Rehabilitation, November 23, 2010 - November 25, Taylor & Francis - Balkema, Zaragoza, Spain, 3-27.

Alonso, E. E., and Pinyol, N. M. (2011). "Slope stability under rapid drawdown conditions." Landslide Hazard Analysis, 11-27.

ASTM D6391-11. (2011). “Standard test method for field measurement of hydraulic conductivity using borehole infiltration.”

Dassault Systèmes Simulia Corp. (2012). “ABAQUS theory manual, 2.8.1 effective stress principle for porous media.” Providence, Rhode Island, USA.

Deng, H. F., Guo, J., Zhu, M., and Lu, T. (2011). "Study on the stability of reservoir landslide under multiple-factors action." Advanced Materials Research, Vols. 243-249, 2552-2555.

Deng, Q. L., Zhu, Z. Y., Cui, Z. Q., and Wang, X. P. (2000). "Mass rock creep and landsliding on the Huangtupo slope in the reservoir area of the Three Gorges Project, Yangtze River, China." Eng. Geol., 58(1), 67-83.

Desai, C. S. and Walter C. S. (1971). "Unconfined transient seepage in sloping banks." Journal of the Soil Mechanics and Foundations Division 97(2), 357-373.Desai, C. S. (1977). "Drawdown analysis of slopes by numerical method." Journal of Geotechnical and Geoenvironmental Engineering 103. ASCE 13054.

Du, J., Yin, K., and Lacasse, S. (2013). "Displacement prediction in colluvial landslides, Three Gorges Reservoir, China." Landslides, 10(2), 203-218.

Feng, Q. (2011). "Seepage analysis for Dashiban landslide applied multi-day rainstorm once in fifty years." 4th International Conference on Technology of Architecture and Structure (ICTAS2011), Trans Tech Publications Ltd, Switzerland, 2493-6.

Fujita, H. (1977). "Influence of water level fluctuations in a reservoir on slope stability." Bulletin of the International Association of Engineering Geology-Bulletin de l'Association Internationale de Géologie de l'Ingénieur, 16(1), 170-173.

GEO-SLOPE International, Ltd. (2008). Geostudio 2007. (Version 7.10) [computer software]. Calgary.

Graham, J., Crooks, J., and Bell, A. (1983). "Time effects on the stress-strain behavior of natural soft clays." Geotechnique, 33(3), 327-340.

He, K. Q., Wang, S. Q., Du, W. and Wang, S. J. (2009). "Dynamic features and effects of rainfall on landslides in the Three Gorges Reservoir region, China: Using the Xintan landslide and the large Huangya landslide as the examples." Environmental Earth Sciences, 59(6), 1267-1274.

He, K. Q., Yan, Q. G., Chen, W. G. and Zhao, M. (2012). "A new dynamic prediction method and its application in prediction of the colluvial landslides induced by rainfall." 2nd International Conference on Civil Engineering, Architecture and Building Materials, CEABM 2012, May 25, 2012 - May 27, Trans Tech Publications, Yantai, China, 3-7.

Hou, T., Xu, G., Shen, Y., Wu, Z., Zhang, N., and Wang, R. (2013). "Formation mechanism and stability analysis of the Houba expansive soil landslide." Eng. Geol., 161, 34-43.

Hu, G., Ding, Y., and Liu, J. (2011). "Study on the landslide stability influenced by the reservoir water lifting and atmospheric rainfall." Advanced Materials Research, 243-249(4), 3289-95.Hu, X. W., Tang, H. M., and Liu Y. R. (2005). “Physical model studies on stability of Zhaoshuling landslide in area of three gorges reservoir.” Chinese Journal of Rock Mechanics and Engineering, 24(12), 2089-2095.

Hu, X., Zhang, M., Sun, M., Huang, K., and Song, Y. (2013). "Deformation characteristics and failure mode of the Zhujiadian landslide in the Three Gorges Reservoir, China." 1-12.

Hu, Y., and Feng, Q. (2012). "The saturated - unsaturated seepage analysis of Hualianshu landslide on the condition of rainfall." Advanced Materials Research, 594-597(1), 387-90.

Huang, R. Q. (2007). “Large-scale landslides and their sliding mechanisms in China since the 20th century.” Chinese Journal of Rock Mechanics and Engineering, 26(3), 433-454.

Hug, C. (2009) “Investigations of the Xiao Tou landslide stabilisation in the Three Gorges catchment area.” Australian Geomechanics Journal, 44(4), 13-17.

ICOLD. (1980). “Deterioration of dams and reservoirs. Examples and their analysis.” ICOLD, Paris. Balkema, Rotterdam.

Kulhawy, F. H. and Mayne, P. W. (1990). “Manual on estimating soil properties for

foundation design.” Final Report, Project 1493-6, EL-6800, Electric Power Research Institute, Palo Alto, California.

Lane, P. A. and Griffiths, D. V. (2000). “Assessment of stability of slopes under drawdown conditions.” Jnl. Geotech. and Geoenv. Engng., 126(5), 443-450.

Lee, K. L. and Duncan, J. M. (1975). “Landslide of April 25, 1974 on the Mantaro River, Peru.” Report to the Committee on Natural Disasters, Commission on Sociotechnical Systems, National Research Council, National Academy of Sciences, Washington, D.C.

Leobacher, A. and Blauhut, A. (2010). “Gerlos power station/Gmünd dam – stabilization of a reservoir slope (Grasegger slope).” Geomechanics and Tunnelling, 3, 462-469.Li, D., and Yin, K. (2011). "Deformation characteristics of landslide with steplike deformation in the Three Gorges Reservoir." 2011 International Conference on Electric Technology and Civil Engineering, ICETCE 2011, April 22, 2011 - April 24,IEEE Computer Society, Lushan, China, 6517-6520.

Li, D., Yin, K., and Leo, C. (2010). "Analysis of Baishuihe landslide influenced by the effects of reservoir water and rainfall." Environmental Earth Sciences, 60(4), 677-687.Li Shaojun, Knappett J. A. and Feng Xiating. (2008). “Centrifugal test on slope instability influenced by rise and fall of reservoir water level.” Chinese Journal of Rock Mechanics and Engineering, 27(8), 1586-1593.

Li, T., Zhang, C., Xu, P., and Li, P. (2009). "Stability assessment and stabilizing approaches for the Majiagou landslide, undergoing the effects of water level fluctuation in the Three Gorges reservoir area." F. Wang, and T. Li, eds., Springer Berlin Heidelberg, 331-352.

Li, X., Liao, Q., Wang, S., Liu, J., and Lee, S. (2008). "On evaluating the stability of the Baiyian ancient landslide in the Three Gorges Reservoir area, Yangtze River: A geological history analysis." Environ. Geol., 55(8), 1699-1711.

Li, Y. R., Wen, B. P., Aydin, A., and Ju, N. P. (2013). "Ring shear tests on slip zone soils of three giant landslides in the Three Gorges Project area." Eng. Geol., 154, 106-115.

Li, Y. J. (2013). "An earthquake fault zone discovered in the Three Gorges reservoir area." Applied Mechanics and Materials, 256, 2207-2211.

Liao, H., Ying, J., Gao, S., and Sheng, Q. (2005). "Numerical analysis on slope stability under variations of reservoir water level." K. Sassa, H. Fukuoka, F. Wang, and G. Wang, eds., Springer Berlin Heidelberg, 305-311.

Lu, S., Yi, Q., and Yi, W. (2012). "Analysis on deformation failure mechanism of Woshaxi landslide in the Three Gorges reservoir area." 2012 Global Conference on Civil, Structural and Environmental Engineering, GCCSEE 2012 and the 3rd International Symposium on Multi-field Coupling Theory of Rock and Soil Media and Its Applications, MCTRSM 2012, October 20, 2012 - October 21, Trans Tech Publications, Yichang, China, 498-501.

Luo, X. Q., Sun, H., Tham, L. G., and Junaideen, S. M. (2010). "Landslide model test system and its application on the study of Shiliushubao landslide in Three Gorges reservoir area." Soils and Foundations, 50(2), 309-317.

Ma, H., Shi, D., Yao, W., and Tang, Z. (2011). "Stability analysis of Nongji Technical School landslide in Three Gorges reservoir." 2011 International Conference on Multimedia Technology, IEEE, Piscataway, NJ, USA, 4586-90.

Miao, H., Wang, G., Yin, K., Kamai, T., and Li, Y. (2014). "Mechanism of the slow-moving landslides in Jurassic red-strata in the Three Gorges reservoir, China." Eng. Geol., 171(0), 59-69.

Micu Mihai, Bălteanu Dan. (2013). "A deep-seated landslide dam in the Siriu reservoir (Curvature Carpathians, Romania)", Landslides, 10(3), 323-329.

Morgenstern. (1963). “Stability charts for earth slopes during rapid drawdown.” Géotechnique, 13(1), 121-131.

Nanjing Hydraulic Research Institute. (1999). “Specific gravity test SL-237-005-1999.” Specification of Soil Test SL-237-1999, 38-41.

Nanjing Hydraulic Research Institute. (1999). “Gradation analysis test SL-237-006-1999.” Specification of Soil Test SL-237-1999, 49-71.

Nanjing Hydraulic Research Institute. (1999). “Atterberg limits test SL-237-007-1999.” Specification of Soil Test SL-237-1999, 72-75.

Pytharouli, S. I., and Stiros, S. C. (2010). "Kinematics and rheology of a major landslide based on signal analysis." Geotechnique, 60(3), 207-22.

Qiao, J. P., Zhu, A. X., Wu, C. Y., and Tian, H. L. (2006). "Bottom factors applied to the zoning study of the risk levels of landslides in the Three Gorges Reservoir area." Wuhan Univ. J. Nat. Sci., 11(4), 761-6.

Richardson, A. M. and Whitman, R. V. (1963). “Effect of strain rate upon undrained shear

resistance of a saturated remolded fat clay.” Geotechnique, 13(4), 310-324.

Riemer, W., Pantzartzis, P., Krapp, L. & Skourtis, C. (1996). “Investigation and monitoring of landslides at the Polyphyton project in Greece.” In Proceedings of the 7th International Symposium on Landslides, Trondheim, 357–362.

Sadrekarimi, A., and Olson, S. M. (2007). "Review of the October 9, 1963 failure of the Vaiont reservoir slope." Geotech. Spec. Publ., (157).

Saurer, E., Prager, C. and Marcher, T. (2013). "Soil slope stability of hydropower reservoirs-from geological site investigation to design of mitigation measures." Proceedings of the 18th International Conference on Soil Mechanics and Geotechnical Engineering, Paris, 2249-2252.

Sherard, J. L., Woodward, R. J. Gizienski, S. F. and Clevenger, W. A. (1963). “Earth and earth-rock dams.” John Wiley and Sons, New York.

Singh, Y., Bhat, G. M., Sharma, V., Pandita, S. K., and Thakur, K. K. (2012). "Reservoir induced landslide at Assar, Jammu and Kashmir: A case study." Journal of the Geological Society of India, 80(3), 435-439.

Skempton A.W. (1964). “Long-term stability of clay slopes.” Geotechnique, 14(2), 77-102.

Tang, H., Hu, X., and Xiong, C. (2012). "Stability prediction of Zhaoshuling landslide by physical model test." 2nd International Conference on Civil Engineering, Architecture and Building Materials, CEABM 2012, May 25, 2012 - May 27, Trans Tech Publications, Yantai, China, 1147-1150.

The Ministry Of Education Key Laboratory of the Three Gorges Reservoir Geological Disasters (2012). “Geological model and numerical modeling report for the assessment and prediction of large reactivated landslides in the Three Gorges reservoir after impoundment.”

Vaid, Y., Robertson, P., and Campanella, R. (1979). "Strain rate behavior of Saint-Jean-Vianney clay." Can. Geotech. J., 16(1), 34-42.

Wang, F., Yin, Y., Huo, Z., and Wang, G. (2013). "Landsliding caused by water level variation in China Three Gorges reservoir." 2nd World Landslide Forum, WLF 2011, October 3, 2011 - October 9, Springer-Verlag Berlin Heidelberg, Rome, Italy, 19-26.

Wang, F., Zhang, Y., Huo, Z., Matsumoto, T., and Huang, B. (2004). "The July 14, 2003

Qianjiangping landslide, Three Gorges Reservoir, China." Landslides, 1(2), 157-162.

Wang, F., Zhang, Y., Huo, Z., Peng, X., Wang, S., and Yamasaki, S. (2008). "Mechanism for the rapid motion of the Qianjiangping landslide during reactivation by the first impoundment of the Three Gorges dam reservoir, China." Landslides, 5(4), 379-386.

Wang, F., Zhang, Y., Wang, G., Peng, X., Huo, Z., Jin, W., and Zhu, C. (2007). "Deformation features of Shuping landslide caused by water level changes in Three Gorges reservoir area, China." Yanshilixue Yu Gongcheng Xuebao/Chinese Journal of Rock Mechanics and Engineering, 26(3), 509-517.

Wang, S. Q. (2009)."Time prediction of the Xintan landslide in Xiling Gorge, the Yangtze River." Landslide Disaster Mitigation in Three Gorges Reservoir, China, Springer Berlin Heidelberg, 411-431.

Wang, X., Chen, S., and Feng, Q. (2013). "Bankside stability analysis under the actions of rainfall and reservoir water level fluctuation." 2nd International Conference on Energy, Environment and Sustainable Development, EESD 2012, October 12, 2012 - October 14, Trans Tech Publications, Jilin, China, 2658-2662.

Wedage A.M.P. (1995). “Influence of rate effects on the residual strength of moving slopes.” Ph.D. Thesis, University of Alberta, Alberta, Canada.

Wu, Y. P., Ou, G. Z., Wang, Z. S. (2013). "Factor analysis of Liangshuijing landslide deformation." Applied Mechanics and Materials, 392, 978-983.

Xia, M., Guang, M. R., and Xin, L. M. (2013). "Deformation and mechanism of landslide influenced by the effects of reservoir water and rainfall, Three Gorges, China." Nat. Hazards, 68(2), 467-82.

Yang, Q., Pan, S., Ding, W., Zhang, Z., Li, Q., and Gao, Y. (2013). "Analysis of the impact of reservoir water level fluctuation on the stability of cohesive colluvial landslide in the Three Gorges reservoir area." 2013 3rd International Conference on Intelligent System Design and Engineering Applications, ISDEA 2013, January 16, 2013 - January 18, IEEE Computer Society, Hong Kong, China, 325-328.

Yi, W., Huang, H., and Lu, S. (2012). “Emergency investigation report for Shuping landslide in Three Gorges reservoir Hubei Zigui County.” 1-33.

Zhang, Z. H., Luo, X. Q., and Wu, J. (2009)."Study on the possible failure mode and mechanism of the Xietan landslide when exposed to water level fluctuation." Landslide

Disaster Mitigation in Three Gorges Reservoir, China, Springer Berlin Heidelberg, 375-385.

Zhu, D., Yan, E., Hu, G., and Lin, Y. (2011). "Revival deformation mechanism of Hefeng landslide in the three gorges reservoir based on FLAC3D software." 2011 International Conference on Advanced in Control Engineering and Information Science, CEIS 2011, August 18, 2011 - August 19, Elsevier Ltd, Dali, Yunnam, China, 2847-2851.

Appendix I Unsaturated Hydraulic Conductivity for Shuping Analysis

Table I.1: Relationship between matric suction and permeability for Shuping SEEP/W model

Ground Surface		R.1	R.2	R.3	R.4	R.5&7	R.6
Matric Suction (kPa)	K_H (m/day)	K_H (m/day)	K_H (m/day)	K_H (m/day)	K_H (m/day)	K_H (m/day)	K_H (m/day)
2.63	2	0.1	2	0.1	0.1	0.5	1
5.26	2.20E-02	1.10E-03	2.20E-02	1.10E-03	1.10E-03	5.50E-03	1.10E-02
10.5	4.73E-03	2.37E-04	4.73E-03	2.37E-04	2.37E-04	1.18E-03	2.37E-03
15.8	1.75E-03	8.73E-05	1.75E-03	8.73E-05	8.73E-05	4.37E-04	8.73E-04
21.1	8.36E-04	4.18E-05	8.36E-04	4.18E-05	4.18E-05	2.09E-04	4.18E-04
26.3	4.66E-04	2.33E-05	4.66E-04	2.33E-05	2.33E-05	1.17E-04	2.33E-04
31.6	2.88E-04	1.44E-05	2.88E-04	1.44E-05	1.44E-05	7.20E-05	1.44E-04
36.8	1.91E-04	9.55E-06	1.91E-04	9.55E-06	9.55E-06	4.78E-05	9.55E-05
42.5	1.42E-04	7.09E-06	1.42E-04	7.09E-06	7.09E-06	3.54E-05	7.09E-05
47.4	9.70E-05	4.85E-06	9.70E-05	4.85E-06	4.85E-06	2.43E-05	4.85E-05
52.6	7.30E-05	3.65E-06	7.30E-05	3.65E-06	3.65E-06	1.82E-05	3.65E-05
57.9	5.64E-05	2.82E-06	5.64E-05	2.82E-06	2.82E-06	1.41E-05	2.82E-05
63.2	4.45E-05	2.22E-06	4.45E-05	2.22E-06	2.22E-06	1.11E-05	2.22E-05
68.4	3.58E-05	1.79E-06	3.58E-05	1.79E-06	1.79E-06	8.96E-06	1.79E-05
73.7	2.93E-05	1.46E-06	2.93E-05	1.46E-06	1.46E-06	7.31E-06	1.46E-05
78.9	2.43E-05	1.21E-06	2.43E-05	1.21E-06	1.21E-06	6.06E-06	1.21E-05
84.2	2.03E-05	1.01E-06	2.03E-05	1.01E-06	1.01E-06	5.07E-06	1.01E-05
89.5	1.72E-05	8.62E-07	1.72E-05	8.62E-07	8.62E-07	4.31E-06	8.62E-06
94.7	1.47E-05	7.35E-07	1.47E-05	7.35E-07	7.35E-07	3.68E-06	7.35E-06
100	1.27E-05	6.34E-07	1.27E-05	6.34E-07	6.34E-07	3.17E-06	6.34E-06

Table I.2: Relationship between matric suction and volumetric water content for Shuping SEEP/W model

Matric Suction (kPa)	10	12	40	60	80	100	120
Volumetric Water Content	0.44	0.39	0.12332	0.090867	0.084	0.081836	0.080971
Matric Suction (kPa)	140	160	180	200	220	240	260
Volumetric Water Content	0.080566	0.080355	0.080235	0.080163	0.080116	0.080086	0.080065

Matric Suction (kPa)	280	300	320	340	360	380	400
Volumetric Water Content	0.08005	0.080039	0.080031	0.080025	0.080021	0.080017	0.080014

Table I.3: Relationship between k_s and saturation for Shuping ABAQUS model

k_s	3.25E-06	3.50E-06	3.75E-06	4.00E-06	4.25E-06	4.50E-06	6.35E-06
Saturation	0.200000	0.200005	0.200015	0.200025	0.200035	0.200408	0.204590
k_s	7.35E-06	8.60E-06	1.02E-05	1.22E-05	1.47E-05	1.79E-05	2.23E-05
Saturation	0.206024	0.207430	0.208864	0.210944	0.215408	0.219957	0.224421
k_s	2.82E-05	3.65E-05	4.85E-05	7.10E-05	9.55E-05	0.000144	0.000233
Saturation	0.235686	0.257187	0.278281	0.298158	0.358972	0.441314	0.525240
k_s	0.000418	0.000875	0.002365	0.011	1	1	-
Saturation	0.607582	0.772000	0.957500	0.982778	0.991378	1	-

Table I.4: Relationship between saturation and pore pressure for Shuping ABAQUS model

Pore Pressure (kPa)	-5000	-3200	-1600	-800	-400	-380	-360
Saturation	0.200000	0.200005	0.200015	0.200025	0.200035	0.200043	0.200053
Pore Pressure (kPa)	-340	-320	-300	-280	-260	-240	-220
Saturation	0.200063	0.200078	0.200098	0.200125	0.200163	0.200215	0.20029
Pore Pressure (kPa)	-200	-180	-160	-140	-120	-100	-80
Saturation	0.200408	0.200588	0.200838	0.201415	0.202428	0.20459	0.21
Pore Pressure (kPa)	-60	-40	-20	-10	-1	0	-
Saturation	0.227168	0.3083	0.625	0.975	0.995	1	-

Appendix II Unsaturated Hydraulic Conductivity for Baishuihe Analysis

Table II.1: Relationship between matric suction and hydraulic conductivity for Baishuihe SEEP/W model

Landslide Mass		Slip Zone	Bedrock
Matric Suction (kPa)	K_H (m/day)	K_H (m/day)	K_H (m/day)
2.63	0.1	0.1	0.5
5.26	1.10E-03	1.10E-03	5.50E-03
10.5	2.37E-04	2.37E-04	1.18E-03
15.8	8.73E-05	8.73E-05	4.37E-04
21.1	4.18E-05	4.18E-05	2.09E-04
26.3	2.33E-05	2.33E-05	1.17E-04
31.6	1.44E-05	1.44E-05	7.20E-05
36.8	9.55E-06	9.55E-06	4.78E-05
42.5	7.09E-06	7.09E-06	3.54E-05
47.4	4.85E-06	4.85E-06	2.43E-05
52.6	3.65E-06	3.65E-06	1.82E-05
57.9	2.82E-06	2.82E-06	1.41E-05
63.2	2.22E-06	2.22E-06	1.11E-05
68.4	1.79E-06	1.79E-06	8.96E-06
73.7	1.46E-06	1.46E-06	7.31E-06
78.9	1.21E-06	1.21E-06	6.06E-06
84.2	1.01E-06	1.01E-06	5.07E-06
89.5	8.62E-07	8.62E-07	4.31E-06
94.7	7.35E-07	7.35E-07	3.68E-06
100	6.34E-07	6.34E-07	3.17E-06

Table II.2: Relationship between matric suction and volumetric water content for Baishuihe SEEP/W model

Matric Suction (kPa)	10	12	40	60	80	100	120
Volumetric Water Content	0.44	0.39	0.12332	0.090867	0.084	0.081836	0.080971
Matric Suction (kPa)	140	160	180	200	220	240	260
Volumetric	0.080566	0.080355	0.080235	0.080163	0.080116	0.080086	0.080065

Water Content							
Matric Suction (kPa)	280	300	320	340	360	380	400
Volumetric Water Content	0.08005	0.080039	0.080031	0.080025	0.080021	0.080017	0.080014

Table II.3: Relationship between k_s and saturation for Baishuihe ABAQUS model

k_s	6.35E-06	7.35E-06	8.60E-06	1.02E-05	1.22E-05	1.47E-05	1.79E-05
Saturation	0.20459	0.206024	0.20743	0.208864	0.210944	0.215408	0.219957
k_s	2.23E-05	2.82E-05	3.65E-05	4.85E-05	7.10E-05	9.55E-05	0.000144
Saturation	0.224421	0.235686	0.257187	0.278281	0.298158	0.358972	0.441314
k_s	0.000233	0.000418	0.000875	0.002365	0.011	1	1
Saturation	0.52524	0.607582	0.772	0.9575	0.982778	0.991378	1

Table II.4: Relationship between saturation and pore pressure for Baishuihe ABAQUS model

Pore Pressure(kPa)	-100	-80	-60	-40	-20	-10	-1	0
Saturation	0.20459	0.21	0.227168	0.3083	0.625	0.975	0.995	1

Appendix III Unsaturated Hydraulic Conductivity for Muyubao landslide

Table III.1: Relationship between matric suction and hydraulic conductivity for Muyubao SEEP/W model

Landslide Mass		Slip Zone	Bedrock
Matric Suction (kPa)	K_H (m/day)	K_H (m/day)	K_H (m/day)
2.63	0.1	851.0	851.0
10.5	2.37E-04	800.9	800.9
21.1	4.18E-05	210.8	210.8
42.5	7.09E-06	25.3	25.3
63.2	2.22E-06	10.1	10.1
84.2	1.01E-06	8.0	8.0
100	6.34E-07	7.4	7.4

Table III.2: Relationship between matric suction and volumetric water content for Muyubao SEEP/W model

Matric Suction (kPa)	10	12	40	60	80	100	120
Volumetric Water Content	0.44	0.39	0.12332	0.090867	0.084	0.081836	0.080971
Matric Suction (kPa)	140	160	180	200	220	240	260
Volumetric Water Content	0.080566	0.080355	0.080235	0.080163	0.080116	0.080086	0.080065
Matric Suction (kPa)	280	300	320	340	360	380	400
Volumetric Water Content	0.08005	0.080039	0.080031	0.080025	0.080021	0.080017	0.080014

Table III.3: Relationship between saturation and pore pressure for Muyubao ABAQUS model

Pore Pressure(kPa)	-100	-80	-60	-40	-20	-10	-1	0
Saturation	0.20459	0.21	0.227168	0.3083	0.625	0.975	0.995	1